MULTIGENERATION POWER: POWER GENERATION FROM RENEWABLE SOURCE

TOH WEE KAI

UNIVERSITI TUNKU ABDUL RAHMAN

MULTIGENERATION POWER: POWER GENERATION FROM RENEWABLE SOURCE

TOH WEE KAI

A project report submitted in partial fulfilment of the requirements for the award of Bachelor of Engineering (Honours) Mechanical Engineering

Lee Kong Chian Faculty of Engineering and Science
Universiti Tunku Abdul Rahman

May 2022

COMMENTS ON FYP REPORT

Name: Toh Wee Kai Student ID: 17UEB02606

Supervisor: Dr. Jun Hieng Kiat Co-supervisor: N/A

Moderator: Dr. Rubina Bahar

Comments by: **Supervisor/Moderator** (delete where not applicable)

Option 1

☐ Marking and give comments on the pdf/word FYP report

Option 2

☐ Marking and give comments on below

Comments on FYP Report

No.	Criteria	Comments
1	Abstract	
2	Introduction	
3	Literature Review	
4	Methodology	
5	Results & Discussion	
6	Conclusion and Recommendation	
7	References	
8	Any other comments	

DECLARATION

I hereby declare that this project report is based on my original work except for citations and quotations which have been duly acknowledged. I also declare that it has not been previously and concurrently submitted for any other degree or award at UTAR or other institutions.

Signature : 

Name : Toh Wee Kai

ID No. : 17UEB02606

Date : 22 April 2022

APPROVAL FOR SUBMISSION

I certify that this project report entitled **"MULTIGENERATION POWER: POWER GENERATION FROM RENEWABLE SOURCE"** was prepared by **TOH WEE KAI** has met the required standard for submission in partial fulfilment of the requirements for the award of Bachelor of Engineering (Honours) Mechanical Engineering at Universiti Tunku Abdul Rahman.

Approved by,

Signature	:	*jun hk*
Supervisor	:	Dr. Jun Hieng Kiat
Date	:	22 April 2022

ACKNOWLEDGEMENTS

I would like to thank everyone who had contributed to the successful completion of this project. I would like to express my gratitude to my research supervisor, Dr. Jun Hieng Kiat for his invaluable advice, guidance and his enormous patience throughout the development of the research.

In addition, I would also like to express my gratitude to my loving parents and friends who had helped and given me encouragement to enable me to complete this research project successfully.

Last but not least, I would like to express my appreciation to ScienceDirect and the authors of the journal "Theoretical and experimental performance analysis of a Fresnel type solar concentrator" - Hani Beltagy, Djaffar Semmar, Christophe Lehaut, and Noureddine Said for allowing me to use the figure in your journal.

ABSTRACT

In recent years, solar-driven multigeneration systems have received a lot of attention due to their ability to produce multiple outputs from solar energy. Cogeneration and trigeneration systems are classified under the category of multigeneration systems. In this study, the cogeneration and trigeneration systems powered by solar energy had been proposed. Both systems utilize solar energy to generate electric power and hydrogen gas concurrently while the trigeneration system with an additional absorption chiller can produce an extra cooling capacity. The proposed systems were modelled in Aspen HYSYS to evaluate the overall performances of the systems. From the simulation results, it was found that when the direct normal irradiation (DNI) is 0.375 kW/m^2, both the cogeneration and trigeneration systems can generate 3 127.5 kW of electric power and 24.58 kg/h of hydrogen gas. The trigeneration system can produce an additional 54.97 kW of cooling capacity other than electric power and hydrogen gas. The efficiencies of the cogeneration and the trigeneration systems are 26.77% and 27.15% respectively. Other than performance evaluation, the life cycles of both systems were also assessed through GaBi software. Since both systems are driven by solar energy, the operations of the systems do not have direct impacts on the environment. However, the generation of electric power to drive the pumps in the systems as well as the processes of producing the working fluids for the systems bring some negative impacts to the environment. In 1 hour of operation, the global warming potential, acidification potential, and human toxicity potential of the cogeneration system are 145.4 kg of CO_2-eq, 0.561 kg of SO_2-eq, and 8.28 kg of 1,4-DCB-eq respectively. On the other hand, the operation of the trigeneration system has slightly higher environmental impacts compared to the cogeneration system due to the additional power and working fluid required by the absorption chiller. It was found that 145.937 kg of CO_2-eq, 0.562 kg of SO_2-eq, and 8.30 kg of 1,4-DCB-eq will be emitted into the atmosphere when the trigeneration system operates for 1 hour.

TABLE OF CONTENTS

DECLARATION **i**
APPROVAL FOR SUBMISSION **ii**
ACKNOWLEDGEMENTS **iv**
ABSTRACT **v**
TABLE OF CONTENTS **vi**
LIST OF TABLES **x**
LIST OF FIGURES **xi**
LIST OF SYMBOLS / ABBREVIATIONS **xiii**
LIST OF APPENDICES **xv**

CHAPTER

1 INTRODUCTION **1**
1.1 General Introduction 1
1.2 Importance of the Study 2
1.3 Problem Statement 3
1.4 Aim and Objectives 4
1.5 Scope and Limitation of the Study 4
1.6 Contribution of the Study 5
1.7 Outline of the Report 5
2 LITERATURE REVIEW **7**
2.1 Introduction 7
2.2 Cogeneration 7
2.2.1 Ideal Cogeneration Plant 7
2.2.2 Cogeneration Plant with Adjustable Loads 9
2.3 Trigeneration 11
2.3.1 Overview of Absorption Chillers 11
2.3.2 Trigeneration System 14
2.4 Advantages of Cogeneration and Trigeneration 15
2.5 Power Generation from Solar Energy 19

2.5.1 Solar Thermal Power Generation 20
2.5.2 Solar Photovoltaic (PV) 25
2.6 Solar-Driven Cogeneration System 26
2.7 Hybrid Photovoltaic-Thermal (PVT) Cogeneration System 29
2.8 Solar-Driven Trigeneration System 30
2.9 Hydrogen Production Methods 33
2.9.1 Steam Methane Reforming 33
2.9.2 Methane Pyrolysis 34
2.9.3 Electrolysis of Water 34
2.10 Summary of Literature Review 38
3 METHODOLOGY AND WORK PLAN 39
3.1 Introduction 39
3.2 Overview of Methodology 39
3.3 The Proposed Solar Cogeneration System 40
3.4 The Proposed Solar Trigeneration System 44
3.5 Performance Evaluation of the Proposed Multigeneration Systems 46
3.5.1 Analysis of Energy Flows in the Solar Field 46
3.5.2 Process Simulation of the Cogeneration System in Aspen HYSYS 48
3.5.3 Mathematical Models for the Cogeneration System 50
3.5.4 Process Simulation of the Trigeneration System in Aspen HYSYS 52
3.5.5 Mathematical Models for the Trigeneration System 54
3.5.6 Criteria for Selecting the Final Operating Parameters of the Proposed Multigeneration Systems 55
3.6 Life Cycle Assessment (LCA) of the Proposed Multigeneration Systems 56
3.6.1 Goal and Scope Definition 57
3.6.2 Life Cycle Inventory Analysis 57

3.6.3 Life Cycle Impact Assessment 59
3.6.4 Summary of Life Cycle Assessment Methodology 59
3.6.5 Life Cycle Assessment of the Cogeneration System in GaBi 60
3.6.6 Life Cycle Assessment of the Trigeneration System in GaBi 62
3.7 Work Plan 62
3.8 Summary 65
4 RESULTS AND DISCUSSION 66
4.1 Introduction 66
4.2 Results of Energy Flow Analysis for the Solar Field 66
4.2.1 Calculations of Energy Transfer Rates in the Solar Field 66
4.2.2 Interpretation of the Calculated Results 67
4.3 Performance Evaluation of the Cogeneration System 68
4.3.1 Results of Process Simulation for the Cogeneration System 68
4.3.2 Outputs and Efficiency of the Cogeneration System 70
4.3.3 Discussion on the Simulation Results and the Performance of the Cogeneration System 72
4.4 Performance Evaluation of the Trigeneration System 75
4.4.1 Results of Process Simulation for the Trigeneration System 76
4.4.2 Outputs and Efficiency of the Trigeneration System 78
4.4.3 Discussion on the Simulation Results and the Performance of the Trigeneration System 79

4.5 Further Discussion on the Performances of the Cogeneration and Trigeneration Systems 82
4.6 Applications of the Proposed Cogeneration and Trigeneration Systems 86
4.7 Life Cycle Assessment of the Solar Cogeneration System 88
4.7.1 Results of Life Cycle Assessment for the Cogeneration System 89
4.7.2 Interpretation of Life Cycle Assessment Results for the Cogeneration System 89
4.8 Life Cycle Assessment of the Solar Trigeneration System 93
4.8.1 Results of Life Cycle Assessment for the Trigeneration System 94
4.8.2 Interpretation of Life Cycle Assessment Results for the Trigeneration System 94
4.9 Further Discussion on Life Cycle Assessment 97
4.10 Summary 97
5 CONCLUSIONS AND RECOMMENDATIONS 98
5.1 Conclusions 98
5.2 Recommendations for Future Work 99
REFERENCES 101
APPENDICES 108

LIST OF TABLES

Table 3.1:	Summary of Life Cycle Assessment Methodology.	59
Table 3.2:	The Main Tasks for Part 1 of the Project.	63
Table 3.3:	The Main Tasks for Part 2 of the Project.	64
Table 4.1:	Parameters Needed for the Calculations of Energy Transfer Rates in the Solar Field.	66
Table 4.2:	The Selected Operating Parameters for the Binary Vapour Cycle.	68
Table 4.3:	Rates of Flow of Energy across the Binary Vapour Cycle.	69
Table 4.4:	Parameters Required for the Calculation of Hydrogen Production Rate.	71
Table 4.5:	Summary of the Calculated Results for the Cogeneration System.	71
Table 4.6:	The Selected Operating Parameters for the Absorption Chiller.	76
Table 4.7:	Rates of Flow of Energy across the Trigeneration System.	77
Table 4.8:	Summary of the Calculated Results for the Trigeneration System.	79
Table 4.9:	The New Operating Parameters for the Cogeneration System.	83
Table 4.10:	The New Energy Flow Rates across the Cogeneration System.	84
Table 4.11:	The LCA Results for the Proposed Cogeneration System.	89
Table 4.12:	The LCA Results for the Proposed Trigeneration System.	94

LIST OF FIGURES

Figure 2.1:	An Ideal Cogeneration Plant.	8
Figure 2.2:	A Cogeneration Plant with Adjustable Loads.	10
Figure 2.3:	Ammonia-Water Absorption Refrigeration Cycle.	13
Figure 2.4:	Gas-Turbine Trigeneration System.	15
Figure 2.5:	Amount of Fuels Required to Generate the Demanded Powers Separately.	17
Figure 2.6:	Amount of Fuels Required to Generate the Demanded Powers in Cogeneration and Trigeneration Plants.	18
Figure 2.7:	Summary of Solar Power Generation Methods.	20
Figure 2.8:	Schematic Diagram of a Parabolic Trough Collector.	22
Figure 2.9:	The Actual Linear Fresnel Reflector System.	23
Figure 2.10:	Schematic Diagram of a Solar Power Tower System.	24
Figure 2.11:	Schematic Diagram of a Parabolic Dish Reflector.	25
Figure 2.12:	Working Principle of Solar Photovoltaic (PV) Cell.	26
Figure 2.13:	The Small-Scale Solar Cogeneration System Proposed by Hong and Shi (2020).	28
Figure 2.14:	The Hybrid Photovoltaic-Thermal (PVT) System Proposed by Liang, et al. (2015).	30
Figure 2.15:	The Small-Scale Modular Trigeneration System Proposed by Wang (2014).	32
Figure 2.16:	Schematic Diagram of Alkaline Water Electrolysis.	35
Figure 2.17:	Schematic Diagram of Proton Exchange Membrane (PEM) Water Electrolysis.	36
Figure 2.18:	Schematic Diagram of Solid Oxide Electrolysis.	37
Figure 3.1:	The Flow Chart of Performing the Study.	40
Figure 3.2:	Schematic Diagram of the Proposed Solar Cogeneration System.	43

Figure 3.3:	Schematic Diagram of the Proposed Solar Trigeneration System.	45
Figure 3.4:	Direct Normal Irradiation (DNI) in Malaysia.	47
Figure 3.5:	Schematic Diagram of Energy Flows in the Solar Field.	47
Figure 3.6:	The Model of the Cogeneration System in Aspen HYSYS.	49
Figure 3.7:	The Model of the Trigeneration System in Aspen HYSYS.	54
Figure 3.8:	The Flow Model for the Proposed Multigeneration Systems.	58
Figure 3.9:	The Solar Cogeneration System Modelled in GaBi.	61
Figure 3.10:	The Solar Trigeneration System Modelled in GaBi.	62
Figure 3.11:	Work Breakdown Structure of the Project.	63
Figure 4.1:	Temperature versus Specific Entropy (*T*-*s*) Diagram for the Binary Vapour Cycle in the Cogeneration System.	70
Figure 4.2:	Effect of Lowering the Lower Pressure Limit of the Steam Cycle.	85

LIST OF SYMBOLS / ABBREVIATIONS

A	total area of heliostats, m^2
$\dot{m}$	mass flow rate, kg/s
$\dot{m}_{H_2}$	hydrogen production rate, kg/s
$\dot{Q}_{CR}$	rate of heat received by the central receiver, kW
$\dot{Q}_{gen}$	rate of heat received by the generator, kW
$\dot{Q}_{helios}$	rate of heat received by the heliostats, kW
$\dot{Q}_{H}$	rate of heat rejected to the warm environment, kW
$\dot{Q}_{L}$	rate of heat transferred from the cold space, kW
$\dot{Q}_{in}$	rate of heat supply, kW
$\dot{Q}_{out}$	rate of heat rejection, kW
$\dot{Q}_{p}$	rate of supply of process heat, kW
$\dot{W}_{elec}$	electric power, kW
$\dot{W}_{net}$	net power generated, kW
$\dot{W}_{in,\ pump}$	input power supplied to pump, kW
$\dot{W}_{out,\ PEM}$	output power of the PEM electrolyzer, kW
$\dot{W}_{out,\ turb}$	output power generated by turbine, kW
ϵ_u	utilization factor
η_{cogen}	efficiency of the cogeneration system
η_{CR}	efficiency of the central receiver
η_{HF}	efficiency of the heliostat field
η_{PEM}	efficiency of the PEM electrolyzer
η_{SG}	efficiency of the single-generation power plant
η_{trigen}	efficiency of the trigeneration system
CCHP	combined cooling, heating and power
CHP	combined heat and power
COP	coefficient of performance
CPC	compound parabolic concentrator
DAR	diffusion absorption refrigerator

DNI	direct normal irradiation
HRSG	heat recovery steam generator
LCA	life cycle assessment
LHV	lower heating value
ORC	organic Rankine cycle
PEM	proton exchange membrane
PV	photovoltaic
PVT	photovoltaic-thermal
SDG	Sustainable Development Goal
STU	solar thermal unit
PEU	power and end-users

LIST OF APPENDICES

Appendix A:	Gantt Charts	108
Appendix B:	List of Successful Simulations for the Cogeneration System	110
Appendix C:	Simulation Results and Calculation of Efficiency for the Single-Generation Power Plant	111
Appendix D:	List of Successful Simulations for the Absorption Chiller in the Trigeneration System	113
Appendix E:	Graphs of Life Cycle Assessment (LCA) for the Cogeneration System	114
Appendix F:	Graphs of Life Cycle Assessment (LCA) for the Trigeneration System	115

CHAPTER 1

INTRODUCTION

1.1 General Introduction

Renewable energy is the energy obtained from a source that is constantly replenished and will never run out. It is commonly known as clean energy due to its lower environmental impacts compared to fossil fuels (Friman, 2017). Some common forms of renewable energy include solar energy, hydropower, wind energy, and geothermal energy. In recent years, renewable energy sources are increasingly replacing fossil fuels in the power generation sectors due to their unlimited supply and lower overall environmental impacts. According to the International Renewable Energy Agency (2021), the worldwide renewable power generation capacity increased by 261 GW in 2020, with 127 GW of power capacity expansion contributed by solar energy.

Perhaps the most significant factor that boosted the expansion of solar power generation is the abundance and wide availability of solar energy. The most common application of solar energy is the generation of electricity through photovoltaic (PV) cells. Other than that, solar energy can also be converted to electricity by means of solar thermal power generation technologies. Unlike the PV cells that directly convert sunlight into electricity, a solar thermal power plant generates electricity via a heat engine. Specifically, the solar thermal power plant generates electricity in a similar fashion as the fossil fuel power plant, except that the combustion of fossil fuels is substituted by the thermal energy obtained from the sun (Poullikkas, 2009).

Moreover, in a conventional power plant, a lot of waste heat is produced from the power generation process. This waste heat is usually transferred to a cooling tower and discharged into the atmosphere in the form of water vapour. However, the heat released into the atmosphere represents a huge waste of energy. Instead of releasing this heat into the atmosphere, utilizing it for other purposes helps to minimize the amount of energy wasted and thus improve the efficiency of the power plant. The waste heat resulting from power generation can be recovered and supplied to other systems or processes to produce more outputs. When the otherwise-wasted heat energy is utilized to

produce more outputs, the power plant is said to operate in multigeneration mode.

Multigeneration systems produce multiple useful outputs from a single source of energy. Cogeneration systems that produce two outputs simultaneously are the first commercially available multigeneration systems. After the successful development of cogeneration systems, trigeneration systems that produce three useful products from a single energy source have been developed (Bamisile, et al., 2019). Some examples of useful outputs that can be produced by multigeneration systems are electric power, cooling and heating capacities, hydrogen gas etc. Conventional multigeneration systems usually rely on the burning of fossil fuels as the heat source for the power generation process. Lately, multigeneration systems powered by renewable energy have been researched and developed to reduce the dependency on non-renewable fossil fuels. Among various types of renewable energy, solar energy shows the most promising potential to replace fossil fuels as the alternative energy source for multigeneration systems. This is because solar energy is essentially inexhaustible, readily available, and non-polluting energy source (Gong, et al., 2019).

In this study, multigeneration systems, specifically cogeneration and trigeneration systems powered by solar energy were proposed. Both of these systems utilize solar energy to produce electric power and hydrogen gas concurrently while the trigeneration system is able to produce an additional output, which is cooling capacity. The performances and the life cycles of these systems were then assessed and compared.

1.2 Importance of the Study

In the world we live in today, more than 80% of the global energy demand is satisfied through the burning of fossil fuels (Mohr, et al., 2015). The U.S. Energy Information Administration (EIA) estimates that the global energy demand will be increased by 47% in the next 30 years due to the continuous growth of economics and the global population (Gordon and Weber, 2021). The increase in global energy demand will undoubtedly increase the demand for fossil fuels. However, it is well-known that fossil fuels are non-renewable energy sources that will be completely used up someday in the future.

Furthermore, fulfilling the energy demand through the combustion of fossil fuels causes some serious environmental issues as this process releases a lot of pollutants into the atmosphere. Hence, it is important to overcome the current status of heavy dependence on fossil fuels as well as to save the environment at the same time.

Adopting renewable energy as an alternative energy source is claimed to be the most effective way to overcome the issues brought by fossil fuels. This is because renewable energy is cleaner, greener, and sustainable (Sagir and Bahadir, 2017). Therefore, the proposal of solar-driven multigeneration systems that are capable of producing power and other useful outputs from solar energy is essential in resolving the issues of fossil fuels depletion and environmental pollution.

1.3 Problem Statement

Cogeneration and trigeneration systems are both classified under the category of multigeneration systems. As the name suggests, cogeneration systems produce two outputs whereas trigeneration systems produce three outputs from a single source of energy. In most literature, it is claimed that the trigeneration system can achieve much higher efficiency than the cogeneration system since it produces an extra output from the same amount of input energy. For instance, in the literature published by Hernández-Santoyo and Sánchez-Cifuentes (2003), it is claimed that a trigeneration system can potentially be 50% more efficient than a cogeneration system of similar size. However, there is no strong evidence or calculation to prove this statement. Therefore, a problem to be solved is to examine whether the efficiency of the trigeneration system can be so much higher than the cogeneration system.

In addition, multigeneration systems typically recover the waste heat produced from power generation and utilize it for other purposes. Generally, the waste heat recovered is supplied to other processes such as absorption cooling, hydrogen production, or desalination processes. Nevertheless, the waste heat resulting from power generation is classified as a low-grade heat source because of its limited temperature (generally 60 ℃ to 200 ℃). Moreover, solar energy itself is a low-grade heat source as the thermal energy collected from the sun may be limited sometimes (Yamamoto, et al., 2001). Hence, the questions to

address in this study are whether the solar-driven multigeneration systems can produce power from the low-grade solar thermal energy and whether the waste heat resulting from solar power generation is sufficient to activate another process.

1.4 Aim and Objectives

The aim of this project is to propose multigeneration power systems such as cogeneration and trigeneration systems that produce multiple useful outputs from renewable energy. The specific objectives of this project are as follows:

(i) To model multigeneration power systems that utilize solar energy as the input source and produce hydrogen gas as one of the outputs.

(ii) To evaluate the overall performances of the proposed multigeneration systems.

(iii) To assess the life cycles of the proposed multigeneration systems.

1.5 Scope and Limitation of the Study

In this study, the cogeneration and the trigeneration systems that are powered by solar energy have been proposed. To achieve the objective of evaluating the performances of the proposed systems, the cogeneration and the trigeneration systems were modelled and simulated in a process simulation software, Aspen HYSYS. However, there are certain limitations of using Aspen HYSYS to model the proposed systems. First of all, the solar field that is responsible for collecting and concentrating the solar radiation could not be modelled in the software. This is because the solar energy data and the solar collectors are not available in Aspen HYSYS. Hence, the solar field was excluded from the process simulations and the solar energy received by the power generation system could only be determined through calculations.

Apart from that, to fulfil the objective of designing multigeneration systems that produce hydrogen gas as one of the outputs, a proton exchange membrane (PEM) electrolyzer is added to the proposed systems to allow hydrogen gas to be produced through the water electrolysis process. However, there is no way to simulate the water electrolysis process in Aspen HYSYS as

the PEM electrolyzer is also not available in the component list of the software. Hence, the amount of hydrogen gas produced by the systems was determined through theoretical calculations.

On the other hand, it was of interest to perform the life cycle assessment (LCA) for the proposed multigeneration systems. The ultimate goal of LCA is to assess the environmental impacts of the multigeneration systems, starting from raw material extraction, production and manufacturing of components needed by the systems, installation of the systems, and operation of the systems. However, performing the LCA for these processes will be extremely complicated as the proposed multigeneration systems are the large power plants that consist of several subsystems such as solar field, power generation unit, PEM electrolyzer etc. Thus, the LCA did in this study only assessed the environmental impacts associated with the operation of the multigeneration systems (i.e. the emissions due to the power generation and hydrogen production processes in the proposed systems).

1.6 Contribution of the Study

Today, sustainable energy production has become a hot topic due to the increased awareness of the energy crisis. The Sustainable Development Goal 7 (SDG 7) established by the United Nations aims to ensure access to affordable, reliable, sustainable, and modern energy for all by 2030. One of the most effective methods to achieve this goal is to adopt renewable energy sources to replace fossil fuels in power generation industries because renewable energy is free, sustainable, and environmentally friendly. Hence, the proposal of solar-driven multigeneration systems can be viewed as an effort that contributes to the achievement of SDG 7.

1.7 Outline of the Report

The report contains five chapters in total. The first chapter of the report is the introduction, in which the background of the project is introduced. Chapter 2 of the report is the literature review. In this chapter, the findings of the literature review are summarized. The contents of this chapter include the definitions and some practical examples of cogeneration and trigeneration systems, various solar power generation technologies, some solar-driven cogeneration and

trigeneration systems proposed by other researchers, as well as the common methods of producing hydrogen gas.

Chapter 3 of the report covers the methodology and the work plan of the project. The proposed cogeneration and trigeneration systems are well described in this chapter. Furthermore, the methods of performing the process simulations and life cycle assessment (LCA) for the proposed systems are also explained in this chapter. In addition, the project management tools used in this project are also included at the end of Chapter 3.

Chapter 4 presents the results and discussion of the research. In this chapter, the simulation and the LCA results are presented along with some compressive discussions. The last chapter is Chapter 5, which is the conclusion and recommendations for future work.

CHAPTER 2

LITERATURE REVIEW

2.1 Introduction

In this chapter, the definitions of cogeneration and trigeneration are explained in detail. The explanations are supported by some practical examples of cogeneration and trigeneration systems. After that, the state-of-the-art of solar power generation technologies are presented. In addition, some solar-driven cogeneration and trigeneration systems proposed by other researchers have been reviewed and discussed. Finally, to achieve the objective of proposing multigeneration systems with hydrogen gas as one of the outputs, the various hydrogen production processes are studied.

2.2 Cogeneration

Cogeneration is the simultaneous production of two useful forms of energy from a single source of energy. In general, electrical (or mechanical) energy and thermal energy are the common outputs generated by the cogeneration systems. Cogeneration systems often capture the heat resulting from power generation and put it to some productive use such as water or space heating, industrial process heating, or as a heat source to drive other systems or devices (Kanoglu and Dincer, 2009). Since cogeneration systems allow electric power and useful heat to be generated at the same time, they are commonly known as combined heat and power (CHP) systems (Onovwiona and Ugursal, 2006).

2.2.1 Ideal Cogeneration Plant

A cogeneration plant can use either a Rankine (vapour power) cycle or a Brayton (gas power) cycle as the power cycle. Figure 2.1 shows an ideal cogeneration plant that is running on the steam Rankine cycle. At state 1, water exists as a saturated liquid and is pumped to the boiler (state 2). In the boiler, the supply of heat energy ($\dot{Q}_{in}$) vaporizes the water into superheated steam (state 2 to 3). After that, the superheated steam is expanded in the turbine to generate an output power of $\dot{W}_{out,\,turb}$ (state 3 to 4). The output power generated by the turbine is

delivered to an electric generator to produce electric power. After expanding in the turbine, the steam leaves the turbine at relatively low pressure and temperature. The low-pressure steam enters the process heater and the heat energy ($\dot{Q}_p$) is extracted to be used in other heating processes (state 4 to 1). Following the loss of heat in the process heater, the steam condenses to form saturated liquid. Finally, the liquid working fluid will be pumped to the boiler (state 1 to 2) and the process repeats. In general, the amount of work required to pump the liquid working fluid is small and negligible.

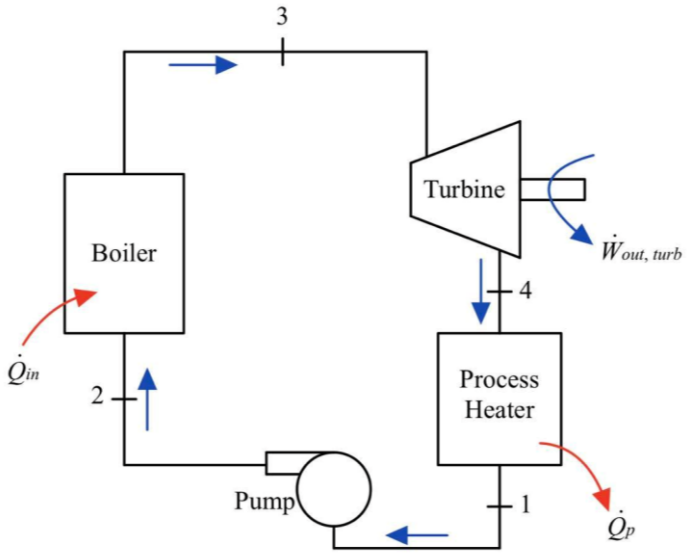

Figure 2.1: An Ideal Cogeneration Plant (Cengel and Boles, 2015).

It can be noticed that the ideal cogeneration plant illustrated in Figure 2.1 is similar to the conventional steam power plant (consists of a pump, a boiler, a turbine, and a condenser), except that the condenser has been replaced by a process heater. With the process heater, the heat energy carried by the exhaust steam is recovered and supplied to the industrial processes that require process heat. Some examples of the industrial processes that require an extensive amount of process heat are steel making, oil production and refining, food processing etc. (Cengel and Boles, 2015). However, the major limitation of this cogeneration plant is the amount of energy that will be used for power generation and process heating cannot be adjusted. This is because all the steam leaving the boiler is expanded in the turbine to generate power first. After producing power, only then the steam enters the process heater to supply process

heat to other processes. The process heat produced in this manner is limited as most of the energy carried by the steam is used for power generation. When the demand for process heat is high, the process heat supplied by the cogeneration plant may be inadequate.

2.2.2 Cogeneration Plant with Adjustable Loads

The limitation of the ideal cogeneration plant described in Section 2.2.1 is remedied by introducing the cogeneration plant with adjustable loads, as shown in Figure 2.2. In this cogeneration plant, the amount of steam that passes through the turbine and the process heater can be adjusted according to the demands for electric power and process heat. Nevertheless, it is noticeable that this cogeneration plant is more complex than the ideal cogeneration plant. Hence, it will be more costly to build such a cogeneration plant.

Similar to the ideal cogeneration plant, the working fluid, which is water, is heated and vaporized into superheated steam in the boiler. In this cogeneration plant, the superheated steam produced in the boiler can be routed to either the turbine or the process heater, depending on the demands for power and process heat. When the demand for process heat is zero, all the superheated steam produced in the boiler will be directed to the turbine to generate a maximum amount of power. After the steam is expanded in the turbine, it leaves the turbine and enters the condenser, where it undergoes a constant pressure cooling process to condense into water. The heat released by the steam during the cooling process represents the waste heat produced by the cogeneration plant. In such a case, since there is no steam passes through the process heater, the cogeneration plant produces zero process heat and operates like an ordinary steam power plant.

When there is a little demand for process heat, a portion of steam will be drawn from the turbine at an intermediate pressure (P_6) and routed to the process heater. If this is not adequate, all the steam that leaves the turbine will be directed to the process heater. Under this condition, no steam passes through the condenser and thus no waste heat is produced from this plant. When the demand for process heat is higher, some of the superheated steam leaving the boiler will be throttled by an expansion valve to the operating pressure of the process heater (P_5). It is also possible to adjust the system such that all the

superheated steam produced in the boiler is throttled to the process heater to generate the highest possible amount of process heat. When the cogeneration plant is operating in this mode, no power will be generated as there is no expansion of steam in the turbine.

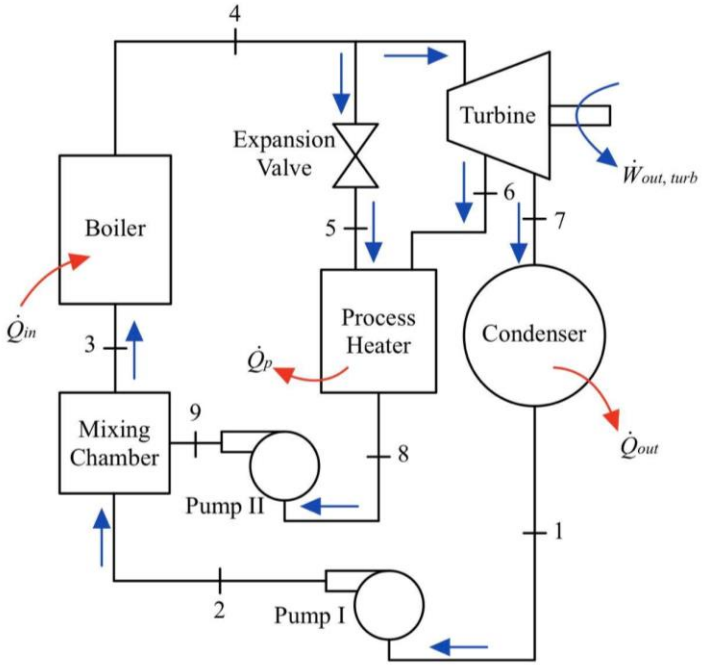

Figure 2.2: A Cogeneration Plant with Adjustable Loads (Cengel and Boles, 2015).

The performance of the cogeneration plant with adjustable loads can be assessed by defining a utilization factor (ϵ_u), which can be evaluated by using the following equation.

$$\epsilon_u = \frac{\dot{W}_{net} + \dot{Q}_p}{\dot{Q}_{in}} \tag{2.1}$$

where

ϵ_u = utilization factor

$\dot{W}_{net}$ = net power generated, kW

$\dot{Q}_p$ = rate of supply of process heat, kW

$\dot{Q}_{in}$ = rate of heat input, kW

Since the cogeneration plants can generate power and process heat at the same time, it is claimed that the utilization factors of the cogeneration plants can be as high as 80%. In recent years, the newly developed cogeneration plants can achieve even higher utilization factors (Cengel and Boles, 2015). This is due to the advanced technology such as the upgraded steam turbines as well as the advanced steam piping systems that help to reduce the leakage of steam and the undesirable heat loss when the working fluid travels from one component to another. As a result, the energy loss is minimized and thus a higher output power can be generated from the same amount of input power.

2.3 Trigeneration

Trigeneration refers to the simultaneous production of three useful outputs from the same energy source. In general, electric power, useful heat energy, and cooling capacity are the three outputs often generated by the trigeneration systems. Due to this reason, trigeneration systems are also known as combined cooling, heating and power (CCHP) systems. Trigeneration is an extension of cogeneration, in which the waste heat produced from the cogeneration system is used to drive a thermally activated cooling system to produce additional cooling output (Deng, et al., 2011). One of the thermally activated cooling technologies that has been widely used in trigeneration systems is the absorption chiller. Thus, a trigeneration system is often described as a cogeneration system integrated with an absorption chiller (Hernández-Santoyo and Sánchez-Cifuentes, 2003).

2.3.1 Overview of Absorption Chillers

Absorption chillers are an alternative to vapour-compression chillers when a continuous heat source is available. Absorption chillers often utilize the waste heat collected from other industrial processes to provide the energy necessary to drive a cooling process. This characteristic makes them suitable to be used as the refrigeration systems to output cooling capacity in the trigeneration plants.

Absorption chillers are classified based on the types of working fluids used. One of the most commonly used absorption chillers is the ammonia-water system, which has been illustrated in Figure 2.3. In the ammonia-water absorption chiller, ammonia (NH_3) is the refrigerant whereas water (H_2O) serves

as the absorbent. In the evaporator, ammonia absorbs heat ($\dot{Q}_L$) from the cold refrigerated space and turns into ammonia vapour. The transfer of heat from the cold refrigerated space to the refrigerant (ammonia) represents the cooling effect produced by the absorption chiller.

After receiving heat from the cold refrigerated space, the ammonia leaves the evaporator in the form of saturated vapour and enters the absorber, where the absorption process takes place. In the absorber, the ammonia vapour is absorbed by the liquid absorbent, which is water. As a result, an ammonia-water mixture solution (NH_3 H_2O) is formed. The absorption of ammonia vapour into water is an exothermic (heat releasing) reaction, which increases the temperature within the absorber. The high temperature in the absorber reduces the amount of ammonia vapour that can be absorbed into the water. Thus, it is necessary to have a stream of cooling water circulating through the absorber to lower its temperature so as to enhance the absorption process. After the absorption process, the ammonia-water solution is pumped to the generator.

In the generator of the absorption chiller, the heat collected from other industrial processes or heat sources is supplied to the ammonia-water solution. Consequently, a portion of the mixture solution vaporizes into vapour form. Since water is a highly volatile liquid, it usually vaporizes with ammonia when the ammonia-water solution receives heat energy from the heat source. As a result, the ammonia vapour (the refrigerant) that leaves the generator usually contains an appreciable amount of water vapour. The presence of water vapour in the refrigerant tends to decrease the cooling capacity of the absorption chiller. In order to maintain the performance of the absorption chiller at the optimum level, it is necessary to include a rectifier in between the generator and the condenser to remove the water vapour from the refrigerant. The rectifier serves as a pre-condenser in the system that cools the vapours leaving the generator. Since the water vapour has a higher saturation temperature than the ammonia vapour, it will condense into water when it is cooled in the rectifier. In this way, the water is separated from the ammonia vapour and is returned to the generator.

The solution in the generator, which is hot and weak in ammonia, is then passed to the regenerator. In the regenerator, the hot and weak solution transfers some heat to the ammonia-water solution leaving the pump. Finally, the weak solution is throttled to the absorber. On the other hand, the ammonia

vapour, which is the refrigerant of the absorption cycle, enters the condenser after leaving the rectifier. In the condenser, the ammonia vapour rejects heat ($\dot{Q}_H$) to the warm environment and condenses to form liquid ammonia. The liquid ammonia is then throttled by the expansion valve to the evaporator pressure. Finally, the ammonia enters the evaporator to absorb heat ($\dot{Q}_L$) from the cold refrigerated space again (Cengel and Boles, 2015; Dossat and Horan, 2002).

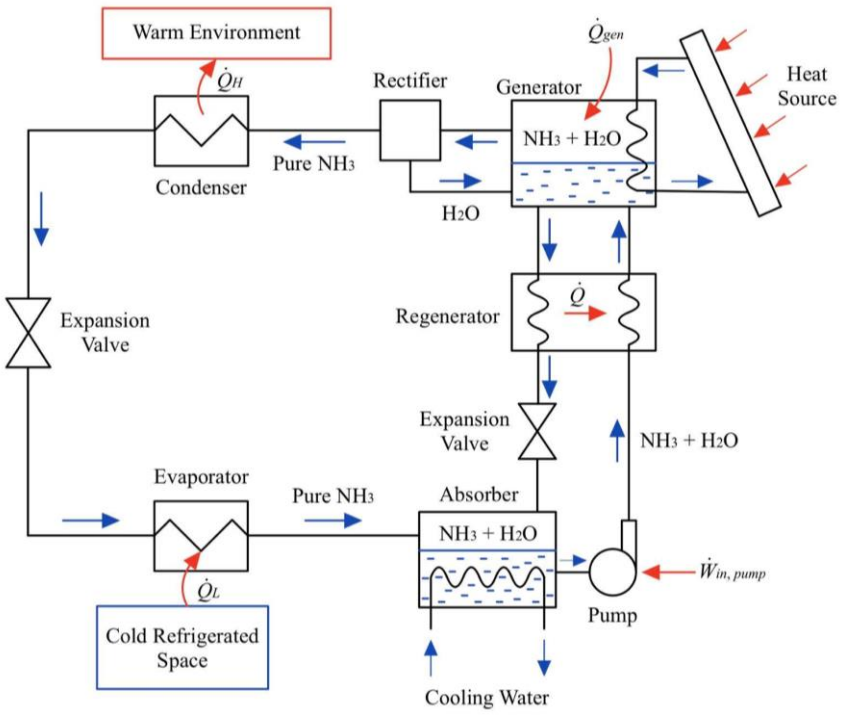

Figure 2.3: Ammonia-Water Absorption Refrigeration Cycle (Cengel and Boles, 2015).

Another commonly used absorption chiller is the water-lithium bromide system, where water (H_2O) serves as the refrigerant and lithium bromide (LiBr) serves as the absorbent. The working principle of the water-lithium bromide systems is basically the same as the ammonia-water systems. Hence, the major components that present in the water-lithium bromide systems are also similar to the ammonia-water systems, with the exception that the rectifiers are removed from the systems. Unlike water, lithium bromide is a non-volatile absorbent. It does not evaporate with water when heat is supplied to the water-lithium bromide solution in the generator. Therefore, the need of a

rectifier in the refrigeration cycle can be eliminated as the water vapour (the refrigerant) can be completely separated from the lithium bromide (the absorbent) in the generator. However, water-lithium bromide systems are limited to the applications where the evaporator is to be maintained at a temperature higher than 0 ℃ (Srikhirin, et al., 2001). Generally, they are widely used in building cooling applications where the evaporator temperatures are ranging from 5 ℃ to 10 ℃. On the other hand, ammonia-water systems are usually used in the commercial and industrial chiller systems where the refrigerants are to evaporate at the temperatures lower than 0 ℃ (Deng, et al., 2011; Dossat and Horan, 2002).

2.3.2 Trigeneration System

Zeng, et al. (2011) proposed a trigeneration system that is driven by a Brayton cycle (gas power cycle) as depicted in Figure 2.4. The working fluid used in the Brayton cycle is the ambient fresh air. In the Brayton cycle, fresh air at atmospheric pressure is sucked into the compressor to undergo a compression process. As a consequence, the temperature and pressure of the air increase. The high-pressure air then enters the combustor, where it is heated at constant pressure to a temperature ranging from 1 000 ℃ to 1 350 ℃ (Kribus, et al., 1998). In this trigeneration system, heat energy is supplied through the combustion of fossil fuels. After being heated, the hot gases are expanded to the atmospheric pressure in the gas turbine. The expansion of gases in the gas turbine causes the turbine blades to rotate, thus generating mechanical power. The mechanical power can further be converted into electrical power via a generator (Brouche and Lahoud, 2018).

In a gas power cycle, the temperature of the gas leaving the gas turbine usually exceeds 500 ℃ (Cengel and Boles, 2015). The high-temperature exhaust gas will then enter a heat recovery steam generator (HRSG), which is an equipment used to recover the heat energy contained in the hot exhaust gas. At the same time, water is being pumped to the HRSG to allow the transfer of heat from the hot exhaust gas to the water. As a result, the water vaporizes and leaves the HRSG as hot steam (Norouzi, et al., 2019). In this trigeneration system, a portion of the hot steam is used to drive a water-lithium bromide absorption chiller to output cooling capacity (discussed in Section 2.3.1). On the

other hand, the remaining hot steam serves as a heat source to supply heat energy to other heat-driven processes.

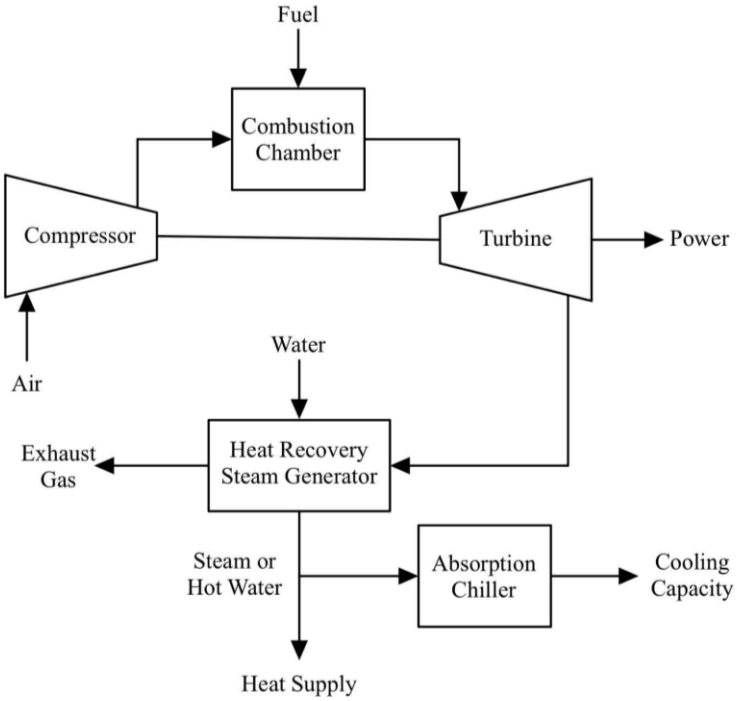

Figure 2.4: Gas-Turbine Trigeneration System (Zeng, et al., 2011).

To summarize, this trigeneration system is able to produce three useful outputs at the same time, which are power (either in mechanical or electrical form), cooling capacity, as well as useful heat energy. With the aid of HRSG, the otherwise-wasted heat energy is utilized to produce steam that can be used to drive an absorption chiller and other processes that require heat energy.

2.4 Advantages of Cogeneration and Trigeneration

Multigeneration systems, such as cogeneration and trigeneration systems, are recognized as an important and effective way to save energy as well as the environment. Today, cogeneration and trigeneration technologies are rapidly growing due to their numerous advantages of being able to produce multiple outputs simultaneously. Perhaps the most striking advantage of multigeneration systems is the increase in overall efficiency. This is due to the fact that multigeneration systems utilize the otherwise-wasted heat energy to produce other useful commodities. For a power plant that generates electricity through

the combustion of fossil fuels, higher efficiency also means that the fuel utilization factor is higher. Thus, in multigeneration power plants, lesser fossil fuels are required to produce the given amount of electricity, thermal energy, and/or cooling capacity compared to the traditional method of generating these outputs separately.

Wu and Wang (2006) performed a theoretical calculation that distinguishes the primary energy utilization between conventional energy supply mode and multigeneration mode. The results of the calculation are summarized in Figure 2.5 and 2.6. The calculation was made with the assumption that 15 units of heating power and 33 units of electrical power are demanded. To meet the electrical demand, a typical power plant with an efficiency of 33% needs 100 units of fuel input. Besides that, a boiler that is operating at 85% of efficiency needs 18 units of fuel to generate the desired heating power. The overall efficiency of producing the demanded electrical and heating powers separately is about 40.7%, with a total of 118 units of fuel required. In contrast, when the power plant is running in cogeneration (combined heat and power) mode, the demand for heating power is fulfilled by recovering the waste heat exhausted from electrical power generation without burning any additional fuel. When 100 units of fuel is supplied to the cogeneration plant, only 33 units of the fuel energy is consumed to generate 33 units of electric power and the remaining 67 units of energy is lost as waste heat. The demand for 15 units of heating power can therefore be fulfilled by recovering 18 units of waste heat exhausted from electrical power generation. Hence, the amount of fuels required to satisfy the power demands reduces from 118 units to 100 units and the overall efficiency of generating the demanded powers raises from 40.7% to 48%.

During hot summer days, there might be an additional demand for cooling power. In the case that 40 units of cooling power are demanded, an electrical air conditioner with a coefficient of performance (COP) of 4 is to be driven by 10 units of electrical power, which in turn requires 30 units of fuel input. Therefore, to produce the demanded electrical, heating, and cooling powers separately, 148 units of fuel are required. The overall efficiency of producing the demanded powers separately is approximately 59.5%. On the other hand, in the trigeneration plant, the waste heat resulting from electrical

power generation is utilized to produce the heating and cooling powers. In addition, the waste heat in the form of exhaust gas makes it feasible to use an absorption chiller instead of the electrical air conditioner to output cooling power. Therefore, the demands for heating and cooling powers are met without supplying additional input energy to the boiler and the absorption chiller. In other words, the trigeneration plant only needs 100 units of fuel to generate the desired electrical, heating, and cooling powers. The reduction in the fuel input brings a significant increase to the overall efficiency of the trigeneration plant, i.e. the overall efficiency increases from 59.5% (separate generation mode) to 81% (trigeneration mode).

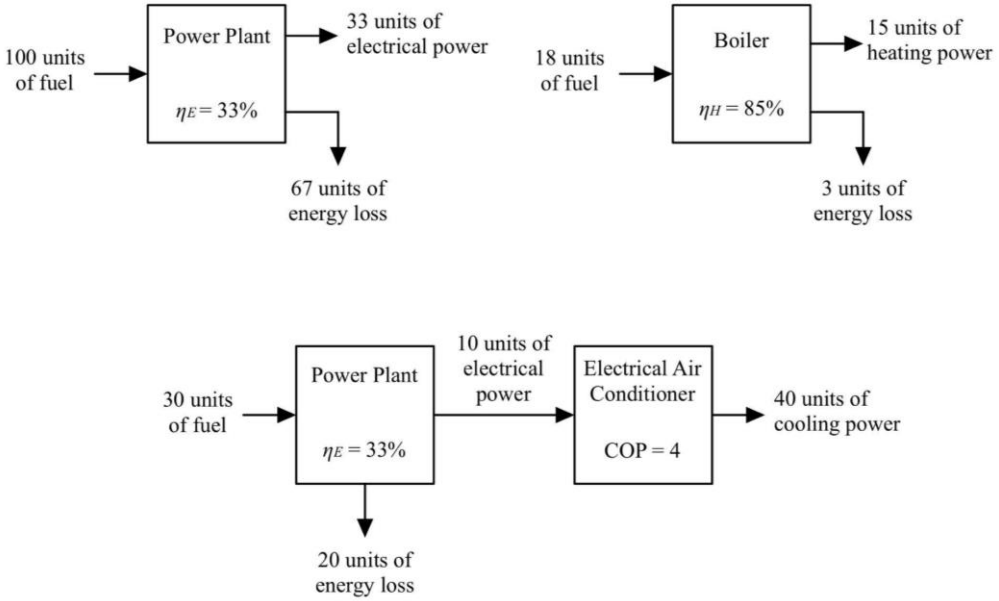

Figure 2.5: Amount of Fuels Required to Generate the Demanded Powers Separately.

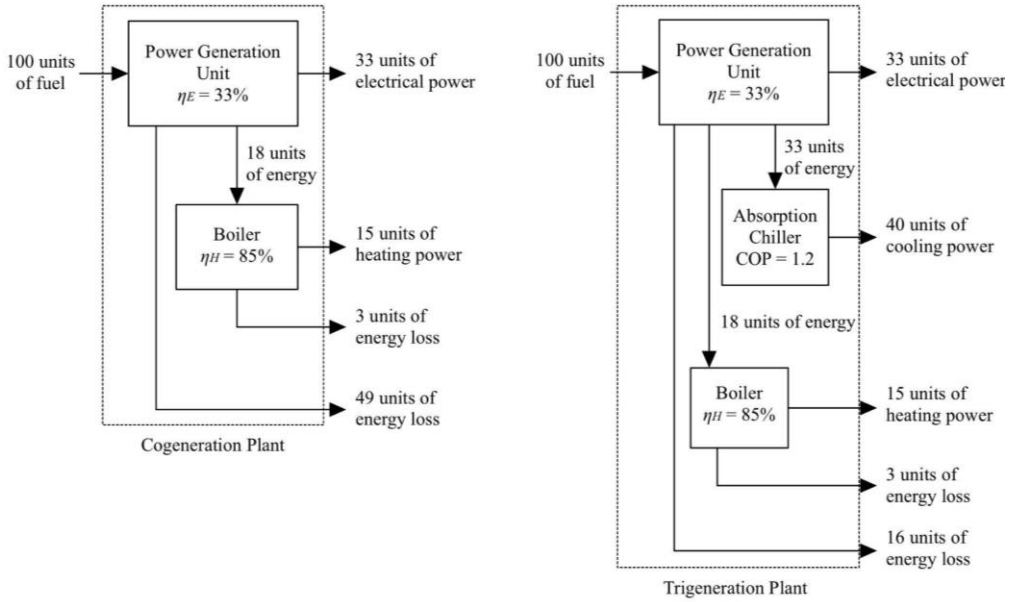

Figure 2.6: Amount of Fuels Required to Generate the Demanded Powers in Cogeneration and Trigeneration Plants.

Another advantage of multigeneration power plants is the reduction of greenhouse gas emissions. As described previously, cogeneration and trigeneration plants require lesser fuel to produce the demanded outputs compared to generating the outputs separately. The reduction in fuel input not only can save the cost of purchasing the fuel, but also reduce the amount of greenhouse gases released into the atmosphere. According to a study conducted by Elsarrag and Alhorr (2013), a typical trigeneration plant consisting of a power generation unit, a heating system, and an absorption chiller can reduce up to 25.1% of carbon dioxide released into the atmosphere in a year. However, the reduction in the emission of carbon dioxide contributed by the absorption chiller does not exceed 1.2%. This is due to the operation of an absorption chiller consumes parasitic power as well as its low coefficient of performance (COP) compared to the vapour-compression chiller. Therefore, a cogeneration plant that consists of a power generation unit and a heating system can also achieve up to 24% of annual carbon dioxide reduction.

Last but not least, multigeneration power plants can also be deployed as decentralized energy generation systems, which are generally more reliable than centralized energy generation systems. In the context of power generation systems, reliability is defined as the capability of an energy system to ensure the

energy is supplied consistently at a reasonable price (Alanne and Saari, 2006). Unlike the centralized power plants where electricity is generated at a large scale and distributed over a long distance, decentralized power stations usually have smaller capacities (ranging from 1 kW to 250 MW) and are located in close proximity to the electricity consumers (Liu, et al., 2017). Centralized power plants are claimed to be less reliable because they are vulnerable to natural disasters and unexpected phenomena such as climate change, terrorism, changes in customer needs and electricity markets etc. The multigeneration power systems that adopt decentralized energy generation technology are able to prevent these threats from happening. In the case that these undesired events occur, decentralized multigeneration power plants allow fast recovery actions to be taken as they are smaller and more flexible compared to the centralized power plants. In addition, decentralized multigeneration power plants will not face the issue of electricity blackouts due to their independence in electricity distribution (Liu, et al., 2014; Wu and Wang, 2006).

2.5 Power Generation from Solar Energy

The Sun provides 174 PW (1 PW = 10^{15} W) of radiation energy to the upper atmosphere of the Earth. After being reflected and absorbed by the atmosphere and the clouds, approximately 89 PW of solar radiation reaches the surface of the Earth (Tian and Zhao, 2013). The enormous amount of solar energy on the Earth makes it one of the most promising and attractive renewable energy sources to generate electricity. Reddy, et al. (2013) summarized the state-of-the-art of solar power generation methods as illustrated in Figure 2.7. In general, electricity can be generated from solar energy in two ways, either through solar thermal or solar photovoltaic (PV) technologies.

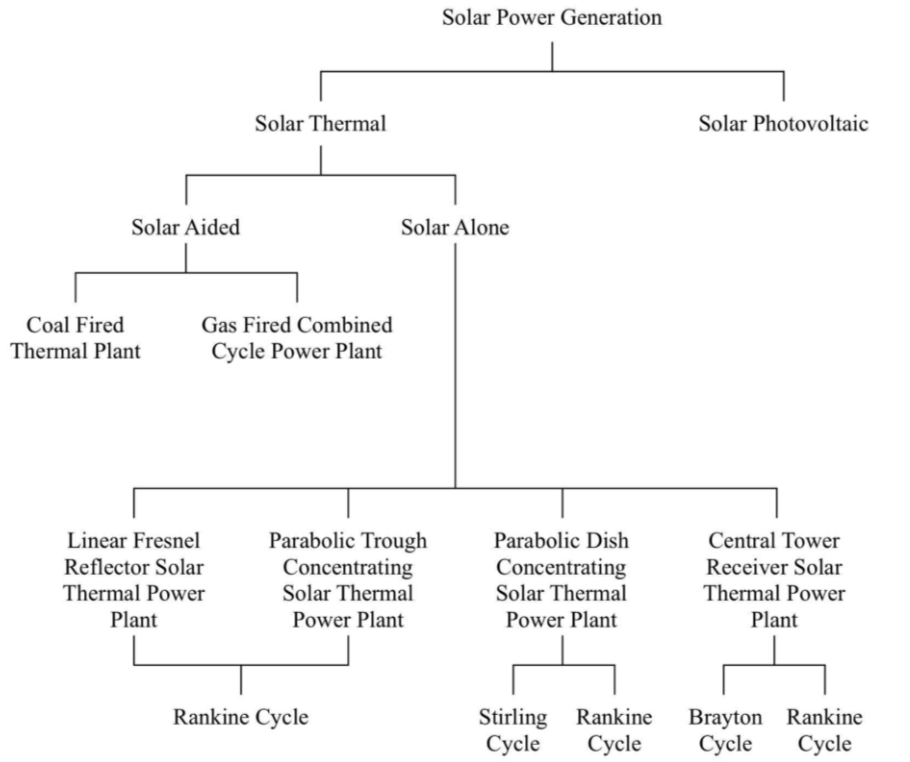

Figure 2.7: Summary of Solar Power Generation Methods (Reddy, et al., 2013).

2.5.1 Solar Thermal Power Generation

Solar thermal power, which is also known as concentrated solar power, involves the use of mirrors to reflect and focus sunlight onto a receiver to produce the heat needed to generate electricity (Garc á, et al., 2011). A heat transfer fluid is circulating through the receiver to absorb the heat energy collected from sunlight. The heat energy is then transferred to the working fluid of the power generating cycle (i.e. water for Rankine cycle or gas for Brayton cycle) through a heat exchanger. The heated working fluid will then expand in a turbine to produce mechanical power. The mechanical power generated can be converted into electricity via a generator. In short, solar thermal power plants generate electricity in a similar fashion as the fossil fuel power plants, except that the thermal energy is obtained from the sun instead of the combustion of fossil fuels (Wagner and Rubin, 2014).

Although solar thermal power plants generate electricity in a cleaner way, they need a relatively high initial investment compared to the fossil fuel power plants. Furthermore, solar thermal power plants are characterized by low thermal efficiency as the thermal energy collected from the sun may be limited

sometimes. To utilize solar energy to generate electricity while compensating the shortcomings of solar thermal power plants, solar thermal collectors are often integrated into the traditional fossil fuel power plants. Such a power plant is called a solar aided power plant. In a solar aided power plant, part of the electricity is generated from solar energy while the remaining electricity is generated through the combustion of fossil fuels. Since lesser fossil fuels are being burned, the emission of greenhouse gases can be reduced significantly. Moreover, solar aided power plants have higher thermal efficiencies than the standalone solar thermal power plants. Therefore, solar aided power generation is proven to be an effective and efficient way of utilizing solar energy to generate electricity (Qin, et al., 2020).

Solar thermal power plants are classified based on the types of solar collectors used. At the present stage, there are four main types of solar thermal collectors, namely parabolic trough collectors, linear Fresnel reflectors, solar power towers, and parabolic dishes. Two of them, which are parabolic trough collectors and linear Fresnel reflectors, work by concentrating the solar radiation onto a line. On the other hand, solar power towers and parabolic dishes reflect and concentrate the incident sunlight onto a point (Garc á, et al., 2011).

2.5.1.1 Parabolic Trough Collectors

Parabolic trough technology is one of the most advanced and mature solar technologies that has been widely used in solar thermal power generation or process heat applications. As the name suggests, a parabolic trough collector is a type of solar thermal collector that is curved into a parabolic shape to concentrate the incident sunlight onto its focal line. To make use of solar energy to generate electricity, a receiver tube covered with a glass envelope is located along the focal line of the parabolic reflector. The purpose of covering the receiver tube with the glass envelope is to minimize the convective heat loss while the heat transfer fluid flows through the tube. When the incident solar rays strike on the parabolic reflector, they will be reflected and focused onto the receiver tube placed on the focal line of the parabolic reflector. As a result, the heat transfer fluid gains energy and heats up. The solar thermal energy absorbed by the heat transfer fluid will then be transferred to the working fluid of the power generation cycle with the purpose of generating electricity.

A typical parabolic trough system has a concentration ratio ranging from 30 to 100 (Kodama, 2003). This means that the energy density concentrated onto the receiver tube can be 30 to 100 times higher than the density of the incident solar energy. Therefore, the heat transfer fluid that flows through the receiver tube can be heated up to 400 ℃. Today, the parabolic trough collectors can be supported with a single-axis tracking system, which allows them to track the sun as the sun moves from east to west throughout the day (Kalogirou, 2004). With the single-axis tracking system, the parabolic trough collectors can always receive the maximum solar energy whenever the sun is available.

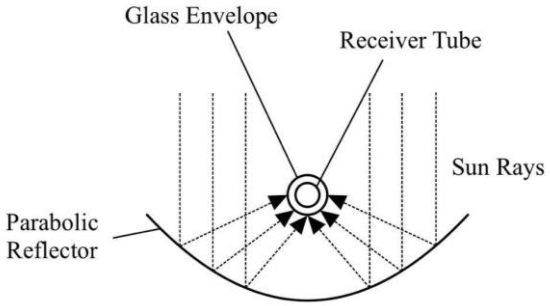

Figure 2.8: Schematic Diagram of a Parabolic Trough Collector.

2.5.1.2 Linear Fresnel Reflectors

A linear Fresnel reflector is a type of line-focus solar collector that is similar to the parabolic trough collector. However, the solar reflector does not have to be in parabolic shape (i.e. it can be a flat or slightly curved mirror) (Kalogirou, 2004). In a linear Fresnel reflector system, a series of mirrors is rotating on a single axis to reflect sunlight onto a receiver, which is usually located at several meters above the ground. Unlike the parabolic trough systems where the receivers are rotating with the parabolic reflectors to track the sun, the receivers in the linear Fresnel reflector systems are fixed in position. The concentration ratios of the linear Fresnel reflectors are lower, which are typically in the range of 10 to 50 (Bellos, 2019). Due to the lower concentration ratios, the temperatures of the fluids that flow through the receiver tubes are also lower, which are generally ranging from 80 ℃ to 250 ℃. Despite not being as efficient as the parabolic trough systems, linear Fresnel reflector systems have the

advantage of being cost-effective as the flat or slightly curved mirrors are cheaper than parabolic reflectors (Liu, et al., 2019).

Figure 2.9: The Actual Linear Fresnel Reflector System (Beltagy, et al., 2017 with License Number: 5286060084907).

2.5.1.3 Solar Power Towers

A solar power tower system employs a large number of mirrors (known as heliostats) to reflect and concentrate the solar radiation onto a central receiver located at the top of a tall tower (Xu, et al., 2011). At the present stage, the typical solar power tower systems can have several hundred or even thousand heliostats, with each heliostat having a reflective surface ranging from 50 m^2 to 150 m^2. Due to the large field of heliostats, solar power tower systems can achieve relatively high concentration ratios, typically ranging from 300 to 1 500. In other words, the energy flux at the central receivers can be higher than the normal solar irradiation by a factor of 300 to 1 500. To utilize this huge amount of energy to generate electricity, heat transfer fluids will be pumped to the central receivers to absorb the concentrated solar thermal energy. The high energy flux in the central receivers allows the heat transfer fluids to be heated to a temperature as high as 1 500 ℃. After that, the heat transfer fluids will transfer the received energy to the working fluids of the power generation cycles. Finally, the high-temperature working fluids run through the power cycles to generate power. In general, the power capacities of solar power tower systems

are higher than 10 MW, which are considerably large compared to the other types of solar thermal power plants (Kalogirou, 2004).

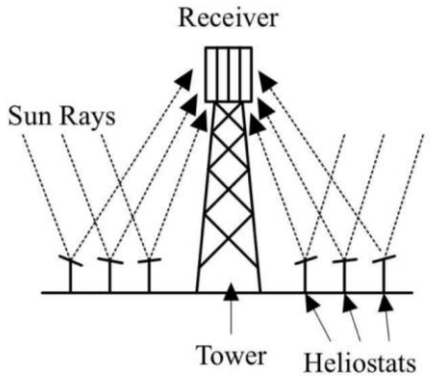

Figure 2.10: Schematic Diagram of a Solar Power Tower System (Kalogirou, 2004).

2.5.1.4 Parabolic Dishes

A parabolic dish is composed of many small mirrors that are arranged to form a large parabolic-shaped reflector. In parabolic dish systems, the large parabolic dish reflectors reflect and focus the incident solar radiation onto the thermal receivers, which are located at the focal points of the parabolic dishes. Unlike the other solar thermal power generation technologies that use concentrated solar energy to drive the steam power cycles (Rankine cycles), parabolic dish systems use a Stirling engine to generate power. In layman's terms, a Stirling engine is a type of heat engine that transforms thermal energy to mechanical energy. In the thermal receivers, the working fluids (typically helium or hydrogen) are heated by concentrated solar energy. The heated working fluids will then expand in a turbine to produce mechanical power. The mechanical power will be converted to electric power via a generator (Hafez, et al., 2017).

Parabolic dishes are usually come with a two-axes tracking system to enable them to track the sun from time to time. Due to this reason, they are highly efficient in converting solar energy to electrical energy. The concentration ratios of parabolic dishes are high, which are generally in the range of 600 to 2 000. Besides, the operating temperature of the parabolic dish systems can be as high as 1 500 ℃ (Kalogirou, 2004).

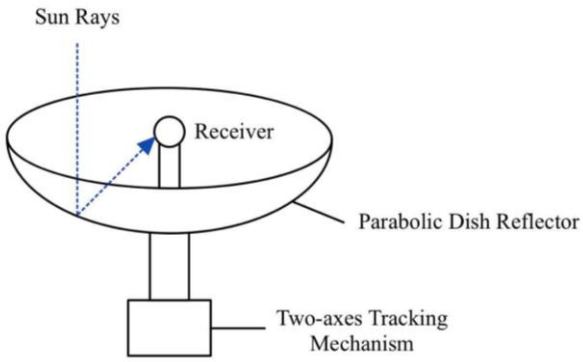

Figure 2.11: Schematic Diagram of a Parabolic Dish Reflector (Kalogirou, 2004).

2.5.2 Solar Photovoltaic (PV)

Another method of generating electricity from solar energy is through solar photovoltaic (PV) system. Unlike the solar thermal power generation technologies discussed in Section 2.5.1, a solar PV cell converts sunlight into electricity without the use of a heat engine. Hence, solar PV systems are relatively simple in design compared to concentrated solar power systems (Parida, et al., 2011).

A solar PV panel is made up of a large number of solar cells that contain semiconducting material (usually silicon). The semiconductor in each solar cell is doped with two different types of impurities to create a layer of N-type (negatively charged) semiconductor and a layer of P-type (positively charged) semiconductor. The N-type semiconductor contains extra electrons whereas the P-type semiconductor has extra holes (the spaces for electrons). The interface where the two layers of semiconductors meet is known as the P-N junction.

When the photons in the sunlight hit the solar cells, some electrons gain enough energy and leave the bonds, creating electron-hole pairs. Due to the electric field created by the P-N junction, the electrons tend to move to the negative electrode while the holes will be drawn to the positive electrode. The negative electrode, the positive electrode, and the external load are connected via a connecting wire to form a series circuit. Therefore, the free-moving electrons will leave the negative electrode, pass through the external load and finally reach the positive electrode (Khan, et al., 2013). The flowing of electrons

from one electrode to another creates a direct current. In this way, electricity is generated from the sunlight directly. The working principle of the solar PV cell is demonstrated in Figure 2.12.

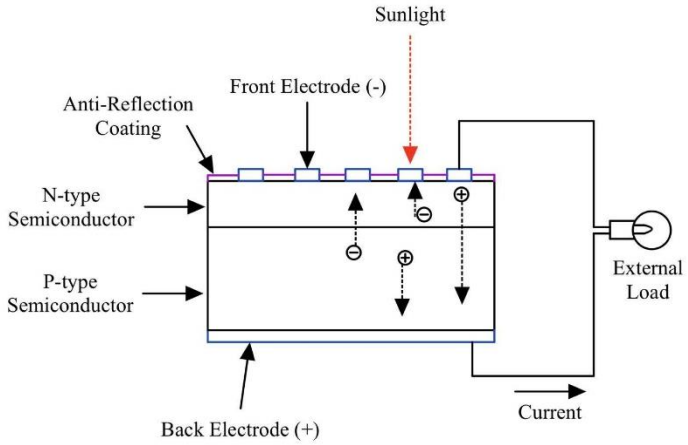

Figure 2.12: Working Principle of Solar Photovoltaic (PV) Cell.

2.6 Solar-Driven Cogeneration System

As of the current status, most of the cogeneration systems rely on the combustion of fossil fuels to obtain the energy required to generate outputs. The burning of fossil fuels can be replaced by solar thermal energy by integrating solar concentrating technologies into the cogeneration systems. Hong and Shi (2020) proposed a small-scale solar-driven cogeneration system that produces electric power and cooling capacity simultaneously. The schematic diagram of the cogeneration system is illustrated in Figure 2.13. In this cogeneration system, compound parabolic concentrators (CPC) are adopted to concentrate solar radiation to warm the heat transfer fluid. A CPC is a type of non-imaging solar concentrator that does not form an image of the light source on the receiver. It is able to collect all the available solar radiation and direct it to the receiver (Vijayakumar, et al., 2019).

The heat transfer fluid used in this cogeneration system is thermal oil. After passing through the CPC, the thermal oil is heated to a high temperature. The hot thermal oil is then stored in a heat storage tank. When the power is to be generated, the thermal oil will be conveyed to the heat exchanger to allow the heat to be transferred to the working fluid of the power generation cycle.

In this cogeneration system, an organic Rankine cycle (ORC) is used as the power cycle to convert the solar thermal energy to mechanical energy. Unlike the ordinary Rankine cycle where water is used as the working fluid, an ORC uses an organic fluid such as refrigerant, hydrocarbon, siloxane, and ether as the working fluid (Rahbar, et al., 2017). This type of fluid has a lower boiling point compared to water, which means that it tends to vaporize into vapour form at a lower temperature. This characteristic makes it suitable to be used as the working fluid of the Rankine cycle when the temperature of the heat source is limited (i.e. low-grade heat source). According to Tartière and Astolfi (2017), ORC performs better than the steam Rankine cycle as well as the gas power cycle (Brayton cycle) when the temperature of the heat source is lower than 400 ℃ and the power output is lower than 20 MW. Since the energy source of this cogeneration system is solar thermal energy, which is a low-grade heat source, an ORC is chosen as the power generation cycle instead of the ordinary steam Rankine cycle.

In the heat exchanger, the organic fluid receives heat from the thermal oil and vaporizes to become superheated vapour. The superheated vapour enters the turbine and expands to the condenser pressure. The expansion of superheated vapour drives the rotation of the turbine, which eventually produces mechanical power. However, organic fluids generally have higher molecular weights compared to water. This means that the turbine will be rotating at a lower speed and hence the magnitude of the power generated is smaller. The electric generator will then convert the mechanical power produced by the turbine to electric power. After the expansion process, the organic fluid leaves the turbine at a lower temperature and enters the condenser.

In this cogeneration system, the condenser of the ORC also serves as the generator of the absorption chiller. Heat is transferred from the organic working fluid to the refrigerant of the absorption chiller in the condenser/generator. The absorption chiller presented in this study is the water-lithium bromide (H_2O-LiBr) system. The working principle of the water-lithium bromide system is similar to the ammonia-water system discussed in Section 2.3.1, except that water is used as the refrigerant while lithium bromide is used as the absorbent. With the heat supplied from the ORC, the absorption cooling process is activated and thus cooling capacity can be produced. Due to the heat

transferred to the refrigerant, the organic working fluid condenses into liquid form. The liquid organic fluid is then pumped to the heat exchanger to repeat the cycle.

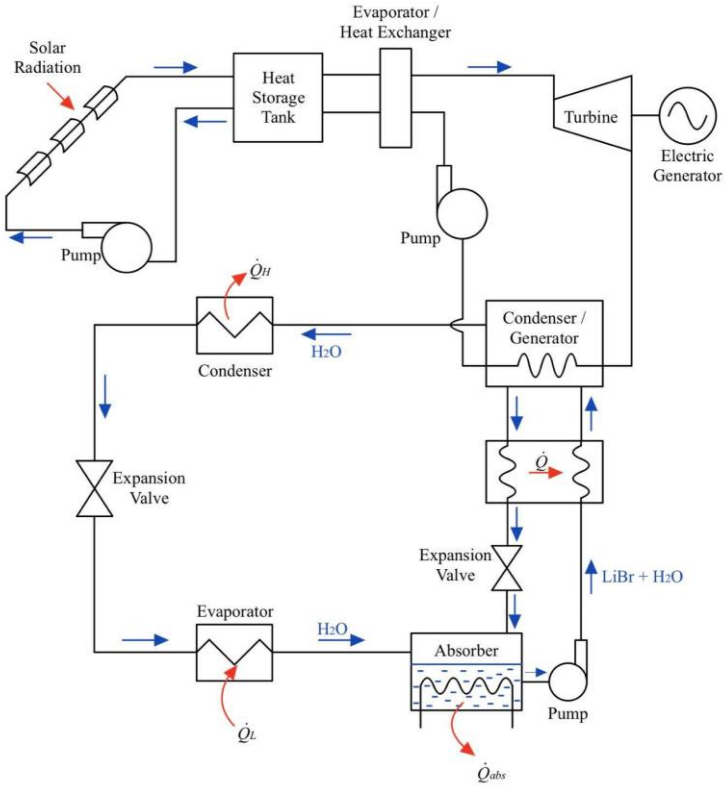

Figure 2.13: The Small-Scale Solar Cogeneration System Proposed by Hong and Shi (2020).

This study considered three different working fluids for the ORC, namely R123, R141b, and R1233zd. Among these three working fluids, R141b shows a better performance than the other two working fluids. The results of this study also show that the cooling output of this cogeneration system is always higher than the electrical power generated. When the thermal oil is heated to a temperature ranging from 100 ℃ to 130 ℃, the cooling capacity produced by the absorption chiller is within the range of 10 kW to 12 kW whereas the maximum electrical power generated is approximately 0.6 kW. The results also show that when the thermal oil is heated to a higher temperature, the electrical power generated will be higher but the cooling capacity produced will be slightly lower (Hong and Shi, 2020).

2.7 Hybrid Photovoltaic-Thermal (PVT) Cogeneration System

As discussed in Section 2.5.2, a solar photovoltaic (PV) panel directly converts solar radiation into electricity. However, as the PV panel is exposed to the sunlight, it gets heated. The increase in the temperature of the PV panel tends to lower the efficiency of the solar cells in converting sunlight to electricity. A method to remedy this situation is to integrate a solar thermal collector into the solar PV panel to collect heat from the PV panel. Such a system is known as a solar photovoltaic-thermal (PVT) system.

In a solar PVT system, pipes are being built at the backside of the solar panel to allow fluid to circulate through the panel and collect heat from it. As the fluid flows through the panel, heat is transferred from the panel to the fluid. As a consequence, the fluid is warmed up while the solar panel is cooled down. The decrease in the temperatures of the solar cells enhances the photoelectric conversion process. Meanwhile, the heat collected by the fluid can be used for other purposes such as water and space heating. Since the solar PVT system generates electricity and useful heat at the same time, it is also considered as a solar cogeneration system (Abdullah, et al., 2020; Dupeyrat, et al., 2014).

Liang, et al. (2015) proposed a hybrid PVT system, as shown in Figure 2.14. This PVT system is designed to generate electricity and provide space heating concurrently. On sunny days, the photons in the sunlight strike the solar PVT collector. As a result, a direct current is generated. To transfer the current to the power grid, it is necessary to include an inverter in the system to convert the direct current to alternating current. At the same time, water flows through the PVT collector to absorb heat from the panel. Consequently, the temperature of the PV panel decreases. The decrease in the temperatures of the solar cells eventually enhances the sunlight-to-electricity conversion process and increases the magnitude of the electric current produced. Meanwhile, the heat collected from the PV panel will be transferred to the water in the heating system via a heat exchanger. The heated water will then enter the radiant floor coils to serve as a radiant heat source for indoor space heating. Due to the intermittent characteristic of the sunlight, an additional electric heater is employed to supply additional heat energy to the space heating system when the heat collected from the sun is insufficient.

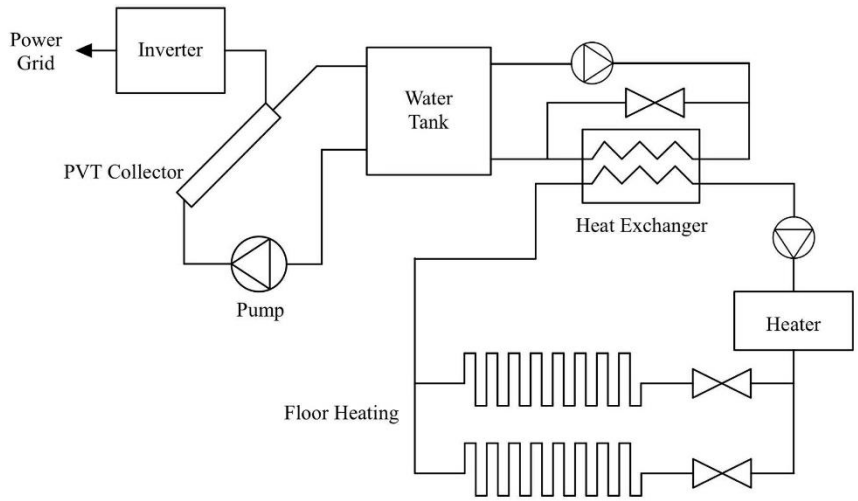

Figure 2.14: The Hybrid Photovoltaic-Thermal (PVT) System Proposed by Liang, et al. (2015).

The hybrid PVT system in Figure 2.14 was simulated in TRNSYS software. The simulation results show that the electricity generated by the solar cells increases as the intensity of the solar radiation increases. When the area of the solar PVT collector is 32 m^2 and the intensity of the solar radiation is 370 W/m^2, the solar cells are able to generate 1 465 W of electric power. This implies that the efficiency of the solar cells in converting solar radiation to electric power is approximately 12.37%. It was also found that the solar cells can generate 4.078 MW of electric power in one year. Furthermore, the results of the study also show that, on a sunny winter day, the auxiliary electric heater is not required to be turned on from 12:00 PM to 6:00 PM. This is because the heat energy gained from solar radiation is sufficient to meet the load demand of space heating.

2.8 Solar-Driven Trigeneration System

Similar to the cogeneration system, a trigeneration system can also be driven by solar energy to produce three useful outputs simultaneously. Wang (2014) proposed a small-scale modular trigeneration system that utilizes solar energy to produce electric power, cooling and heating capacities. The proposed trigeneration system is illustrated in Figure 2.15.

The trigeneration system consists of two main parts, namely solar thermal unit (STU) and power and end-users (PEU). The solar and thermal unit

consists of parabolic trough collectors, an auxiliary heater, a thermal storage tank, a heat exchanger, and the first fluid pump. The function of the STU part is to collect solar thermal energy and transfer it to the PEU part for power generation. The fluid that circulates in the STU loop is thermal oil. After flowing through the parabolic trough collectors, the thermal oil is heated to a temperature ranging from 150 ℃ to 250 ℃. In the case that the temperature of the thermal oil cannot reach the desired range, the auxiliary heater supplies additional heat to the thermal oil through the combustion of fossil fuels. Additionally, a thermal storage tank is included in the STU part. It serves to store excess heat energy that can be used to generate power when the sunlight is not available. The thermal oil will then transfer the heat energy to the water in the PEU part via the heat exchanger.

On the other hand, the power and end-users (PEU) part of this trigeneration system is made up of a heat exchanger, a power generator, a diffusion absorption refrigerator (DAR), a water heater, a cooling unit, and the second fluid pump. The PEU part of this trigeneration system is running on the ordinary steam Rankine cycle. In the heat exchanger, the water receives heat energy from the thermal oil and is vaporized into superheated steam. The superheated steam expands in the turbines to produce mechanical power. Since the turbine is connected to a power generator, the mechanical power produced will be converted to electrical power. The working fluid then leaves the turbine in the form of a saturated water-vapour mixture. It enters the DAR to produce cooling capacity and supply coolant to the users. After supplying heat to the DAR, the temperature of the saturated water-vapour mixture is still high enough to produce domestic hot water. Thus, the working fluid enters the water heater to transfer heat to the domestic water. If the temperature of the working fluid is still high when it leaves the water heater, it will be cooled in the cooling unit to turn into saturated water. Finally, the saturated water will be pumped by the second fluid pump to the heat exchanger to receive heat from the thermal oil again.

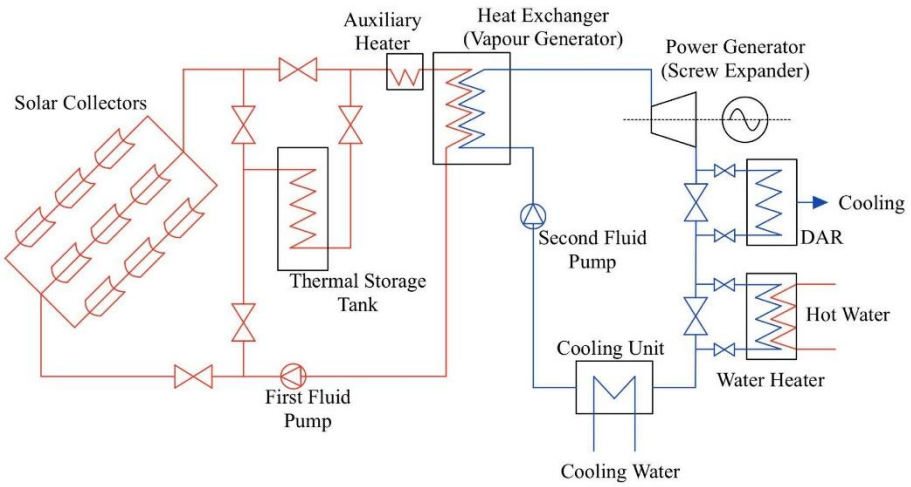

Figure 2.15: The Small-Scale Modular Trigeneration System Proposed by Wang (2014).

The results of this study show that when the system is operating as a single solar thermal power system (without producing domestic hot water and cooling capaciy), the input power required to generate 10 kW of electrical power is 126.41 kW. Furthermore, the second fluid pump requires an input power of 2.235 kW to pump the working fluid to the heat exchanger. Hence, the net power generated is reduced to 7.765 kW. The overall efficiency of the single solar thermal power system is only 6.14%.

In contrast, when the system is operating in trigeneration mode, it is able to produce 10 kW of electrical power, 16.51 kW of cooling capacity and 49.13 kW of heating capacity from the same amount of input power. The power consumed by the pump is slightly higher, which is 2.875 kW. This leads to an overall efficiency of 57.56%.

Therefore, it is clear that the trigeneration system can achieve a much higher efficiency compared to the single solar thermal power system. This is because the trigeneration system utilizes the heat energy contained in the exhaust vapour to provide additional cooling and heating effects instead of releasing it into the atmosphere as waste heat. In this solar trigeneration system, the water heater contributes the highest output. It was found that the domestic water can be heated from 20 ℃ to approximately 60 ℃ from the heat energy gained from the exhaust vapour (Wang, 2014).

2.9 Hydrogen Production Methods

Hydrogen is the lightest and the most abundant element in this universe. It is considered a clean fuel as it emits only water vapour when it is being consumed (Sharma and Ghoshal, 2015). Hydrogen is a highly reactive element. Hence, it does not exist as a free element in nature as it usually reacts with other elements to form compounds (Koroneos, et al., 2004). To obtain pure hydrogen, it must be separated from the elements for which it forms the compounds. In general, the common processes that separate hydrogen from the other elements include steam methane reforming, methane pyrolysis, and water electrolysis processes.

2.9.1 Steam Methane Reforming

At present, steam methane reforming is the most commonly used method to produce hydrogen gas at industrial scale. In a steam methane reforming process, methane (CH_4) is reacted with high-temperature steam to produce hydrogen gas (H_2) and carbon monoxide (CO). Natural gas is the primary source of methane, but other hydrocarbons such as ethane, butane, light and heavy naphtha etc. can also be used as the feedstock for the steam methane reforming process. The reaction between methane and hot steam is highly endothermic. Thus, steam methane reforming process is often carried out at high temperatures (about 850 ℃ to 950 ℃) to ensure the methane can be completely converted into the end products. Moreover, nickel is often used as the catalyst to enhance the rate of the reaction between methane and hot steam. The chemical equation that represents the reaction between methane and steam is as follow:

$$CH_4 + H_2O \rightarrow CO + 3H_2 \qquad (2.2)$$

To increase the amount of hydrogen gas produced, the carbon monoxide produced from the above reaction is further reacted with steam to produce additional hydrogen gas. This reaction is known as the water-gas shift reaction. Other than hydrogen gas, carbon dioxide is also produced as the by-product of the water-gas shift reaction. The carbon dioxide produced will then be filtered out from the gas mixture. As a result, pure hydrogen gas is obtained (Nieva, et al., 2014; Nikolaidis and Poullikkas, 2017). The water-gas shift reaction is described by the Equation 2.3.

$$CO + H_2O \rightarrow CO_2 + H_2 \quad (2.3)$$

2.9.2 Methane Pyrolysis

Methane pyrolysis is a cleaner way to generate hydrogen gas because it does not involve the combustion of fossil fuels. As a result, no greenhouse gas will be released into the atmosphere (Sánchez-Bastardo, et al., 2020). Methane pyrolysis is a process to decompose methane into hydrogen gas and solid carbons. It is an endothermic reaction and is conducted at high temperatures. In the absence of a catalyst, the formation of solid carbons and hydrogen gas starts when the temperature reaches around 300 ℃. However, without any catalyst, a high temperature that exceeds 1 200 ℃ is required to convert a large portion of methane into the end products. Therefore, to lower the temperature required to activate the conversion process, methane pyrolysis is usually carried out in the presence of a catalyst. One of the catalysts that has been widely used in methane pyrolysis is the molten nickel-bismuth (NiBi) alloy. In this process, methane is fed into the bottom of a bubble column reactor filled with molten NiBi. After that, heat is supplied to the reactor to raise the temperature of the reactant to the range of 600 ℃ to 900 ℃. During the heating process, the methane is decomposed to form solid carbons and hydrogen gas. The solid carbons produced can be separated easily because they have a low density and hence will float to the top of the molten catalyst (Msheik, et al., 2021; Rahimi, et al., 2019). In short, the chemical equation that describes the methane pyrolysis process is given as follows:

$$CH_4 \rightarrow C + 2H_2 \quad (2.4)$$

2.9.3 Electrolysis of Water

Electrolysis of water is another common way of producing hydrogen gas. It is a process that uses electricity to decompose water into oxygen and hydrogen gases. The decomposition of water takes place in an electrolyzer, which consists of an anode (positive terminal), a cathode (negative terminal), and a membrane that separates the two terminals. In general, electrolysis of water can be classified into three main types, namely alkaline water electrolysis, proton exchange membrane (PEM) water electrolysis, and solid oxide electrolysis.

2.9.3.1 Alkaline Water Electrolysis

In the alkaline water electrolysis process, an alkaline solution is used as the electrolyte for the electrolysis process. Potassium hydroxide (KOH) and sodium hydroxide (NaOH) are the common alkaline solutions used in this process. Alkaline water electrolysis is usually carried out at a temperature ranging from 30 ℃ to 80 ℃. When an electric current is supplied to the electrodes, water molecules in the cathode region gain electrons and undergo a reduction process. As a result, hydrogen gas (H_2) and hydroxide ions (OH^-) are formed at the cathode. The hydroxide ions will then pass through the diaphragm to reach the anode region. At the anode, the hydroxide ions undergo oxidation by giving out electrons to produce oxygen gas (O_2) and water (H_2O). At present, a typical alkaline electrolyzer has an efficiency ranging from 60% to 80% and is able to produce hydrogen gas of up to 99% of purity (Ahmad Kamaroddin, et al., 2021). The schematic diagram and chemical equations for alkaline water electrolysis are as follows:

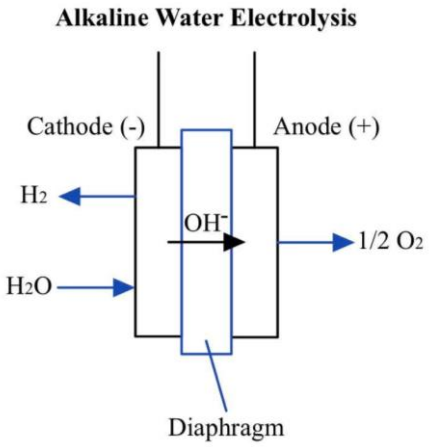

Figure 2.16: Schematic Diagram of Alkaline Water Electrolysis.

$$\text{Anode: } 2OH^- \rightarrow \frac{1}{2}O_2 + H_2O + 2e^- \quad (2.5)$$

$$\text{Cathode: } 2H_2O + 2e^- \rightarrow H_2 + 2OH^- \quad (2.6)$$

$$\text{Overall Equation: } H_2O \rightarrow \frac{1}{2}O_2 + H_2 \quad (2.7)$$

2.9.3.2 Proton Exchange Membrane (PEM) Water Electrolysis

As the name suggests, a proton exchange membrane (PEM) electrolyzer contains a PEM to separate the anode and the cathode. In some literature, it is also known as a polymer electrolyte membrane electrolyzer. In PEM water electrolysis, water is introduced to the anode of the PEM electrolyzer. Once an electric current is applied, water at the anode will start to decompose to form oxygen gas (O_2), hydrogen ions (H^+), and electrons (e^-). The electrons will then travel to the cathode side through an external circuit. Meanwhile, the hydrogen ions formed at the anode will diffuse across the membrane to reach the cathode side of the electrolyzer. Once the hydrogen ions reach the cathode side, they receive the electrons and are reduced to hydrogen gas (Kumar and Himabindu, 2019). Generally, PEM water electrolysis is conducted at a temperature between 20 ℃ to 100 ℃ (Carmo, et al., 2013). Hydrogen gas with up to 99.995% of purity can be produced from this electrolysis process (Ahmad Kamaroddin, et al., 2021). The PEM water electrolysis process is depicted in Figure 2.17 and the chemical equations for the PEM electrolysis process are shown in Equations 2.8 to 2.10.

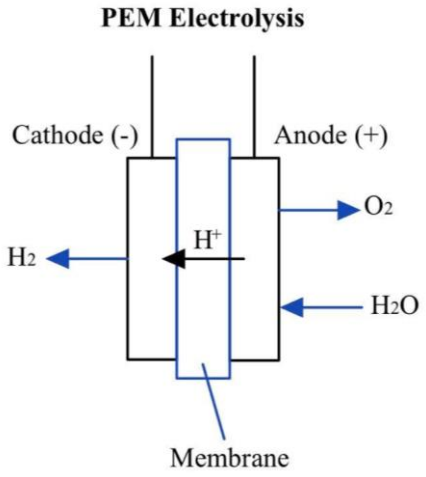

Figure 2.17: Schematic Diagram of Proton Exchange Membrane (PEM) Water Electrolysis.

$$\text{Anode: } 2H_2O \rightarrow O_2 + 4H^+ + 4e^- \quad (2.8)$$

$$\text{Cathode: } 4H^+ + 4e^- \rightarrow 2H_2 \quad (2.9)$$

$$\text{Overall Equation: } 2H_2O \rightarrow O_2 + 2H_2 \quad (2.10)$$

2.9.3.3 Solid Oxide Electrolysis

Solid oxide electrolysis produces hydrogen gas in a slightly different way compared to alkaline and PEM water electrolysis processes. In a solid oxide electrolyzer, a solid ceramic membrane is used as the electrolyte. Besides that, the operation of this process requires a relatively high temperature, which is generally ranging from 500 ℃ to 1 000 ℃ (Ahmad Kamaroddin, et al., 2021). Due to the high temperature, the water fed into the electrolyzer is often in the form of steam (Kumar and Himabindu, 2019). At the cathode, steam undergoes a reduction process by receiving electrons from the external circuit. As a consequence, hydrogen gas (H_2) and oxygen ions (O^{2-}) are formed at the cathode. The negatively charged oxygen ions will then move to the anode side by passing through the membrane. At the anode, the oxygen ions release their electrons and turn into oxygen gas (O_2). The electrons produced will then travel to the cathode via the external circuit. To summarize, the illustration and chemical equations of solid oxide electrolysis are shown as follows:

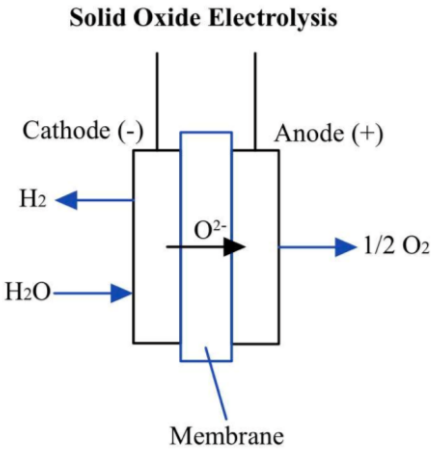

Figure 2.18: Schematic Diagram of Solid Oxide Electrolysis.

$$\text{Anode: } O^{2-} \rightarrow \frac{1}{2}O_2 + 2e^- \quad (2.11)$$

$$\text{Cathode: } H_2O + 2e^- \rightarrow H_2 + O^{2-} \quad (2.12)$$

$$\text{Overall Equation: } H_2O \rightarrow H_2 + \frac{1}{2}O_2 \quad (2.13)$$

2.10 Summary of Literature Review

In summary, cogeneration systems can produce two useful outputs while trigeneration systems can produce three useful outputs from a single source of energy. The operations of the cogeneration and the trigeneration systems can be driven by solar energy, either through solar thermal power generation or solar photovoltaic (PV) technologies. Parabolic troughs, linear Fresnel reflectors, solar power towers, and parabolic dishes are the common methods of concentrating solar energy for power generation. Last but not least, hydrogen gas can be produced through steam methane reforming, methane pyrolysis, and water electrolysis processes.

The cogeneration and trigeneration systems reviewed in this chapter are mainly designed to produce power, heat energy, and cooling capacity. In these systems, the heat energy produced is mainly supplied to other industrial processes or used for space or water heating purposes. However, none of the cogeneration or trigeneration system proposed by other researchers is capable of producing hydrogen gas as one of the outputs. Hence, an unexplored area that requires further research is the investigation of the suitable hydrogen production process that can be applied to the cogeneration and trigeneration systems to enable the systems to produce hydrogen gas as one of the outputs. This further research is important in order to achieve the first objective of the project, which is to propose multigeneration systems that produce hydrogen gas as one of the outputs.

CHAPTER 3

METHODOLOGY AND WORK PLAN

3.1 Introduction

This chapter outlines the methodology of conducting the research. Besides that, the proposed multigeneration (cogeneration and trigeneration) systems are described in detail. Apart from that, the models of the proposed systems in Aspen HYSYS are presented and the mathematical equations for evaluating the efficiencies of the systems are derived. In addition, the steps involved in performing life cycle assessments (LCA) for the proposed cogeneration and trigeneration systems are explained. Last but not least, the project management tools used for this project are included at the end of this chapter.

3.2 Overview of Methodology

Understanding the project scope and requirements is always the first step to start off a project. This step was not an exception in this project. This project dealt with proposing and modelling multigeneration systems that produce multiple commodities from solar energy. To understand the definition and principles of multigeneration, literature review was conducted to investigate the multigeneration systems proposed by other researchers. After the completion of literature review, the ideas of solar-driven multigeneration systems were developed. In this study, the proposed multigeneration systems were the cogeneration and trigeneration systems powered by solar energy.

Before performing process simulations for the proposed systems, the operating parameters such as the operating pressures and mass flow rates of the working fluids were decided. With the decided operating parameters, the proposed cogeneration and trigeneration systems were modelled in the simulation software, which was Aspen HYSYS. After performing the process simulations, the efficiencies, which represent the overall performances of the systems, were evaluated based on the simulation results. If the efficiencies of the systems were not impressive, a new set of operating parameters was decided and the process simulation was run again. Once the efficiencies of the systems were satisfied, the input and output energies of the systems were keyed in to

GaBi software to assess the life cycles of the proposed systems. After that, the efficiencies and the life cycles of the cogeneration and the trigeneration systems were compared. The last step was to complete the report by presenting the simulation results, discussion, conclusion etc. In summary, the flowchart in Figure 3.1 shows the main steps involved in this study.

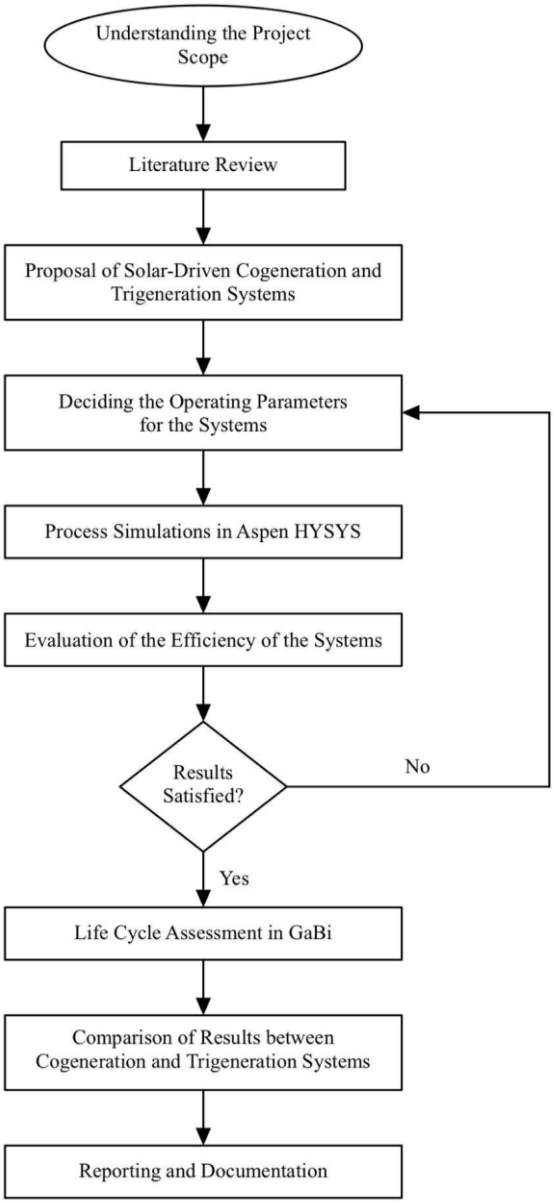

Figure 3.1: The Flow Chart of Performing the Study.

3.3 The Proposed Solar Cogeneration System

Figure 3.2 illustrates the proposed solar cogeneration system that produces two useful outputs simultaneously. The proposed solar cogeneration system consists

of three main subsystems, namely a solar field, a binary vapour cycle, and a proton exchange membrane (PEM) electrolyzer. The solar field is made up of a solar power tower and a number of reflecting mirrors known as heliostats. It was assumed that the solar field consists of 560 heliostats, with each heliostat having an area of 100 m^2. During the daytime, the heliostats reflect and concentrate the incident solar radiation onto the central receiver located at the top of the solar power tower. At the same time, the working fluid of the power generation cycle is pumped to the central receiver to receive the concentrated solar energy for the sake of power generation.

A binary vapour cycle was chosen as the power generation cycle for the proposed cogeneration system. As the name suggests, a binary vapour cycle consists of two vapour power cycles (i.e. Rankine cycles), with each cycle generating its own power. The topping cycle uses water as the working fluid and thus operates like an ordinary steam Rankine cycle, except that the boiler has been replaced by the central receiver of the solar power tower. To make use of concentrated solar energy to generate power, the water is pumped to the central receiver to receive the concentrated solar energy. As a consequence, the water vaporizes and turns into superheated steam. The superheated steam will then expand in the turbine to rotate the turbine shaft. To produce electric power from the power cycle, an electric generator is connected to the shaft of the turbine. With the electric generator, the mechanical energy of the turbine shaft will be transformed into electrical energy. Thus, the first desired output of the cogeneration system, which is the electric power, is generated at the topping cycle. After the steam is expanded in the turbine, its temperature and pressure are lowered. This is because part of its internal energy is converted to work. Nevertheless, the steam leaving the turbine still contains a substantial amount of energy which is adequate to drive another vapour power cycle, i.e. the bottoming cycle. Hence, the steam enters the heat exchanger to transfer its heat to the working fluid of the bottoming cycle.

The working principle of the bottoming cycle is similar to the topping cycle. However, instead of using water as the working fluid, n-butane (C_4H_{10}) was chosen to be the working fluid of the bottoming cycle due to its lower boiling point compared to water. Unlike the topping cycle where the water receives an enormous amount of solar energy in the central receiver, the heat

energy transferred to the bottoming cycle is limited since the heat source of the bottoming cycle is the waste heat rejected by the topping cycle. Therefore, the heat source of the bottoming cycle has a relatively low temperature compared to the topping cycle. To utilize the heat obtained from the low-temperature heat source, it is necessary to replace water with a working fluid that has a lower boiler point. n-Butane is one of the organic fluids that has a lower boiling point than water. It is also commonly used as the working fluid of the organic Rankine cycle (ORC) (discussed in Section 2.6). At atmospheric pressure, the boiling point of n-butane is approximately -1 ℃ (Naeem, et al., 2014). The low boiling point of n-butane allows it to vaporize into superheated vapour at a lower temperature. With this property, the heat energy supplied by the topping cycle is sufficient to completely vaporize the n-butane into superheated vapour.

After receiving heat from the steam in the heat exchanger, the n-butane leaves the heat exchanger in the form of superheated vapour and enters the turbine, where it undergoes an expansion process to generate power. After the expansion process, the n-butane leaves the turbine at a lower temperature and pressure. The low-temperature n-butane will then enter the condenser to transfer the remaining heat energy to the cooling water. The cooling water serves as a transport medium to transfer the heat rejected by the n-butane to the cooling tower. The cooling tower will then dissipate this heat load into the atmosphere as the waste heat (Lakovic, et al., 2016). As the heat is transferred to the cooling water, the n-butane condenses into liquid and leaves the condenser. Finally, the liquid n-butane will be pumped to the heat exchanger to receive heat energy from the topping cycle.

Besides working fluid, another difference between the topping and the bottoming cycles is the presence of an additional PEM electrolyzer in the bottoming cycle. The electric generator in the bottoming cycle is connected to the PEM electrolyzer, which is the water-splitting equipment that decomposes water into hydrogen (H_2) and oxygen (O_2) gases with the aid of electricity. To utilize the PEM electrolyzer to conduct the water electrolysis process, the two primary inputs are electric current and water. In the proposed cogeneration system, the electricity generated by the bottoming cycle is supplied to the PEM electrolyzer. Concurrently, water is introduced to the PEM electrolyzer to allow the electrolysis of water to happen. The PEM electrolyzer will use the electricity

generated by the bottoming cycle to decompose the water into hydrogen and oxygen gases. In this way, hydrogen gas, which is the second desired output of the cogeneration system, can be produced. For the detailed discussion on the PEM water electrolysis process, kindly refer to Section 2.9.3.2.

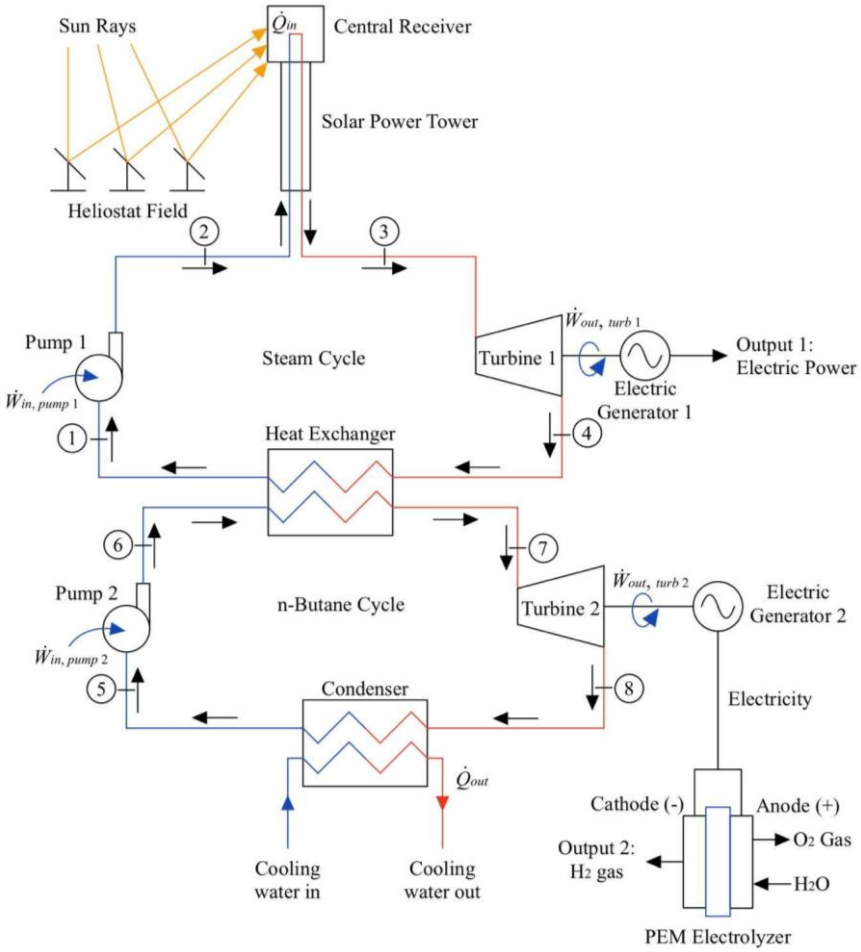

Figure 3.2: Schematic Diagram of the Proposed Solar Cogeneration System.

In summary, the proposed solar cogeneration system uses a large array of heliostats to focus the incoming solar radiation onto the central receiver. The concentrated solar energy is then converted to electric power via the binary vapour cycle. Both the topping and bottoming cycles produce electricity. The electricity generated by the bottoming cycle is fed to the PEM electrolyzer to initiate the water electrolysis process. As a consequence, hydrogen gas is produced. Hence, the proposed cogeneration system is able to produce two useful outputs from solar energy, which are electric power and hydrogen gas.

3.4 The Proposed Solar Trigeneration System

In the cogeneration system depicted in Figure 3.2, the n-butane leaving Turbine 2 still contains a considerable amount of heat energy. This heat energy can be further utilized to activate another process instead of being discharged into the atmosphere as the waste heat. As discussed in Section 2.3, one of the heat-driven systems that is feasible to be incorporated into the cogeneration system is the absorption chiller. When an absorption chiller is integrated with the solar cogeneration system presented in Section 3.3, the resulting overall system is the solar trigeneration system.

The proposed solar trigeneration system is shown in Figure 3.3. It can be observed that the proposed trigeneration system is very much similar to the cogeneration system, except that an additional absorption chiller has been connected to the bottoming cycle. The absorption chiller chosen for the trigeneration system is the ammonia-water ($NH_3 - H_2O$) system, in which ammonia serves as the refrigerant while water serves as the absorbent. The purpose of adding the absorption chiller to the bottoming cycle is to extract some heat energy from the n-butane leaving the turbine to activate the absorption cooling process. With the absorption chiller, the trigeneration system is able to produce an extra cooling capacity other than electric power and hydrogen gas.

The absorption chiller is linked to the bottoming cycle of the binary vapour cycle via the generator. After the n-butane vapour is expanded in Turbine 2, it enters the generator of the absorption chiller to transfer some of its heat to the ammonia-water solution. The remaining heat energy carried by the n-butane is released into the atmosphere via a cooling tower. Meanwhile, the ammonia-water solution in the generator receives heat from the n-butane and is vaporized into vapour form. The ammonia vapour, which is the refrigerant of the absorption chiller, then travels to the remaining parts of the absorption chiller. In the condenser, the ammonia vapour releases heat and condenses into liquid ammonia. The liquid ammonia is then being throttled by the expansion valve so that its pressure is decreased to the lower operating pressure of the absorption chiller. After that, the low-pressure ammonia enters the evaporator to absorb heat from the cold space. After receiving heat from the cold space, the ammonia leaves the evaporator in the form of saturated vapour and enters the absorber to be dissolved in the water. The transfer of heat from the cold space to the

ammonia refrigerant through the evaporator represents the cooling capacity output by the absorption chiller, as this process helps to maintain the cold space at a low temperature. For the complete description of the working principle of the ammonia-water absorption chiller, kindly refer to Section 2.3.1.

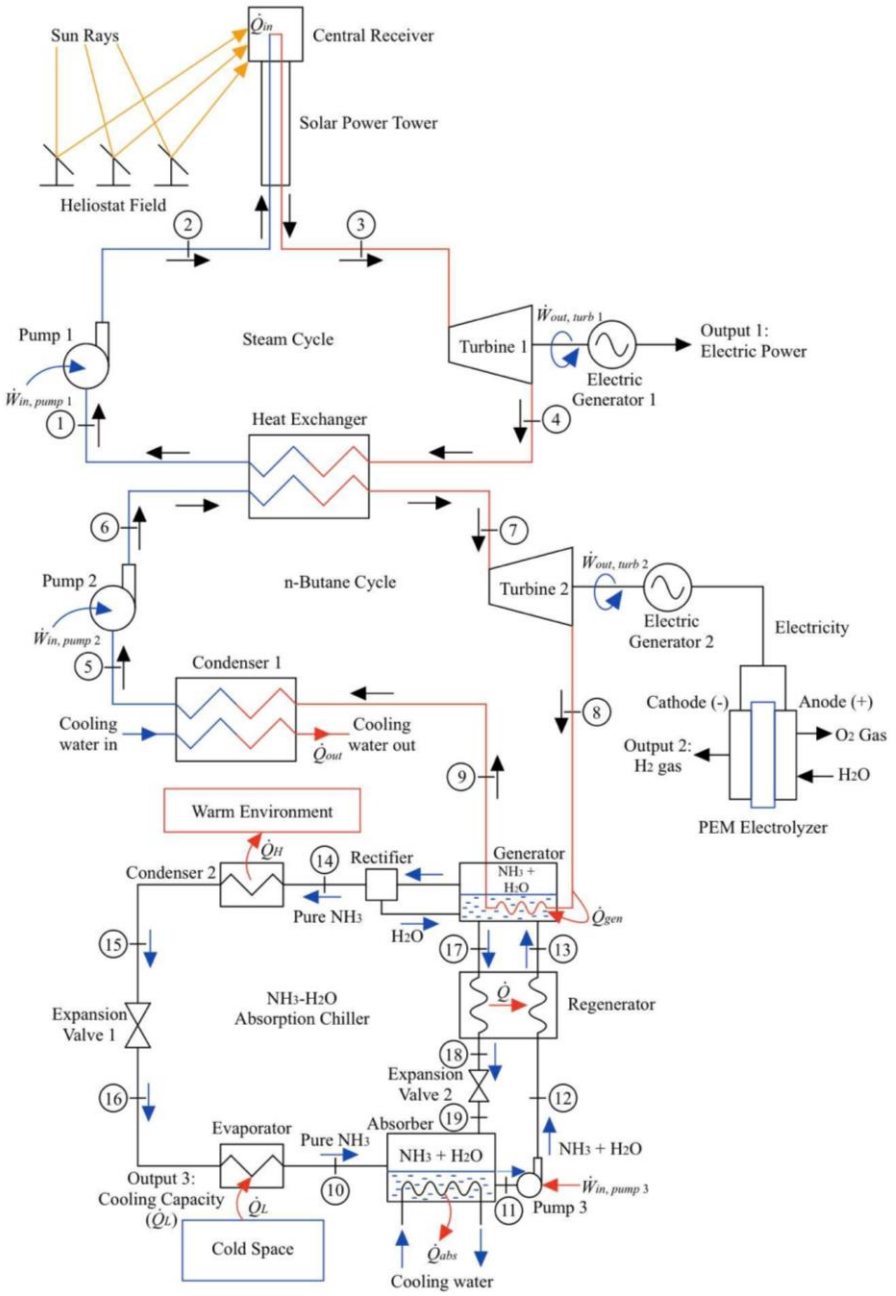

Figure 3.3: Schematic Diagram of the Proposed Solar Trigeneration System.

To summarize, the proposed solar trigeneration system is the solar cogeneration system added with an absorption chiller. Similar to the solar cogeneration system, the solar energy concentrated by the heliostats is supplied

to the binary vapour cycle. The product of the topping cycle is electric power whereas the product of the bottoming cycle is hydrogen gas. Before the waste heat produced by the binary vapour cycle is discharged into the atmosphere, a portion of heat is recovered to drive the absorption chiller to generate cooling capacity. Therefore, the trigeneration system is able to produce electric power, hydrogen gas, and cooling capacity from the concentrated solar energy.

3.5 Performance Evaluation of the Proposed Multigeneration Systems

After the solar cogeneration and trigeneration systems have been proposed, it is essential to assess how well the systems perform. The performances of the proposed cogeneration and trigeneration systems can be assessed by evaluating their efficiencies. This can be done with the aid of process simulation software. In this study, the process simulation software chosen to model the proposed systems was Aspen HYSYS. With this software, the energy flows at all stages of the cycles could be determined effortlessly.

To proceed to evaluate the performances of the proposed systems, the solar cogeneration and trigeneration systems illustrated in Figure 3.2 and 3.3 were modelled in Aspen HYSYS. However, the solar field that consists of the solar power tower and the heliostats could not be modelled in the software. This is because the components of the solar power tower and heliostats as well as the solar energy data are not available in Aspen HYSYS. A solution to this problem was to analyze the energy flows that occur in the solar field through calculations.

3.5.1 Analysis of Energy Flows in the Solar Field

In the proposed solar multigeneration systems, the heliostats reflect and focus the incident solar radiation onto the central receiver to heat the water that flows through the central receiver. The amount of solar energy received by the water could be estimated by searching for the data of direct normal irradiation (DNI). DNI is defined as the amount of solar energy received by a unit of surface area that is positioned perpendicularly to the sun (Asrori, et al., 2020). Since DNI varies with location, it was necessary to decide on a location for the proposed systems to determine the total amount of solar radiation received by the heliostats. In this study, it was assumed that the solar cogeneration and trigeneration systems were to be built in the state of Pahang, Malaysia. From

the solar resource map of Malaysia shown in Figure 3.4, it is reasonable to assume the daily total DNI in Pahang is approximately 3.0 kWh/m^2. By further assuming the location receives 8 hours of solar radiation per day, the DNI for the state of Pahang is equivalent to 0.375 kW/m^2. This means that each unit area of the heliostat will receive about 0.375 kW of solar radiation during the daytime.

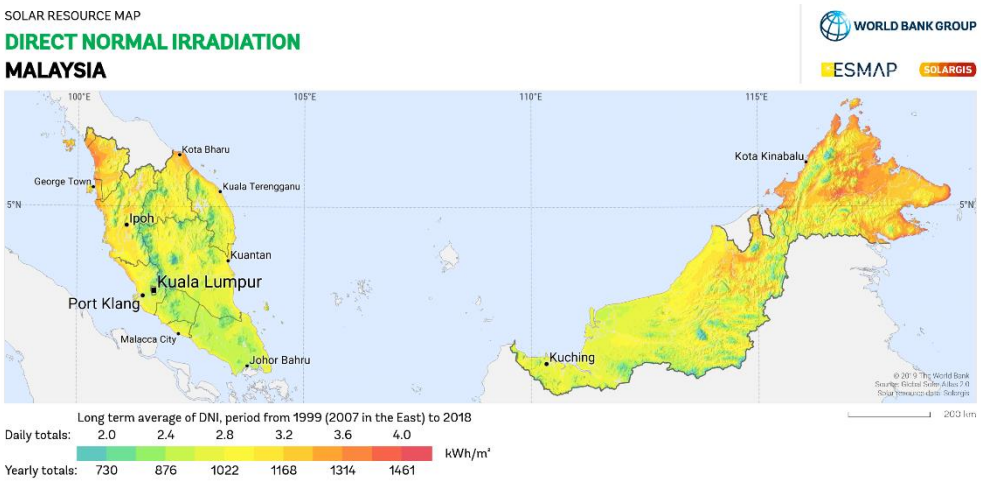

Figure 3.4: Direct Normal Irradiation (DNI) in Malaysia (The World Bank and Solargis, 2020).

Besides DNI, the other parameters that were necessary for this analysis included the efficiencies of the heliostat field and the central receiver. In this study, the efficiencies of the heliostat field and the central receiver were assumed to be 75% and 90% respectively. These values were obtained from the literature published by Xu, et al., (2011). In short, the energy flows that occur in the solar field are demonstrated in Figure 3.5 and the total amount of solar energy received by the water was calculated by using Equations 3.1 to 3.3.

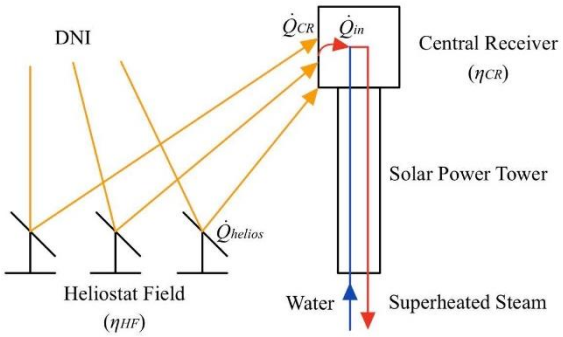

Figure 3.5: Schematic Diagram of Energy Flows in the Solar Field.

$$\dot{Q}_{helios} = A \times DNI \tag{3.1}$$

$$\dot{Q}_{CR} = \eta_{HF}\dot{Q}_{helios} \tag{3.2}$$

$$\dot{Q}_{in} = \eta_{CR}\dot{Q}_{CR} \tag{3.3}$$

where

$\dot{Q}_{helios}$ = rate of heat received by the heliostats, kW

$\dot{Q}_{CR}$ = rate of heat received by the central receiver, kW

$\dot{Q}_{in}$ = rate of heat received by the water, kW

A = total area of heliostats, m^2

DNI = direct normal irradiation, kW/m^2

η_{HF} = efficiency of the heliostat field

η_{CR} = efficiency of the central receiver

After the rate of heat received by the water was known, the value was input to Aspen HYSYS to enable the process simulations for the cogeneration and the trigeneration systems. With this method, the solar field could be omitted from the process simulations since the output of the solar field, which is the total energy supplied to the water, had been determined through calculations.

3.5.2 Process Simulation of the Cogeneration System in Aspen HYSYS

After the energy flow analysis for the solar field was done, the next step was to model the cogeneration system in Aspen HYSYS. This step was done by adding all the components, energy streams, and material streams of the cogeneration system in the simulation window, as depicted in Figure 3.6. The energy streams were represented by the red arrows whereas the material streams were represented by the blue arrows in Figure 3.6. Moreover, since the water is heated in the central receiver of the solar power tower, a heater was added to simulate the water heating process in the central receiver.

Next, the properties of working fluids at different stages of the cycle were defined. These properties included the mass flow rates, pressures, and dryness fractions of the working fluids (water in the topping cycle and n-butane in the bottoming cycle) at different stages. However, since there were no guidelines on how to decide the operating pressures of the binary vapour cycle,

several sets of operating pressures were input to the software and the set of operating pressures that provided the highest efficiency was selected as the final operating pressures for this study. In other words, the operating pressures of the binary vapour cycle were decided based on the trial and error approach. Other than that, the rate of heat received by the water determined from Equation 3.3 was also input to the software to determine the end state of the water after receiving the concentrated solar energy.

Furthermore, the isentropic efficiencies of the pumps and the turbines also played an important role in this process simulation as they would affect the powers needed to drive the pumps and the output powers generated by the turbines. Isentropic efficiency is defined as the extent to which an actual pump or turbine approximates an isentropic (idealized) pump or turbine. In the process simulation of the binary vapour cycle, the isentropic efficiencies for all the pumps and turbines were set to 85%. Once all the input parameters were fully defined, the powers required to drive the pumps and the output powers generated by the turbines were obtained from the simulation results.

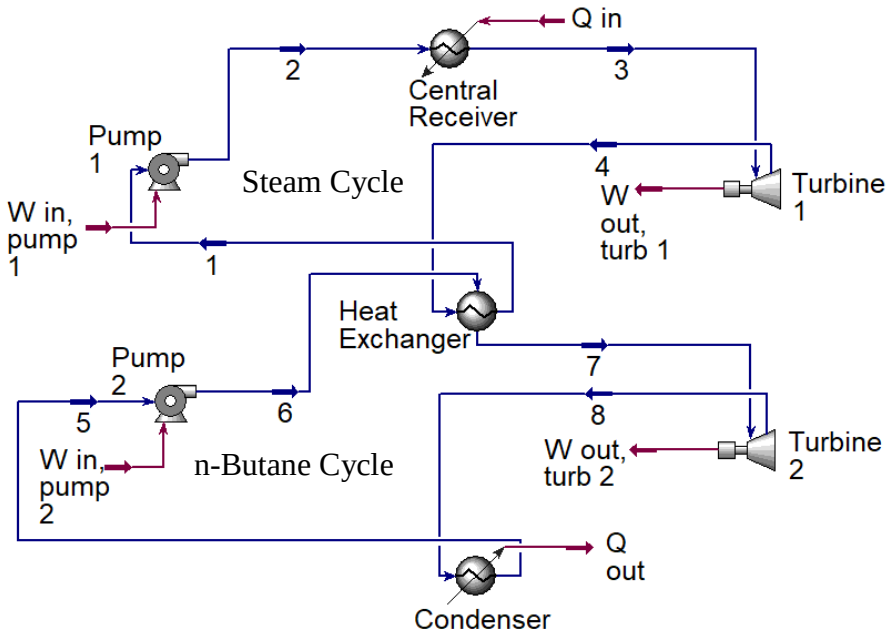

Figure 3.6: The Model of the Cogeneration System in Aspen HYSYS.

By comparing the proposed cogeneration system in Figure 3.2 with the model in Figure 3.6, it can be noticed that the electric generators and the proton

exchange membrane (PEM) electrolyzer were not included in the process simulation in Aspen HYSYS. This is due to the software does not have the electric generator and the PEM electrolyzer in its component list. This implies that only the mechanical powers produced by the turbines could be determined from the simulation results. However, the mechanical powers generated by the turbines are not the desired outputs of the cogeneration system. Based on the proposed cogeneration system, the desired outputs of the system are the electric power generated by the electric generator and the hydrogen gas produced by the PEM electrolyzer. Since there was no way to simulate the electric power generation and the water electrolysis processes in the software, the only method to determine the outputs produced by the system was through calculations.

3.5.3 Mathematical Models for the Cogeneration System

With the process simulation results obtained from Aspen HYSYS, the mathematical equations to compute the electric power and the rate at which hydrogen gas is produced by the cogeneration system could be developed. After that, the equation to calculate the efficiency of the cogeneration system could be derived.

3.5.3.1 Electric Powers Generated by the Electric Generators

After the magnitudes of the mechanical powers generated by the turbines were obtained from the simulation results, the electric powers produced by the cogeneration system could be determined. To calculate the electric powers produced by the system, it was necessary to assume the efficiency of the electric generators. In this study, both electric generators employed in the cogeneration system were assumed to have an efficiency of 90%. This means that the electric generators convert 90% of the input mechanical power into electric power. With this assumption, the magnitudes of the electric powers produced in the topping cycle and the bottoming cycle could be calculated by using the following equations:

$$\dot{W}_{elec\ 1} = 0.9\dot{W}_{out,\ turb\ 1} \tag{3.4}$$

$$\dot{W}_{elec\ 2} = 0.9\dot{W}_{out,\ turb\ 2} \tag{3.5}$$

where

$\dot{W}_{elec\,1}$ = electric power produced by Electric Generator 1, kW

$\dot{W}_{elec\,2}$ = electric power produced by Electric Generator 2, kW

$\dot{W}_{out,\,turb\,1}$ = mechanical power produced by Turbine 1, kW

$\dot{W}_{out,\,turb\,2}$ = mechanical power produced by Turbine 2, kW

3.5.3.2 Hydrogen Production Rate

The second desired output of the cogeneration system is the hydrogen gas (H_2) produced through the proton exchange membrane (PEM) water electrolysis process. Therefore, it was essential to determine the rate at which the hydrogen gas can be produced by the cogeneration system. Ratlamwala, et al. (2012) developed an equation to determine the hydrogen production rate of the water electrolysis process. The equation is given as follows:

$$\dot{m}_{H_2} = \frac{\eta_{PEM}\dot{W}_{elec\,2}}{LHV} \tag{3.6}$$

where

$\dot{m}_{H_2}$ = rate of hydrogen production, kg/s

η_{PEM} = efficiency of the PEM electrolyzer

LHV = lower heating value of hydrogen, kJ/kg

To apply Equation 3.6 to calculate the hydrogen production rate, the electric power supplied to the PEM electrolyzer ($\dot{W}_{elec\,2}$), the lower heating value (LHV) of hydrogen, and the efficiency of the PEM electrolyzer (η_{PEM}) must be determined. The electric power supplied to the PEM electrolyzer could be calculated from Equation 3.5 whereas the LHV of hydrogen and the efficiency of the PEM electrolyzer were determined from the literature. According to Dufo-López and Bernal-Agustín (2008), the LHV of hydrogen is approximately 33.3 kWh/kg, which is equivalent to 119 880 kJ/kg. Furthermore, the energy efficiency of the water electrolysis process is generally ranging from 50% to 70% (Sánchez-Bastardo, et al., 2021). In this study, the efficiency of the PEM electrolyzer was considered to be 70%. Once the values of the required parameters were defined, the rate of hydrogen production could be determined.

3.5.3.3 Efficiency of the Cogeneration System

To achieve the objective of evaluating the performance of the proposed system, the efficiency of the cogeneration system was calculated. The efficiency of a system can be evaluated by taking the ratio of output power to input power. The desired outputs of the proposed cogeneration system are electric power and hydrogen gas. These two outputs were determined from Equation 3.4 and 3.6 respectively. However, it should be noted that both of these outputs were measured in different units. Combining the electric power and the hydrogen production rate into one equation will therefore result in unbalance of the equation. Hence, to calculate the total output produced by the cogeneration system, the output of the PEM electrolyzer was expressed in terms of power (kW) instead of hydrogen production rate (kg/s). The output power of the PEM electrolyzer could be determined by using the following equation:

$$\dot{W}_{out,\,PEM} = \eta_{PEM}\dot{W}_{elec\,2} = 0.9\eta_{PEM}\dot{W}_{out,\,turb\,2} \tag{3.7}$$

where

$\dot{W}_{out,\,PEM}$ = output power of the PEM electrolyzer, kW

By expressing the output of the PEM electrolyzer in terms of power, the overall efficiency of the cogeneration system could be evaluated through the following equation:

$$\eta_{cogen} = \frac{(\dot{W}_{elec\,1} - \dot{W}_{in,\,pump\,1}) + (\dot{W}_{out,\,PEM} - \dot{W}_{in,\,pump\,2})}{\dot{Q}_{in}} \times 100\% \tag{3.8}$$

where

η_{cogen} = efficiency of the cogeneration system

$\dot{W}_{in,\,pump\,1}$ = power supplied to Pump 1, kW

$\dot{W}_{in,\,pump\,2}$ = power supplied to Pump 2, kW

3.5.4 Process Simulation of the Trigeneration System in Aspen HYSYS

As described earlier, the proposed trigeneration system is the extension of the cogeneration system, in which an ammonia-water absorption chiller is added to

the cogeneration system. Therefore, the simulation procedure was essentially the same as the cogeneration system, except that the components in the absorption cycle were added to the simulation window.

Figure 3.7 illustrates the overall trigeneration system modelled in Aspen HYSYS. In this model, a distillation column was used to represent the generator and the rectifier in the absorption chiller. In the proposed trigeneration system, the n-butane in the bottoming cycle enters the generator of the absorption chiller to transfer some heat energy to the ammonia-water solution in the generator. However, in Aspen HYSYS, heat energy could only be supplied to the distillation column in the form of an energy stream. This means that it was not possible to connect the n-butane stream at state point 8 to the generator of the absorption chiller. Hence, to model the trigeneration system in Aspen HYSYS, a pre-condenser was added to the n-butane cycle to output an energy stream (Q_{gen} in Figure 3.7) to the generator of the absorption chiller.

Another difference between the proposed trigeneration system in Figure 3.3 and the model in Figure 3.7 is in the absorber part. In an absorption chiller, the absorber is where the ammonia vapour mixes with the water. Additionally, as described in Section 2.3.1, it is necessary to decrease the temperature in the absorber to optimize the absorption of ammonia vapour into the water. Thus, there are two processes that occur in the absorber, which are mixing and cooling. In Aspen HYSYS, the mixing process occurs in a mixer whereas the cooling process happens in a cooler. Therefore, the absorber in the absorption chiller was represented by the combination of the mixer and the cooler (named as the absorber in Figure 3.7).

Similar to the binary vapour cycle of the cogeneration system, the operating parameters of the absorption cooling cycle, such as the operating pressures, temperatures, and the mass flow rate of the refrigerant were also decided based on the trial and error approach. After running several successful simulations, the set of operating parameters that provides the highest cooling capacity was selected as the final operating parameters of the absorption chiller. Also, to compare the performances of the cogeneration and the trigeneration systems, the operating parameters of the binary vapour cycle in the trigeneration system were set to follow exactly the same as in the cogeneration system.

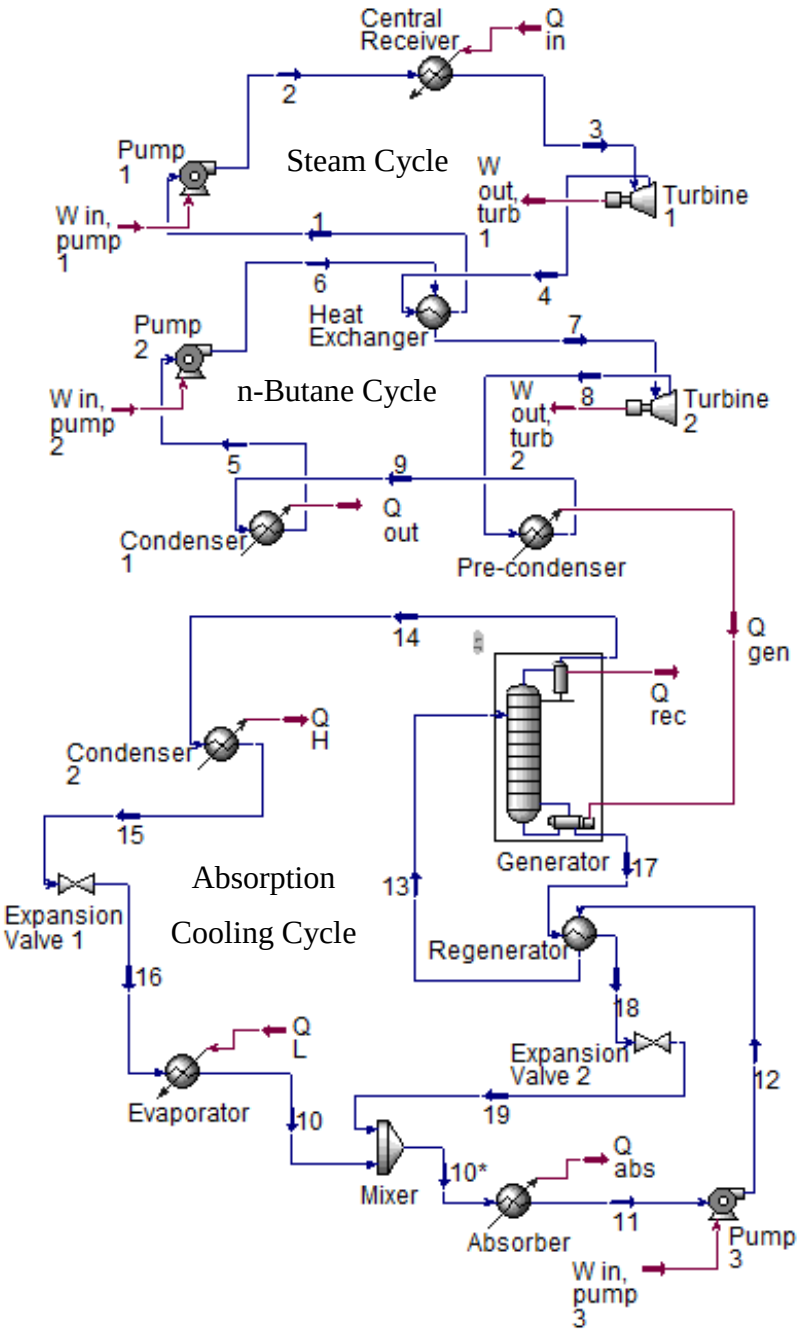

Figure 3.7: The Model of the Trigeneration System in Aspen HYSYS.

3.5.5 Mathematical Models for the Trigeneration System

Similar to the cogeneration system, the trigeneration system produces electric power and hydrogen gas. Thus, the equations developed for calculating the outputs of the cogeneration system could also be applied to the trigeneration system. The electric power and the hydrogen production rate of the trigeneration system were determined from Equation 3.4 and 3.6 respectively.

3.5.5.1 Coefficient of Performance (COP) of the Absorption Chiller

The performance of the absorption chiller was assessed by evaluating its coefficient of performance (COP). The COP of the absorption chiller could be calculated by using Equation 3.9. All the parameters required for this calculation could be determined from the simulation results in Aspen HYSYS.

$$COP_{AC} = \frac{\dot{Q}_L}{\dot{Q}_{gen} + \dot{W}_{in,\,pump\,3}} \tag{3.9}$$

where

COP_{AC} = coefficient of performance of the absorption chiller

$\dot{Q}_L$ = rate of heat removed from the cold space, kW

$\dot{Q}_{gen}$ = rate of heat transferred to the generator of the absorption chiller, kW

$\dot{W}_{in,\,pump\,3}$ = power supplied to Pump 3 in the absorption chiller, kW

3.5.5.2 Efficiency of the Trigeneration System

The efficiency of the trigeneration system could be determined by using a similar equation as the cogeneration system. Additionally, the cooling capacity output by the absorption chiller was taken into account while evaluating the efficiency of the trigeneration system. Thus, the mathematical equation for calculating the efficiency of the trigeneration system is as follows:

$$\eta_{trigen} = \frac{(\dot{W}_{elec\,1} - \dot{W}_{in,\,pump\,1}) + (\dot{W}_{out,\,PEM} - \dot{W}_{in,\,pump\,2}) + (\dot{Q}_L - \dot{W}_{in,\,pump\,3})}{\dot{Q}_{in}} \times 100\% \tag{3.10}$$

where

η_{trigen} = efficiency of the trigeneration system

3.5.6 Criteria for Selecting the Final Operating Parameters of the Proposed Multigeneration Systems

As mentioned previously, the operating parameters of the binary vapour cycle and the absorption chiller were decided based on the trial and error approach. The final operating pressures, temperatures, and mass flow rates of the working

fluids were selected from the list of successful runs that provided the highest efficiency for the system. However, not all the successful simulations were acceptable. To select the most appropriate operating parameters for the proposed multigeneration systems, the simulation results must satisfy several criteria, as listed below:

(i) In most solar power tower systems today, the heat transfer fluid can be heated up to 565 ℃ in the central receiver (Singer, et al., 2014). Therefore, the upper temperature limit of the steam after receiving concentrated solar energy in the central receiver (state point 3) was assumed to be 565 ℃.

(ii) The dryness fractions (the amount of vapour that presents in the saturated liquid-vapour mixture) at the turbine exits (state points 4 and 8) must be higher than 90%. This is because a lower dryness fraction implies that a higher portion of working fluid is condensed into the liquid phase during the expansion process in the turbine. This situation is undesirable as the liquid working fluid can erode the turbine blades.

(iii) In order to supply heat energy to activate the absorption cooling process, the temperature of the n-butane at state point 8 must be higher than 100 ℃ to ensure an efficient heat transfer from the n-butane to the ammonia-water solution in the generator of the absorption chiller.

(iv) The autoignition temperature of n-butane is 405 ℃. Beyond 405 ℃, the n-butane will be spontaneously ignited without any source of ignition (Engineering ToolBox, 2003). Thus, the temperature of the n-butane at any stage of the bottoming cycle must not exceed 405 ℃.

3.6 Life Cycle Assessment (LCA) of the Proposed Multigeneration Systems

Life cycle assessment (LCA) is a method for examining the environmental impacts and resources used throughout the whole life cycle of a product. Specifically, LCA enables the quantification of environmental burdens over the stages of raw material extraction, production, usage, and waste disposal of a

product. Other than product, LCA can also be used to evaluate the environmental impacts of a process, a service, or an activity. In general, an LCA study consists of four main phases as defined by ISO Standards 14040 and 14044. The four phases are goal and scope definition, life cycle inventory analysis, life cycle impact assessment, and interpretation of results (Finnveden, et al., 2009; Azapagic, 1999).

3.6.1 Goal and Scope Definition

Defining an explicit goal and scope was the first step of performing an LCA. In this study, it was of interest to assess the life cycles of the proposed multigeneration systems. However, the proposed systems are the huge power plants that consist of a number of subsystems such as the solar field, the binary vapour cycle, and the proton exchange membrane (PEM) electrolyzer. The analysis of assessing the environmental impacts due to the construction of these power systems will therefore be extremely complex. Hence, to simplify the analysis, the LCA performed in this study only focused on the processes that happen in the cogeneration and the trigeneration systems. That is to say, only the environmental impacts due to the production of electric power, hydrogen gas, and cooling capacity (for the trigeneration system) were examined. The functional unit of the analysis was defined as 1 hour, which means that the analysis evaluated environmental impacts when the systems operate for 1 hour.

3.6.2 Life Cycle Inventory Analysis

Once the goal and scope of the LCA were defined, the life cycle inventory analysis was performed. This step was basically to collect data on the inputs and outputs of the processes. The inputs and outputs of the multigeneration systems are mainly energies. The flow model in Figure 3.8 summarizes the energies that flow across the systems. Other than energy, the power generation systems will not work without the working fluids. Hence, the working fluids that circulate in the binary vapour cycle and the absorption cooling cycle (for the trigeneration system) were also considered as the inputs of the processes.

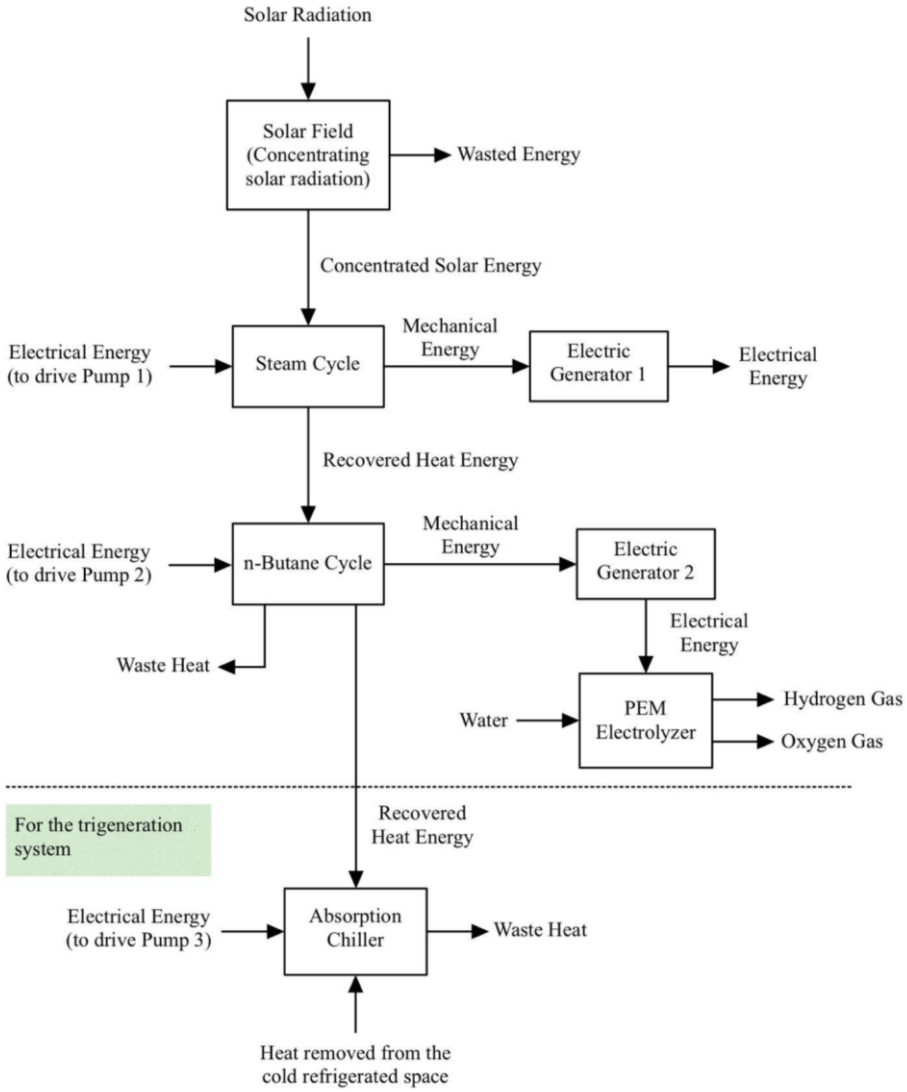

Figure 3.8: The Flow Model for the Proposed Multigeneration Systems.

In the proposed multigeneration systems, pumps are the inevitable components as they are responsible to raise the pressure of the working fluids. In general, a pump converts electrical energy to mechanical energy to transfer a fluid from one location to another. Hence, for the cogeneration and the trigeneration systems to work, electrical energy must be supplied to the pumps. In this study, it was assumed that the electrical energy supplied to the pumps was generated by the fossil fuel power station. In other words, the electrical energy consumed by the pumps was assumed to be generated through the combustion of fossil fuels. The process of generating the electricity needed to drive the pumps had also been considered while evaluating the environmental impacts of the cogeneration and the trigeneration processes.

Furthermore, the working fluids of the systems were also considered as the inputs of the processes. The processes of producing the working fluids (water, n-butane, and ammonia for the absorption chiller) were also taken into account while performing the LCA for the proposed multigeneration systems. However, both the binary vapour cycle and the absorption cooling cycle (for the trigeneration system) are closed cycles. In closed cycles, the working fluids are not discharged from the systems and are recirculating after the completion of each cycle. By further assuming that no working fluids are leaked out from the systems, the masses of the working fluids remain constant throughout the operation of the multigeneration systems. Hence, the emissions due to the production of working fluids could be considered as one-time emissions.

3.6.3 Life Cycle Impact Assessment

Life cycle impact assessment was the third phase for conducting the LCA. This step was accomplished with the aid of LCA software. The LCA software chosen for this purpose was GaBi. By modelling the flow model illustrated in Figure 3.8 in GaBi, the environmental impacts of producing electric power, hydrogen gas, and cooling capacity in the proposed multigeneration systems could be determined. In this study, the impact categories chosen to be analyzed were global warming potential, acidification potential, and human toxicity potential.

3.6.4 Summary of Life Cycle Assessment Methodology

The key points defined during the first three phases of the LCA are summarized in Table 3.1. The last phase of the LCA, which is the interpretation of results, will be presented in Chapter 4.

Table 3.1: Summary of Life Cycle Assessment Methodology.

Phase	Description
Goal and Scope	• To assess the environmental impacts caused by the processes of generating electric power, hydrogen gas, and cooling capacity (for trigeneration system) in the proposed multigeneration systems. • Functional unit: 1 hour of operation

Table 3.1 (Continued)

Life Cycle Inventory Analysis	• Inputs: Solar energy, electrical energy to drive the pumps, and the working fluids of the binary vapour cycle (water and n-butane) and the absorption cooling cycle (ammonia and water) • Outputs: Electric power, hydrogen gas, and the waste heat emitted to the atmosphere • Assumption 1: The electricity needed to power the pumps is generated through the combustion of fossil fuels. • Assumption 2: No working fluids are leaked from the systems and thus the productions of working fluids are one-time process.
Life Cycle Impact Assessment	• LCA Software: GaBi • Impact Categories: Global warming potential, acidification potential, and human toxicity potential

3.6.5 Life Cycle Assessment of the Cogeneration System in GaBi

As mentioned previously, GaBi was the software chosen to evaluate the environmental impacts of the processes that take place in the proposed multigeneration systems. To achieve the goal of the LCA, the flow model depicted in Figure 3.8 was modelled in GaBi. The solar cogeneration system modelled in GaBi is shown in Figure 3.9.

In GaBi, all the processes that occur in the solar cogeneration system were created and the inputs and outputs of each process were defined. The magnitudes of the input and output energies and the amount of working fluids required by the system were determined from the simulation results obtained from Aspen HYSYS. For instance, after the process simulation was done in Aspen HYSYS, the energies consumed by the pumps and the mechanical energies generated by the turbines could be known. The magnitudes of these energies were then input to the processes created in GaBi to perform the LCA for the proposed cogeneration system.

In comparison with the flow model in Figure 3.8, it can be noticed that the model in Figure 3.9 contains two processes that are not directly related to the cogeneration system. The two processes are the generation of electricity needed to drive the pumps (named as “Electricity grid mix” in the model in

Figure 3.9) and the butane refinery process. In GaBi, the input energy or material supplied to a process must be linked to a production process that produces that particular energy or material. Therefore, the electricity supplied to the steam and the n-butane cycles (for powering the pumps) must be connected to an electricity generation process. It should be kept in mind that the electricity supplied to the pumps was assumed to be generated through the combustion of fossil fuels as explained in Section 3.6.2. Similarly, a butane refinery process had been added to the model to supply the required amount of butane to the n-butane cycle. These two processes had also been taken into account while evaluating the overall environmental impacts caused by the processes in the cogeneration system.

Furthermore, it is quite obvious that certain inputs and outputs shown in the flow model in Figure 3.8 are missing from the actual model of the cogeneration system in Figure 3.9. For example, the solar radiation, water, and waste heat emitted to the atmosphere are absent from the model in Figure 3.9. In fact, these inputs and outputs are not missing, they are just not being displayed in the system modelled in GaBi. In GaBi, these "missing" inputs and outputs are known as elementary flows, which are defined as the flows that have direct interaction with the environment (i.e. the energy or material that is directly taken from or released into the environment). Elementary flows do not visually appear on the model created in GaBi. Hence, the solar radiation, water, and waste heat emitted to the atmosphere are not displayed in the model of the cogeneration system created in GaBi as they are all classified as elementary flows.

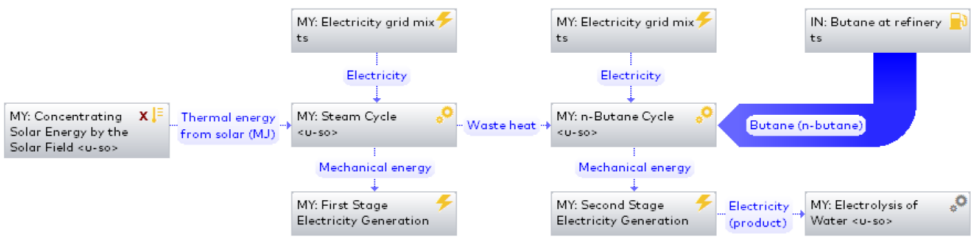

Figure 3.9: The Solar Cogeneration System Modelled in GaBi.

3.6.6 Life Cycle Assessment of the Trigeneration System in GaBi

Similar to the solar cogeneration system, the life cycle of the solar trigeneration system was also assessed through GaBi software. By referring to the flow model in Figure 3.8, the processes that happen in the trigeneration system are essentially the same as in the cogeneration system, except that an additional absorption cooling process has taken place in the trigeneration system. Thus, an absorption cooling process that utilizes the waste heat rejected by the n-butane cycle had been added to the cogeneration model in Figure 3.9 to form the model of the trigeneration system in GaBi.

The trigeneration system modelled in GaBi is illustrated in Figure 3.10. For the absorption cooling process to happen, electrical energy must be supplied to the pump in the absorption chiller so that the pump can transfer the ammonia-water solution from the absorber to the generator. Hence, the absorption cooling process created in GaBi was connected to an electricity generation process as shown in Figure 3.10. Also, like what has been mentioned earlier, the refrigerant used in the absorption chiller is ammonia. To enable the cooling process to occur, an ammonia production process was added to supply the required amount of ammonia to the absorption cooling process. The electric power needed by the pump and the amount of ammonia required by the absorption chiller were determined from the results of the process simulation in Aspen HYSYS.

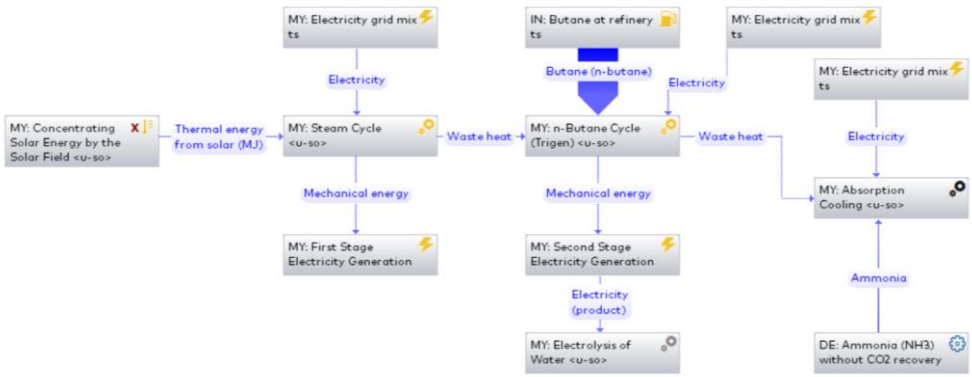

Figure 3.10: The Solar Trigeneration System Modelled in GaBi.

3.7 Work Plan

A proper work plan is necessary to ensure the project's goals can be achieved. After understanding the project scope and requirements, a work breakdown

structure was prepared to break the project into smaller tasks. Also, to constantly monitor the work progress and avoid any unnecessary delays, the Gantt charts that illustrate the project schedules had been prepared. The work breakdown structure is illustrated in Figure 3.11 whereas the Gantt charts for the project can be found in Appendix A.

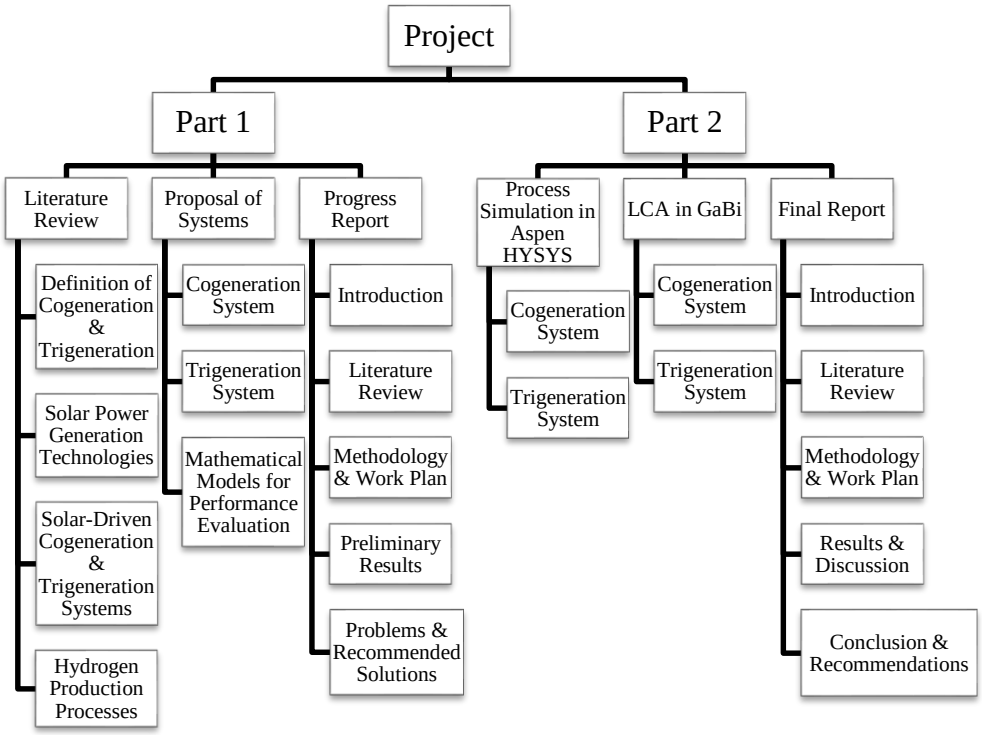

Figure 3.11: Work Breakdown Structure of the Project.

Table 3.2: The Main Tasks for Part 1 of the Project.

Task	Duration	Description
Literature Review	5 weeks	• To understand the definitions and concepts of cogeneration and trigeneration. • To study the various technologies of solar power generation. • To study and investigate the solar-driven cogeneration and trigeneration systems proposed by other researchers. • To discover the various hydrogen production processes.

Table 3.2 (Continued)

Proposal of Multigeneration Systems	3 weeks	• To develop cogeneration and trigeneration systems that produce hydrogen and other useful output(s) from solar energy. • To derive mathematical equations for evaluating the performances (efficiencies) of the proposed cogeneration and trigeneration systems.
Progress Report Writing	9 weeks	• To introduce the background and objectives of the project. • To summarize the findings of literature review. • To describe the proposed cogeneration and trigeneration systems. • To present the methodology and work plan of the project.

Table 3.3: The Main Tasks for Part 2 of the Project.

Task	**Duration**	**Description**
Process Simulations in Aspen HYSYS	4 weeks	• To learn to use the process simulation software, which is Aspen HYSYS. • To model the proposed cogeneration and trigeneration systems in Aspen HYSYS and perform the process simulations. • To evaluate the efficiencies of the proposed systems based on the simulation results.
Life Cycle Assessment (LCA) in GaBi	4 weeks	• To learn to use the LCA software, which is GaBi. • To model the proposed cogeneration and trigeneration systems in GaBi and perform the LCA. • To evaluate the environmental impacts caused by the processes in the proposed systems.

Table 3.3 (Continued)

Final Report Writing	8 weeks	• To present and discuss the simulation results. • To present and discuss the LCA results. • To compare the performances and the environmental impacts of the proposed cogeneration and trigeneration systems. • To conclude the project and suggest recommendations for improvements.

3.8 Summary

In summary, the proposed cogeneration system utilizes solar energy to produce electric power and hydrogen gas simultaneously. The trigeneration system is the cogeneration system added with an absorption chiller. Hence, the trigeneration system can produce an additional cooling capacity. The analysis of energy flows in the solar field was done through calculations. On the other hand, the binary vapour cycle and the absorption cooling cycle (for the trigeneration system) were modelled in Aspen HYSYS with the purpose of determining the efficiencies of the multigeneration systems. Additionally, GaBi software was used to evaluate the environmental impacts caused by the power generation, hydrogen production, and absorption cooling processes that take place in the proposed multigeneration systems.

CHAPTER 4

RESULTS AND DISCUSSION

4.1 Introduction

In this chapter, the results of solar field energy analysis, process simulations, and life cycle assessment (LCA) for the proposed multigeneration systems are presented. Besides that, the outputs and the efficiencies of the multigeneration systems are calculated. In addition, some compressive discussions on the results and the performances of the multigeneration systems are also covered.

4.2 Results of Energy Flow Analysis for the Solar Field

The solar field in the proposed multigeneration systems serves to reflect and focus solar radiation onto the central receiver to produce high-temperature heat to vaporize the water into superheated steam. Hence, the ultimate goal of performing the energy flow analysis for the solar field was to determine the rate of concentrated solar energy supplied to the water in the binary vapour cycle.

4.2.1 Calculations of Energy Transfer Rates in the Solar Field

As discussed in Section 3.5.1, the energy flow analysis for the solar field was done through calculations since the solar field was unable to be modelled in the process simulation software. The parameters required for this analysis and their values are summarized in Table 4.1.

Table 4.1: Parameters Needed for the Calculations of Energy Transfer Rates in the Solar Field.

Parameter	Value	Source
Number of Heliostats	560	Assumption
Area of each Heliostat	100 m^2	Assumption
Total Area of Heliostats (*A*)	56 000 m^2	N/A
Direct Normal Irradiation (*DNI*)	0.375 kW/m^2	The World Bank and Solargis (2020)

Table 4.1 (Continued)

Efficiency of the Heliostat Field (η_{HF})	75%	Xu, et al. (2011)
Efficiency of the Central Receiver (η_{CR})	90%	Xu, et al. (2011)

With the values listed in Table 4.1, the calculations of energy transfer rates in the solar field could be done. The calculations were performed by using Equations 3.1 to 3.3 as explained in Section 3.5.1.

Rate of heat received by the heliostats ($\dot{Q}_{helios}$):

$$\dot{Q}_{helios} = A \times DNI = 56\,000\ \text{m}^2 \times 0.375\ \text{kW/m}^2 = 21\,000\ \text{kW}$$

Rate of heat received by the central receiver ($\dot{Q}_{CR}$):

$$\dot{Q}_{CR} = \eta_{HF}\dot{Q}_{helios} = 0.75 \times 21\,000\ \text{kW} = 15\,750\ \text{kW}$$

Rate of heat received by the water in the central receiver ($\dot{Q}_{in}$):

$$\dot{Q}_{in} = \eta_{CR}\dot{Q}_{CR} = 0.90 \times 15\,750\ \text{kW} = 14\,175\ \text{kW}$$

4.2.2 Interpretation of the Calculated Results

Based on the results of the calculations, it can be deduced that, on the days when the DNI is 0.375 kW/m^2, the heliostats with a total area of 56 000 m^2 will receive solar radiation at a rate of 21 000 kW. However, it is important to keep in mind that not all the solar radiation received by the heliostats will be reflected and concentrated onto the central receiver located at the top of the solar power tower. It is unavoidable that part of the solar radiation will be reflected to other directions (not to the central receiver) and the fact that the existence of the solar power tower may block some solar radiation from reaching the heliostats (shadowing effect). Therefore, at a heliostat field efficiency of 75%, the rate of solar thermal energy received by the central receiver is 15 750 kW.

It is well known that none of the systems in this world can achieve 100% of efficiency. The central receiver is not an exception. By having an efficiency of 90%, the central receiver allows the water to receive concentrated solar

energy at a rate of 14 175 kW. The remaining 10% of energy is lost mainly due to the heat transfer processes such as conduction, convection, and radiation that happen in the central receiver.

4.3 Performance Evaluation of the Cogeneration System

In order to evaluate the performance of the cogeneration system, the binary vapour cycle in the cogeneration system was modelled in Aspen HYSYS to enable the process simulation to be performed. The rate of concentrated solar energy received by the water determined from the solar field energy analysis serves as an input to the process simulation. After running the process simulation, the efficiency, which indicates the performance of the cogeneration system, could be evaluated.

4.3.1 Results of Process Simulation for the Cogeneration System

As mentioned in Section 3.5.2, the operating parameters of the cogeneration system, such as the lower and upper pressure limits, the temperatures, and the mass flow rates of the working fluids were decided based on the trial and error approach. In this study, several sets of operating parameters had been input to Aspen HYSYS and their simulation results were tabulated. The tabulated results can be found in Appendix B. From the list of simulation results in Appendix B, the set of operating parameters that provides the highest efficiency for the cogeneration system is listed in Table 4.2. In addition, the simulation results for the rates of flow of energy across the binary vapour cycle in the cogeneration system are tabulated in Table 4.3.

Table 4.2: The Selected Operating Parameters for the Binary Vapour Cycle.

Cycle	State Point	Pressure (kPa)	Temperature (℃)	Dryness Fraction	Phase
Steam Cycle ($\dot{m}_{steam}$ = 5 kg/s)*	1	500*	151.80	0*	Saturated Liquid
	2	13 000*	153.60	0	Subcooled Liquid
	3	13 000*	564.70	1	Superheated Steam

Table 4.2 (Continued)

	4	500*	165.00	1	Superheated Steam
n-Butane Cycle ($\dot{m}_{butane}$ = 21 kg/s) *	5	450*	46.49	0*	Saturated Liquid
	6	2 000*	47.66	0	Subcooled Liquid
	7	2 000*	148.70	1	Superheated Vapour
	8	450*	103.70	1	Superheated Vapour

Remark: The values with the symbol * represent the input values of the process simulation.

Table 4.3: Rates of Flow of Energy across the Binary Vapour Cycle.

Cycle	**Component**	**Type of Energy Flow**	**Rate of Flow of Energy (kW)**	**Isentropic Efficiency**
Steam Cycle	Central Receiver	Input Heat Energy ($\dot{Q}_{in}$)	14 175.00*	N/A
	Pump 1	Input Power ($\dot{W}_{in,\,pump\,1}$)	81.52	85%
	Turbine 1	Output Power ($\dot{W}_{out,\,turb\,1}$)	3 475.00	85%
n-Butane Cycle	Pump 2	Input Power ($\dot{W}_{in,\,pump\,2}$)	70.05	85%
	Turbine 2	Output Power ($\dot{W}_{out,\,turb\,2}$)	1 299.00	85%
	Condenser	Rate of Heat Rejection ($\dot{Q}_{out}$)	9 552.78	N/A

With the simulation results, a temperature versus specific entropy (*T*-*s*) diagram for the binary vapour cycle can be sketched. The sketched *T*-*s* diagram is illustrated in Figure 4.1.

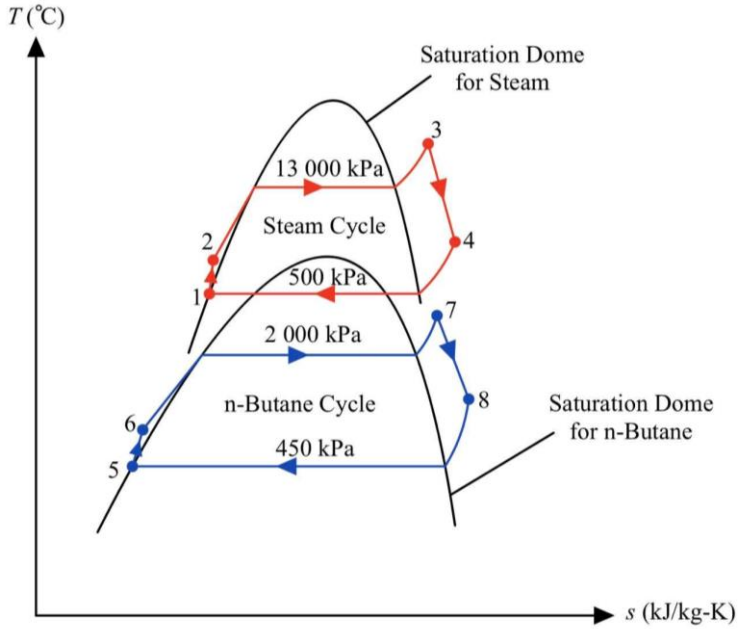

Figure 4.1: Temperature versus Specific Entropy (*T*-*s*) Diagram for the Binary Vapour Cycle in the Cogeneration System.

4.3.2 Outputs and Efficiency of the Cogeneration System

After performing the process simulation, the electric power and hydrogen production rate of the cogeneration system could be computed. Consequently, the efficiency of the cogeneration system could be evaluated. Please take note that the equations applied to the following calculations are explained in Section 3.5.3.

The magnitudes of electric powers generated by the cogeneration system:

$$\dot{W}_{elec\ 1} = 0.9\dot{W}_{out,\ turb\ 1} = 0.9\ (3\ 475\ \text{kW}) = 3\ 127.5\ \text{kW}$$

$$\dot{W}_{elec\ 2} = 0.9\dot{W}_{out,\ turb\ 2} = 0.9\ (1\ 299\ \text{kW}) = 1\ 169.1\ \text{kW}$$

The rate of hydrogen production by the cogeneration system could be determined from Equation 3.6. The parameters required for this calculation are summarized in Table 4.4.

Table 4.4: Parameters Required for the Calculation of Hydrogen Production Rate.

Parameter	Value	Source
Efficiency of the PEM Electrolyzer (η_{PEM})	70%	Sánchez-Bastardo, et al. (2021)
Electric Power Generated by Electric Generator 2 ($\dot{W}_{elec\,2}$)	1 169.1 kW	Simulation and Calculated Results
Lower Heating Value (LHV) of Hydrogen	119 880 kJ/kg	Dufo-López and Bernal-Agustín (2008)

Hence, the rate of hydrogen produced by the cogeneration system is:

$$\dot{m}_{H_2} = \frac{\eta_{PEM}\dot{W}_{elec\,2}}{LHV} = \frac{0.70 \times 1169.1\ \text{kW}}{119\ 880\ \text{kJ/kg}} = 6.827 \times 10^{-3}\ \text{kg/s} = 24.58\ \text{kg/h}$$

The output power of the PEM electrolyzer ($\dot{W}_{out,\,PEM}$):

$$\dot{W}_{out,\,PEM} = \eta_{PEM}\dot{W}_{elec\,2} = 0.70\ (1\ 169.1\ \text{kW}) = 818.37\ \text{kW}$$

Therefore, the overall efficiency of the cogeneration system is:

$$\eta_{cogen} = \frac{(\dot{W}_{elec\,1} - \dot{W}_{in,\,pump\,1}) + (\dot{W}_{out,\,PEM} - \dot{W}_{in,\,pump\,2})}{\dot{Q}_{in}} \times 100\%$$

$$\eta_{cogen} = \frac{(3\ 127.5\ \text{kW} - 81.52\ \text{kW}) + (818.37\ \text{kW} - 70.05\ \text{kW})}{14\ 175.00\ \text{kW}} \times 100\%$$

$$\eta_{cogen} = 26.77\%$$

Table 4.5: Summary of the Calculated Results for the Cogeneration System.

Parameters	Values
Electric Power	3 127.5 kW
Hydrogen Production Rate	24.58 kg/h
Output Power of the PEM Electrolyzer	818.37 kW
Efficiency of the Cogeneration System	26.77%

4.3.3 Discussion on the Simulation Results and the Performance of the Cogeneration System

After running several successful process simulations, the set of operating parameters that provides the highest efficiency for the cogeneration system is tabulated in Table 4.2. By referring to the results in Table 4.2, it can be found that the steam cycle operates within the pressure limits of 500 kPa and 13 000 kPa. Although it makes sense that increasing the upper pressure limit can increase the output power generated by the turbine, it is important to keep in mind that there are several criteria that must be fulfilled by the simulation results, as explained in Section 3.5.6. The first criteria stated in Section 3.5.6 requires the maximum temperature of the steam to be lower than 565 ℃. If the upper pressure limit is increased further, the temperature of the steam at state point 3 will exceed 565 ℃. For instance, when the upper pressure limit is increased to 14 000 kPa, the temperature of steam at state point 3 will be 569.6 ℃ for the same amount of solar energy received. Obviously, this temperature has exceeded the maximum allowable limit stated in Section 3.5.6. For that reason, the upper pressure limit of the steam cycle is capped at 13 000 kPa, in which the temperature of the steam at state point 3 is 564.7 ℃.

Moreover, it is worth taking note that both pumps in the binary vapour cycle have an isentropic efficiency of 85%. This indicates that, for a given input power, the pumps can achieve 85% of work done by an isentropic (idealized) pump. As an example, Pump 1 in the topping cycle which has an isentropic efficiency of 85% consumes 81.52 kW of power to raise the pressure of the water from 500 kPa to 13 000 kPa. If the isentropic efficiency of Pump 1 is now increased to 100% (the idealized pump), the power required to drive the pump to perform a similar workload will be reduced to 69.29 kW, which is 15% lower than the power consumed by the non-isentropic pump. Hence, the higher the isentropic efficiency of the pump, the higher the extent to which the pump behaves like an idealized pump, and thus the lower the amount of power required by the pump to perform a given workload.

Similarly, the turbines in the binary vapour cycle are also having an isentropic efficiency of 85%. Unlike the pumps, turbines are the components that generate powers, which are the desired outputs of the system. With the isentropic efficiency of 85%, the powers produced by the turbines are 15%

lower than the powers generated by the isentropic (idealized) turbines under similar operating conditions. By taking Turbine 2 in the bottoming cycle as an example, the power produced by Turbine 2 is 1 299 kW when its isentropic efficiency is 85%. In the case that its isentropic efficiency is increased to 100%, its output power will be increased to 1 528 kW. Therefore, one can deduce that an increment in the isentropic efficiency of the turbine will lead to a higher power being generated. Thus, the overall efficiency of the cogeneration system can be increased.

Although it seems like it would be better to increase the isentropic efficiencies of the pumps and the turbines to 100% to improve the efficiency of the cogeneration system, it should always be remembered that an isentropic process is not possible to happen in reality. An isentropic process can be viewed as an idealized process that is adiabatic and reversible (Gyӧrke, et al., 2018). However, in actual power plants, an adiabatic process is not possible to achieve since there is always some heat loss from the working fluid to the surrounding when the working fluid flows from one component to another. In addition, irreversibility such as fluid friction and viscous dissipation also cause the processes in the binary vapour cycle to be irreversible (Adesanya and Makinde, 2015). Therefore, all processes that occur in actual power plants are non-isentropic since both the adiabatic and reversible processes are not possible to happen in the real world. To make the proposed cogeneration system reflects the operation of the actual power plant, the isentropic efficiencies of the pumps and the turbines were considered to be 85%. In other words, the pumping of working fluids in the pumps and the expansion of working fluids in the turbines are not isentropic processes. Due to this reason, processes 1 to 2, 3 to 4, 5 to 6, and 7 to 8 do not appear as vertical straight lines in the temperature versus specific entropy (*T*-*s*) diagram shown in Figure 4.1.

Furthermore, the operating pressures of the n-butane cycle are 450 kPa and 2 000 kPa, which are much lower compared to the steam cycle. This is because the n-butane cycle utilizes the waste heat rejected by the steam cycle to produce additional output. To generate power in the turbine, the n-butane must be completely vaporized into superheated vapour after receiving heat from the steam in the topping cycle. Hence, to allow heat transfer process to take place in the heat exchanger while ensuring the n-butane can be completely vaporized

into superheated vapour, the saturation temperature (boiling point) of the n-butane must be lower than the temperature of the heat source (steam at state point 4). By referring to Table 4.2, the temperature of the steam at state point 4 is 165 ℃. On the other hand, the saturation temperature of n-butane at 2 000 kPa is approximately 114 ℃. Therefore, by running the bottoming cycle at an upper pressure of 2 000 kPa, heat energy can be effectively transferred from the steam to the n-butane in the heat exchanger while completely turning the n-butane into superheated vapour. If the pressure is increased further, the n-butane might not be completely vaporized into superheated vapour since the saturation temperature of a fluid increases with its pressure.

Other than operating pressure, another important parameter that decides whether the n-butane can be completely vaporized into superheated vapour is the mass flow rate. If the mass flow rate of the n-butane is too high, the amount of heat supplied by the topping cycle will not be sufficient to vaporize the n-butane completely. In contrast, if the mass flow rate of the n-butane is too low, the outlet temperature of the n-butane (at state point 7) will be unreasonably high (higher than the temperature of the steam at state point 4). Thus, the mass flow rate of the n-butane has to be properly adjusted to ensure the successfulness of the simulation. After several iterations, it was found that the optimum mass flow rate for the n-butane was 21 kg/s. At the mass flow rate of 21 kg/s, the n-butane can be completely vaporized into superheated vapour and its temperature at the outlet of the heat exchanger is 148.70 ℃. This outlet temperature is justified as logical and reasonable as it is lower than the temperature of the heat source.

In terms of performance, it was found that the efficiency of the cogeneration system is around 26.77%. With an input solar thermal energy of 14 175 kW, the mechanical powers produced by the topping and bottoming cycles are 3 475 kW and 1 299 kW respectively. By connecting the turbines' shafts to the electric generators with 90% of efficiency, the electric powers generated in the topping and bottoming cycles are 3 127.5 kW and 1 169.1 kW respectively. The remaining 10% of energy is dissipated as heat due to the electrical resistance offered by the wires and other parts of the electric generators. The electric power generated by the topping cycle is the first desired output of the cogeneration system whereas the electric power produced by the

bottoming cycle is fed to a proton exchange membrane (PEM) electrolyzer with an energy efficiency of 70%. As a result, the output power produced by the PEM electrolyzer is 818.37 kW. The output of the PEM electrolyzer can also refer to the rate of hydrogen production. Since the PEM electrolyzer is producing energy at the rate of 818.37 kJ/s and 1 kg of hydrogen carries 119 880 kJ of energy (based on the lower heating value of hydrogen), it can be estimated that the PEM electrolyzer is producing hydrogen at the rate of 6.827×10^{-3} kg/s, which is equivalent to 24.58 kg/h. In summary, the cogeneration system utilizes solar energy to produce two useful outputs simultaneously, which are 3 127.5 kW of electric power and 24.58 kg/h of hydrogen gas.

Although the efficiency of the cogeneration system is not very impressive, it is still more efficient than a single-generation power plant. By considering a single-generation power plant that operates under the same conditions as the proposed cogeneration system (i.e. the ordinary steam power cycle without the n-butane cycle), the efficiency of the single-generation power plant is approximately 21.49% (the calculation of efficiency can be found in Appendix C). Under single-generation mode, approximately 10 780.56 kW of thermal energy is transferred to the cooling tower to be released into the atmosphere as waste heat. Instead of letting this huge amount of heat energy to go wasted, utilizing it for other purposes helps to boost the efficiency of the power plant. The proposed cogeneration system clearly illustrates that by using the otherwise-wasted heat energy to power the n-butane cycle, an additional output, which is hydrogen gas, can be produced without having to supply extra energy to the system. The production of additional output from the same amount of input energy implies that the overall efficiency of the system is higher.

4.4 Performance Evaluation of the Trigeneration System

Similar to the cogeneration system, the proposed trigeneration system was modelled in Aspen HYSYS and the process simulation was performed to evaluate the performance of the system. The input and output energies of the trigeneration system could be determined from the simulation results. After that, the efficiency of the trigeneration system could be calculated.

4.4.1 Results of Process Simulation for the Trigeneration System

As described previously, the proposed trigeneration system is similar to the cogeneration system, except that an absorption chiller has been added to the system to produce cooling capacity. To compare the contrast the performances between the cogeneration and trigeneration systems, the binary vapour cycle in the trigeneration system was set to have the same operating parameters as the cogeneration system. The operating parameters for the binary vapour cycle are listed in Table 4.2.

Similar to the binary vapour cycle, the operating parameters of the absorption chiller were decided based on the trial and error approach since there were no explicit guidelines on how to determine the operating parameters of the absorption chiller. To achieve this, the absorption chiller had been modelled in Aspen HYSYS and several iterations of process simulation had been run. The list of simulation results for the absorption chiller can be found in Appendix D. From the list of successful iterations, the set of operating parameters that provides the highest cooling capacity is listed in Table 4.6. Besides that, the simulation results for the input and output energies of the trigeneration system are recorded in Table 4.7.

Table 4.6: The Selected Operating Parameters for the Absorption Chiller.

State Point	Pressure (kPa)	Temperature (℃)	Mass Fraction of Working Fluid	Mass Flow Rate (kg/s)	Phase of Working Fluid
10	200	-18.52	100% NH_3	0.05	Saturated Vapour
11	200	6.71	52% NH_3 + 48% H_2O	0.20	Liquid
12	1 300	6.82	52% NH_3 + 48% H_2O	0.20	Liquid
13	1 300	40.00	52% NH_3 + 48% H_2O	0.20	Liquid
14	1 300	33.94	100% NH_3	0.05	Saturated Vapour

Table 4.6 (Continued)

15	1 300	33.94	100% NH_3	0.05	Saturated Liquid
16	200	-18.53	100% NH_3	0.05	Saturated Liquid-Vapour Mixture
17	1 300	94.80	36% NH_3 + 64% H_2O	0.15	Liquid
18	1 300	51.29	36% NH_3 + 64% H_2O	0.15	Liquid
19	200	32.92	36% NH_3 + 64% H_2O	0.15	Saturated Liquid-Vapour Mixture

Table 4.7: Rates of Flow of Energy across the Trigeneration System.

Cycle	**Component**	**Type of Energy Flow**	**Rate of Flow of Energy (kW)**	**Isentropic Efficiency**
Steam Cycle	Central Receiver	Input Heat Energy ($\dot{Q}_{in}$)	14 175.00	N/A
	Pump 1	Input Power ($\dot{W}_{in,\,pump\,1}$)	81.52	85%
	Turbine 1	Output Power ($\dot{W}_{out,\,turb\,1}$)	3 475.00	85%
n-Butane Cycle	Pump 2	Input Power ($\dot{W}_{in,\,pump\,2}$)	70.05	85%
	Turbine 2	Output Power ($\dot{W}_{out,\,turb\,2}$)	1 299.00	85%
	Condenser 1	Rate of Heat Rejection ($\dot{Q}_{out}$)	9 441.67	N/A

Table 4.7 (Continued)

Absorption Cooling Cycle	Pump 3	Input Power ($\dot{W}_{in,\,pump\,3}$)	0.33	85%
	Generator	Rate of Heat Supplied to the Absorption Chiller ($\dot{Q}_{gen}$)	111.11	N/A
	Evaporator	Cooling Capacity ($\dot{Q}_L$)	54.97	N/A
	Condenser 2	Rate of Heat Rejected to the Warm Environment ($\dot{Q}_H$)	58.56	N/A
	Absorber	Rate of Heat Rejected by the Absorber ($\dot{Q}_{abs}$)	101.78	N/A

4.4.2 Outputs and Efficiency of the Trigeneration System

The trigeneration system utilizes solar energy to produce electric power, hydrogen gas, and cooling capacity concurrently. Since it was assumed that the binary vapour cycle of the trigeneration system operates under the same conditions as the cogeneration system, the electric power and hydrogen production rate of the trigeneration system will be similar to the cogeneration system. Hence, the trigeneration system produces 3 127.5 kW of electric power and 24.58 kg/h of hydrogen gas. Other than that, the trigeneration system with the absorption chiller can produce 54.97 kW of cooling capacity. The performance of the absorption chiller was evaluated by calculating its coefficient of performance (COP) using Equation 3.9.

$$COP_{AC} = \frac{\dot{Q}_L}{\dot{Q}_{gen} + \dot{W}_{in,\,pump\,3}} = \frac{54.97\ \text{kW}}{111.11\ \text{kW} + 0.33\ \text{kW}} = 0.4933$$

To evaluate the overall performance of the trigeneration system, the efficiency of the trigeneration system was calculated using Equation 3.10.

$$\eta_{trigen} = \frac{(\dot{W}_{elec\,1} - \dot{W}_{in,\,pump\,1}) + (\dot{W}_{out,\,PEM} - \dot{W}_{in,\,pump\,2}) + (\dot{Q}_L - \dot{W}_{in,\,pump\,3})}{\dot{Q}_{in}} \times 100\%$$

$$\eta_{trigen} = \frac{(3\,127.50\ \text{kW} - 81.52\ \text{kW}) + (818.37\ \text{kW} - 70.05\ \text{kW}) + (54.97\ \text{kW} - 0.33\ \text{kW})}{14\,175.00\ \text{kW}} \times 100\%$$

$$\eta_{trigen} = 27.15\%$$

Table 4.8: Summary of the Calculated Results for the Trigeneration System.

Parameters	Values
Electric Power	3 127.5 kW
Hydrogen Production Rate	24.58 kg/h
Output Power of the PEM Electrolyzer	818.37 kW
Cooling Capacity	54.97 kW
COP of the Absorption Chiller	0.4933
Efficiency of the Trigeneration System	27.15%

4.4.3 Discussion on the Simulation Results and the Performance of the Trigeneration System

The proposed solar trigeneration system consists of a solar field, a binary vapour cycle, a proton exchange membrane (PEM) electrolyzer, and an absorption chiller. Since it is the extension of the cogeneration system, the number of heliostats in the solar field, as well as the operating parameters of the binary vapour cycle were assumed to follow exactly the same as in the cogeneration system. Thus, the concentrated solar energy received by the water in the central receiver as well as the input and output powers of the binary vapour cycle are the same as the cogeneration system. Other than that, the rate at which hydrogen gas is produced by the trigeneration system is also similar to the cogeneration system. This is because the n-butane cycles in both systems deliver an equal magnitude of electricity to the PEM electrolyzers under similar operating parameters. Therefore, the electric power and the hydrogen production rate of

the trigeneration system are basically the same as the cogeneration system since both of them are having similar operating parameters.

The biggest difference between the cogeneration and the trigeneration systems is the existence of an absorption chiller in the trigeneration system. The n-butane in the bottoming cycle has a temperature of 103.70 ℃ after expanding in Turbine 2. To supply heat energy to activate the absorption cooling process, the n-butane at state point 8 enters the generator of the absorption chiller to transfer some heat energy to the ammonia-water solution in the generator. Due to the temperature difference, heat is transferred at a rate of 111.11 kW from the n-butane to the ammonia-water solution in the generator. With the heat energy supplied by the n-butane, a portion of the ammonia vaporizes to form saturated ammonia vapour. The saturated ammonia vapour with 100% of purity then leaves the generator at a rate of 0.05 kg/s. On the other hand, due to the formation of ammonia vapour, the remaining ammonia-water solution in the generator will be having a lower concentration of ammonia. The mass fractions of the water and the ammonia in the weak ammonia-water solution are 64% and 36% respectively. The weak ammonia-water solution is then returned to the absorber at a rate of 0.15 kg/s.

The ammonia vapour, which is the refrigerant of the absorption chiller, enters the condenser to reject heat at a rate of 58.56 kW. The heat rejection process occurs at constant pressure and temperature as the ammonia vapour is changing its phase from saturated vapour to saturated liquid (phase change process always occurs at constant temperature). After that, the saturated liquid ammonia undergoes a throttling process in the expansion valve. As a consequence, the pressure of the ammonia decreases from 1 300 kPa to 200 kPa. The ammonia leaves the expansion valve as a saturated liquid-vapour mixture with a temperature of -18.53 ℃. It enters the evaporator to absorb the heat transferred from the cold space. The transfer of heat from the cold space to the ammonia in the evaporator is the desired cooling output as this process helps to keep the chilled space at a low temperature. From the simulation results, it was found that the rate of heat transferred from the cold space to the ammonia is 54.97 kW. The ammonia eventually vaporizes into saturated vapour after receiving heat from the cold space. Similar to the heat rejection process in the condenser, the process whereby the ammonia receives heat from the chilled

space occurs at constant pressure and temperature. This is because the ammonia is changing its phase from saturated liquid-vapour mixture to saturated vapour.

After leaving the evaporator, the saturated ammonia vapour mixes with the weak ammonia-water solution in the absorber. As explained in Section 3.5.4, the absorber in the absorption chiller was represented by a combination of a mixer and a cooler in Aspen HYSYS. In the mixer, the ammonia vapour mixes with the weak ammonia-water solution to form a rich ammonia-water solution that composes of 52% of ammonia and 48% of water. The absorption process is an exothermic reaction and the heat generated from this process is removed from the absorber at a rate of 101.78 kW. Due to the absorption process, the rich ammonia-water solution leaves the absorber at a mass flow rate of 0.20 kg/s, which is the sum of the mass flow rates of the ammonia vapour (0.05 kg/s) and the weak ammonia-water solution (0.15 kg/s). Finally, the rich ammonia-water solution is transferred to the generator by the pump to receive heat energy from the n-butane in the bottoming cycle.

The power consumed by the pump in the absorption chiller is negligible, which is only 0.33 kW. This is perhaps the most attractive benefit of an absorption chiller compared to the conventional vapour-compression chiller. In the absorption chiller, the liquid ammonia-water solution is being compressed instead of vapour. In general, the power required to compress a fluid increases as the specific volume of the fluid increases. Since the specific volume of liquid is usually smaller than vapour, the power required to compress liquid is much smaller than vapour (Cengel and Boles, 2015). Thus, the power consumed by the pump in the absorption chiller is much smaller than the power consumed by the compressor in the vapour-compression chiller.

In the matter of performance, it is discovered that the efficiency of the trigeneration system is about 27.15%, which is slightly higher than the cogeneration system (η_{cogen} = 26.77%) under similar operating conditions. The small increment in the efficiency of the trigeneration system is due to the additional cooling capacity offered by the absorption chiller. By referring to the outputs generated by the trigeneration system listed in Table 4.8, it can be found that the cooling capacity delivered by the absorption chiller is much smaller than the electric power and the output power of the PEM electrolyzer. This is because absorption chillers are characterized by low coefficients of performance (COP).

Unlike the conventional vapour-compression chillers where the COP are usually higher than 1, the COP of actual absorption chillers, on the other hand, are normally less than 1 (Cengel and Boles, 2015). With a COP of less than 1, the cooling capacity output by the absorption chiller will be even smaller than the heat energy supplied to the generator of the absorption chiller. In the proposed trigeneration system, the heat source of the absorption chiller is the n-butane at state point 8, which has a temperature of 103.70 ℃ based on the simulation results. Since the temperature of the n-butane at state point 8 is rather low, it is considered as a low-grade heat source. Due to this reason, the heat energy that can be supplied to the absorption chiller is limited to 111.11 kW. With this limited heat supply, the inefficient absorption chiller can only produce 54.97 kW of cooling capacity. By taking the power consumed by the pump into consideration, the COP of the absorption chiller employed in the trigeneration system is only 0.4933.

To cut a long story short, the cooling capacity produced by the absorption chiller is not significant compared to the output powers of the electric generator and the PEM electrolyzer. Due to this reason, the efficiency of the trigeneration system is very close to the cogeneration system, despite being able to produce additional cooling output. Although the cooling capacity generated by the absorption chiller is limited, it does help to remove heat from the cold space to keep the space chilled. What makes it more attractive is that it recovers the waste heat produced by the n-butane cycle to activate the cooling process. By recovering some waste heat produced by the n-butane cycle, the absorption cooling process can be accomplished without requiring additional input heat energy.

4.5 Further Discussion on the Performances of the Cogeneration and the Trigeneration Systems

There is always a question regarding whether the trigeneration system is more efficient than the cogeneration system. It makes sense to assume that the trigeneration system can achieve higher efficiency than the cogeneration system since it produces an extra output from the same amount of input energy. This statement has also been verified by the calculations of efficiencies demonstrated in Section 4.3.2 and 4.4.2, where the efficiency of the cogeneration system is

26.77% whereas the efficiency of the trigeneration system is 27.15%. However, it should be bear in mind that, in this study, the cogeneration and trigeneration systems were set to have the same operating parameters so that the comparison of performances between the two systems was more meaningful. As explained in Section 3.5.6, there are four criteria that the simulation results have to fulfill. The third criteria stated in Section 3.5.6 requires the temperature of the n-butane at state point 8 to be higher than 100 ℃ in order to drive the absorption chiller. Since the cogeneration system does not have an absorption chiller, this criteria is optional to the cogeneration system. Meaning to say, in the cogeneration system, the temperature of the n-butane at state point 8 does not have to be higher than 100 ℃.

Now, let's consider a similar cogeneration system that operates under the following parameters:

Table 4.9: The New Operating Parameters for the Cogeneration System.

Cycle	**State Point**	**Pressure (kPa)**	**Temperature (℃)**	**Dryness Fraction**	**Phase**
Steam Cycle ($\dot{m}_{steam}$ = 5 kg/s)*	1	250*	127.40	0*	Saturated Liquid
	2	13 000*	128.90	0	Subcooled Liquid
	3	13 000*	521.90	1	Superheated Steam
	4	250*	127.40	0.9545	Saturated Liquid-Vapour Mixture
n-Butane Cycle ($\dot{m}_{butane}$ = 21 kg/s) *	5	300*	32.09	0*	Saturated Liquid
	6	1 500*	32.89	0	Subcooled Liquid
	7	1 500*	121.90	1	Superheated Vapour

Table 4.9 (Continued)

	8	300*	76.22	1	Superheated Vapour

Remark: The values with the symbol * represent the input values of the process simulation.

Table 4.10: The New Energy Flow Rates across the Cogeneration System.

Cycle	Component	Type of Energy Flow	Rate of Flow of Energy (kW)	Isentropic Efficiency
Steam Cycle	Central Receiver	Input Heat Energy ($\dot{Q}_{in}$)	14 175.00*	N/A
	Pump 1	Input Power ($\dot{W}_{in,\,pump\,1}$)	81.14	85%
	Turbine 1	Output Power ($\dot{W}_{out,\,1}$)	3 747.00	85%
n-Butane Cycle	Pump 2	Input Power ($\dot{W}_{in,\,2}$)	52.52	85%
	Turbine 2	Output Power ($\dot{W}_{out,\,2}$)	1 330.00	85%
	Condenser	Rate of Heat Rejection ($\dot{Q}_{out}$)	9 230.56	N/A

Hence, the outputs produced by the cogeneration system that operates under the new parameters listed in Table 4.9 are:

$$\dot{W}_{elec\,1,\,new} = 0.9\dot{W}_{out,\,turb\,1} = 0.9\ (3\ 747.00\ \text{kW}) = 3\ 372.3\ \text{kW}$$

$$\dot{W}_{elec\,2,\,new} = 0.9\dot{W}_{out,\,turb\,2} = 0.9\ (1\ 330.00\ \text{kW}) = 1\ 197.0\ \text{kW}$$

$$\dot{W}_{out,\,PEM\,(new)} = \eta_{PEM}\dot{W}_{elec\,2,\,new} = 0.70\ (1\ 197.0\ \text{kW}) = 837.9\ \text{kW}$$

$$\dot{m}_{H_2,\,new} = \frac{\eta_{PEM}\dot{W}_{elec\,2,\,new}}{LHV} = \frac{0.70 \times 1\ 197.0\ \text{kW}}{119\ 880\ \text{kJ/kg}} = 6.989 \times 10^{-3}\ \text{kg/s} = 25.16\ \text{kg/h}$$

Therefore, the new efficiency of the cogeneration system is:

$$\eta_{cogen,\,new} = \frac{(3\,372.3\ \text{kW} - 81.14\ \text{kW}) + (837.90\ \text{kW} - 52.52\ \text{kW})}{14\,175.00\ \text{kW}} \times 100\%$$

$$\eta_{cogen,\,new} = 28.76\%$$

Thus, it is clear that the cogeneration system is possible to achieve higher efficiency than the trigeneration system. From Table 4.9, it can be found that the temperature of the n-butane at state point 8 is 76.22 ℃, which does not fulfil the third criteria stated in Section 3.5.6. Nevertheless, this is not an issue since the n-butane in the cogeneration system does not need to supply heat energy to the absorption chiller. The n-butane with a lower temperature at state point 8 implies that more energy is converted to work during the expansion process in Turbine 2. As a result, the net power produced by the n-butane cycle is higher.

Furthermore, without having to fulfil the third criteria in Section 3.5.6, the lower pressure limit of the steam cycle can be lower. In general, a reduction in the lower pressure limit can increase the net power output and thus the efficiency of the vapour power cycle (Herath, et al., 2020). The temperature versus specific entropy (*T*-*s*) diagram in Figure 4.2 illustrates the increment in the net power output as a result of decreasing the lower pressure limit of the steam cycle.

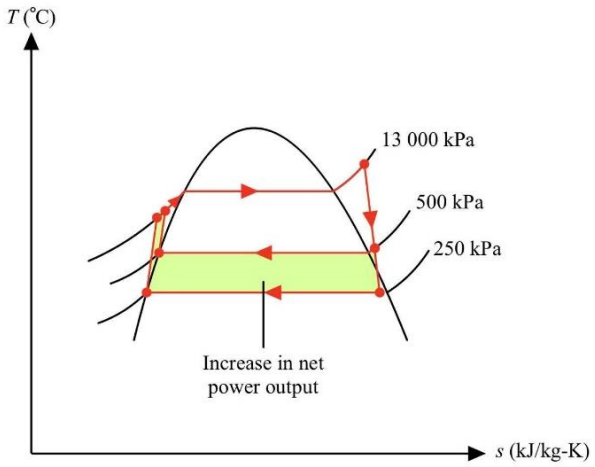

Figure 4.2: Effect of Lowering the Lower Pressure Limit of the Steam Cycle.

By reducing the lower pressure limit of the steam cycle from 500 kPa to 250 kPa, the net mechanical power (difference between the power generated by the turbine and the power consumed by the pump) generated by the steam cycle increases from 3 393.48 kW to 3 665.86 kW. As a consequence, the overall efficiency of the cogeneration system increases from 26.77% to 28.76%, which is even higher than the efficiency of the trigeneration system. Although it can be argued that the trigeneration system that employs the new set of operating parameters tabulated in Table 4.9 can also achieve higher efficiency, it should be kept in mind that the trigeneration system needs to fulfil the third criteria stated under Section 3.5.6 in order to drive the absorption chiller. According to Shirazi, et al. (2018), a single-effect absorption chiller generally requires a heat source that has a minimum temperature ranging from 80 ℃ to 100 ℃ to drive the cooling process. Based on the results in Table 4.9, the temperature of the n-butane after expanding in Turbine 2 is only 76.22 ℃, which may not be adequate to activate the absorption cooling process. Due to this reason, the new set of operating parameters listed in Table 4.9 is not applicable to the proposed trigeneration system.

Despite the fact that the efficiency of the trigeneration system may be lower than the cogeneration system, it is not completely infeasible since it has the merit of being able to produce cooling capacity. The proposed trigeneration can still be a better option for some applications, especially the industries that require low-temperature applications. Some possible applications of the proposed cogeneration and trigeneration systems will be discussed in the next section.

Remark: The operating parameters listed in Table 4.9 are only for additional discussion purposes. The remaining parts in this report only consider the cogeneration system that operates with the parameters listed in Table 4.2.

4.6 Applications of the Proposed Cogeneration and Trigeneration Systems

The proposed cogeneration and trigeneration systems are considered as small-scale power plants since their power capacities are below 10 MW (3.1275 MW for both systems). Furthermore, the proposed systems are completely driven by

solar energy without relying on fossil fuels. These characteristics make them suitable to be deployed as decentralized energy generation systems. As discussed in Section 2.4, decentralized energy systems are located closer to the sites where the energy is being consumed and usually have a power capacity ranging from 1 kW to 250 MW (Liu, et al., 2017). Hence, the proposed multigeneration systems are suitable for decentralized applications and can be built at locations near the consumers.

Other than that, both of the proposed systems are capable of producing hydrogen. Hydrogen is a useful substance that has been widely used in many industries. For example, metallurgical industries use hydrogen in the production of nickel, electronics manufacturing industries utilize hydrogen as a reducing agent to produce silicon, and fertilizer industries produce fertilizer through the reaction of hydrogen and nitrogen (Ramachandran and Menon, 1998). Certainly, all these industries need electric power to run the production processes. Hence, the proposed multigeneration systems are suitable to be deployed as the decentralized energy systems that supply electric power and hydrogen to these industries.

The trigeneration system with the capability of producing cooling capacity can be applied to the industries that require low-temperature applications. From the simulation results tabulated in Table 4.6, the ammonia refrigerant receives heat from the cold space and vaporizes into saturated vapour at -18.53 ℃. By considering the temperature difference for an efficient heat transfer, the absorption chiller in the trigeneration system may be suitable for the applications that require the temperature of the cold space to be maintained at -5 ℃ to 0 ℃. One of the industries that require low-temperature application is the food industry. Furthermore, some food industries need hydrogen to carry out the hydrogenation process, which is a process of converting a liquid fat (such as vegetable oil) into a solid fat through the addition of hydrogen (Fletcher, 2021). Therefore, the proposed trigeneration system may be applied in such food industries as it produces electric power, hydrogen, and cooling capacity simultaneously.

Although the proposed solar-driven multigeneration systems are small scale power systems, they require a large area for installation. This is because the proposed systems consist of 560 heliostats with each heliostat having an area

of 100 m^2. Thus, the solar field in the proposed system will occupy a lot of space. Moreover, to build such a huge solar power system, a huge initial investment is needed, although the costs of purchasing fossil fuels can be saved once the construction of the power system is done. Furthermore, the proposed multigeneration systems are weather dependent since they generate power and other outputs from solar energy. It is generally known that the availability and the intensity of solar radiation are totally out of human control. In this study, the outputs produced by the systems were determined with the assumption that the direct normal irradiation (DNI) is 375 W/m^2. When the sunlight is not available or at the time that the intensity of solar radiation is lower, the outputs produced by the systems will be lower. Hence, to deploy the proposed solar-driven multigeneration systems as decentralized energy systems, factors such as the area required and economic feasibility should be taken into consideration while assessing the practicality of the systems.

4.7 Life Cycle Assessment of the Solar Cogeneration System

The environmental impacts of the power generation and hydrogen production processes in the proposed solar cogeneration system were examined through GaBi software. The input and output energies of the processes are listed in Table 4.3. Since the functional unit was defined to be 1 hour, the energies keyed in to the software were in the unit of kWh.

Besides energy, the environmental impacts caused by the production of working fluids for the cogeneration system were also considered in this life cycle assessment (LCA). Based on the simulation results in Table 4.2, the mass flow rates of the water and n-butane are 5 kg/s and 21 kg/s respectively. This means that 5 kg of water is circulating in the topping cycle and 21 kg of n-butane is circulating in the bottoming cycle. Although it was supposed to convert the unit of mass flow rate to kg/h since the functional unit was defined as 1 hour, it should be kept in mind that both the steam and n-butane cycles are closed cycles, in which the working fluids are not discharged from the system. As highlighted in Section 3.6.2, one of the assumptions made for this LCA was no working fluids are leaked out from the system. Hence, the masses of working fluids remain constant throughout the operation of the cogeneration system. Therefore, only 5 kg of water and 21 kg of n-butane are required by the cogeneration system.

Once the processes were created in GaBi and the inputs and outputs of each process were fully defined, the emissions of pollutants due to the cogeneration process were calculated by the software.

4.7.1 Results of Life Cycle Assessment for the Cogeneration System

The results of LCA for the cogeneration system are summarized in Table 4.11. In GaBi, the LCA results are displayed in graphical form. The graphs of LCA results for the cogeneration system can be found in Appendix E.

Table 4.11: The LCA Results for the Proposed Cogeneration System.

Process	Global Warming Potential (kg CO_2-eq)	Acidification Potential (kg SO_2-eq)	Human Toxicity Potential (kg 1,4-DCB-eq)
Butane Refinery	19.3	0.139	2.28
Generation of Electricity for Pump 1	67.8	0.227	3.23
Generation of Electricity for Pump 2	58.3	0.195	2.77
Total	145.4	0.561	8.28

Remark: The abbreviation eq stands for equivalent.

4.7.2 Interpretation of Life Cycle Assessment Results for the Cogeneration System

As defined earlier, the LCA in this study refers to evaluating the environmental impacts associated with the production of electric power and hydrogen gas in the proposed solar cogeneration system. By referring to the LCA results in Table 4.11, it can be found that the power generation and hydrogen production processes in the cogeneration system do not contribute to environmental issues. This is because the power generation process in the cogeneration system is totally driven by solar energy. Moreover, the n-butane cycle that delivers electric power to the proton exchange membrane (PEM) electrolyzer is powered by the waste heat supplied by the steam cycle. Hence, the power generation

processes in the cogeneration system are completely free from fossil fuels combustion. Since there is no burning of fossil fuels involved, the operation of the cogeneration system does not emit pollutants into the atmosphere. Therefore, one can conclude that generating power from solar energy is environmentally friendly and pollution-free.

However, the operation of the cogeneration system is not completely clean because of the consumption of electrical energy by the pumps in the binary vapour cycle. Following the assumption made in the earlier phase of the LCA, the electrical energy delivered to the pumps is generated by the fossil fuel power station. The generation of electricity required to drive the pumps will therefore release some pollutants that are harmful to the environment and humans. From the simulation results in Table 4.3, the powers consumed by Pump 1 and Pump 2 are 81.52 kW and 70.05 kW respectively. The power consumed by Pump 1 is approximately 1.16 times higher than Pump 2. As a consequence, all the emissions due to the generation of electricity needed to power Pump 1 are about 1.16 times higher than Pump 2.

Apart from that, the butane refinery process also contributes some significant emissions to the environment. Butane refinery is an essential process to produce the working fluid for the bottoming cycle of the cogeneration system. In general, butane is mainly produced through the crude oil refinery process. In a crude oil refinery process, the crude oil is heated in a furnace before being introduced into a distillation tower. The heating of crude oil involves the combustion of fuel gas or fuel oil, which eventually emits pollutants into the atmosphere and thus contributes to environmental issues (Young, 2006). However, as mentioned previously, the n-butane cycle in the cogeneration system is a closed cycle, in which the working fluid is not renewed and is recirculating in the cycle. Therefore, the emissions due to the production of n-butane required by the cogeneration system can be considered as one-time emissions.

Although the generation of electricity required to drive the pumps and the butane refinery process are not occurring in the proposed cogeneration system, they are still the important processes that enable the operation of the cogeneration system. In the following subsections, the environmental impacts caused by these processes will be discussed.

4.7.2.1 Global Warming Potential

Nowadays, one of the most concerning environmental issues is global warming. Global warming is mainly caused by greenhouse gases that prevent heat from escaping from the atmosphere to space. A measure of the amount of heat that could be trapped by the greenhouse gases in 100 years is known as global warming potential (Forabosco, et al., 2017). Global warming potential is usually measured in kilograms of carbon dioxide equivalent (kg of CO_2-eq).

From the LCA results in Table 4.11, the global warming potential of the butane refinery process and the generation of electricity to drive Pump 1 and Pump 2 are 19.3 kg of CO_2-eq., 67.8 kg of CO_2-eq, and 58.3 kg of CO_2-eq respectively. It should be aware that the unit of kg of CO_2-eq does not mean that only CO_2 is released into the atmosphere or only CO_2 is contributing to global warming. Instead, some other gases that contribute to global warming are converted to CO_2-equivalent. For instance, the generation of electricity required to power the pumps involves the combustion of fossil fuels, which emits mainly CO_2 and a small amount of nitrous oxide (N_2O) and methane (CH_4). In order to evaluate the overall global warming potential as well as to compare the impacts of different greenhouse gases on global warming, these gases are often converted to CO_2-equivalent. In general, 1 kg of CH_4 is considered as 25 kg of CO_2-eq whereas 1 kg of N_2O is regarded as 298 kg of CO_2-eq (Khan, et al., 2018). With the aid of GaBi software, all the greenhouse gases that cause global warming were automatically converted to CO_2-equivalent. Based on the LCA results obtained from GaBi, it can be concluded that a total of 145.4 kg of CO_2-eq is released into the atmosphere due to the production of electricity and n-butane required by the cogeneration system.

It is arguable that the waste heat rejected by the n-butane cycle can also lead to global warming. Based on the simulation results in Table 4.3, the condenser in the n-butane cycle rejects 9 552.78 kW of waste heat (about 34.39 GJ of waste heat in 1 hour) to the cooling water. The cooling water will then carry this heat to the cooling tower and release it into the atmosphere in the form of water vapour. Since water vapour is also a type of greenhouse gas, it is also contributing to global warming by trapping the heat emitted from the Earth's surface and preventing it from going out to space. However, unlike other greenhouse gases, water vapour remains in the atmosphere for a relatively short

period. As an example, CO_2, which is the most well-known greenhouse gas, stays in the atmosphere for 50 to 200 years. In contrast, water vapour in the atmosphere typically condenses and precipitates to form raindrops in less than two weeks. Due to the short duration of staying in the atmosphere, the water vapour emitted into the atmosphere is not taken into consideration while evaluating global warming potential in LCA (Dotson, 2010; Sherwood, et al., 2018). Hence, the waste heat rejected by the n-butane cycle was not included in the LCA results for global warming potential, as it is released into the atmosphere in the form of water vapour.

4.7.2.2 Acidification Potential

Another environmental impact that had been analyzed is the acidification potential. Acidification potential is defined as the emission of pollutants that increase the acidity concentration of the environment (water and soil). Some examples of these pollutants are sulphur dioxide (SO_2) and nitrogen oxides (NO_x). The emission of these acidic gases into the atmosphere tends to cause acid rain, which is a terrible phenomenon that damages buildings, threaten the ecosystem, and affects human health (Nematchoua, 2022). Generally, acidic gases are often converted to SO_2-equivalent while evaluating the acidification potential of a process.

Based on the results of the LCA in Table 4.11, the acidification potentials of the butane refinery process and the generation of electricity needed to drive Pump 1 and Pump 2 are 0.139 kg of SO_2-eq, 0.227 kg of SO_2-eq, and 0.195 kg of SO_2-eq respectively. The emission of acidic gases is mainly due to the combustion of fossil fuels (Chungsangunsit, et al., 2009). In the proposed solar cogeneration system, electric power and hydrogen gas are produced from solar energy. Since there is no combustion of fossil fuels involved, the power generation and water electrolysis processes that take place in solar cogeneration system do not contribute to acidification potential. However, the pumps employed in the cogeneration system consume electricity from external sources to pump the working fluids. Since it was assumed that the electricity supplied to the pumps is generated through the burning of fossil fuels, the operation of the cogeneration system will contribute to acidification potential indirectly.

Other than electricity generation, the process of refining the n-butane required by the cogeneration system also contributes to acidification potential because the crude oil refinery process involves the combustion of fuel oil in the furnace. Nevertheless, with the assumption that no working fluids are leaked from the binary vapour cycle, the production of n-butane for the cogeneration system will only happen once. Furthermore, the emission of acidic gases due to the butane refinery process is lower than the electricity generation process. Therefore, the acidification potential of producing the n-butane for the cogeneration system may be considered negligible.

4.7.2.3 Human Toxicity Potential

As stated previously, the combustion of fossil fuels produces pollutants such as nitrogen oxides (NO_x), sulphur dioxide (SO_2) etc. These pollutants are not only causing acidification of the environment but also affecting human health in a negative way. To measure how harmful are these pollutants to human health, human toxicity potential is evaluated. In LCA, toxic pollutants are often converted to 1,4-dichlorobenzene (DCB) equivalent (a potentially carcinogenic substance) while evaluating human toxicity potential (Wang, et al., 2019).

Based on the LCA results in Table 4.11, it can be inferred that the operation of the cogeneration system emits a total of 8.28 kg of 1,4-DCB-eq into the atmosphere. Operating the two pumps in the binary vapour cycle for 1 hour emits 6 kg of 1,4-DCB-eq into the atmosphere, mainly due to the process of burning fossil fuels to generate the required electricity. Besides that, to produce 21 kg of n-butane for the cogeneration system, 2.28 kg of 1,4-DCB-eq is released into the atmosphere due to the combustion of fuel oil in the crude oil refinery process. However, the emission due to the butane refinery process is considered as one-time emission since the n-butane is only required to be supplied to the cogeneration system once.

4.8 Life Cycle Assessment of the Solar Trigeneration System

The power generation and water electrolysis processes in the trigeneration system are the same as in the cogeneration system. Nevertheless, the trigeneration system has an extra absorption cooling process. The input and output energies of the trigeneration process are listed in Table 4.7. Additionally,

the operation of the absorption chiller requires ammonia, which serves as the refrigerant of the absorption cooling cycle. Hence, an ammonia production process had been added to the model of the trigeneration system in GaBi to supply the required amount of ammonia to the absorption cooling cycle.

4.8.1 Results of Life Cycle Assessment for the Trigeneration System

Table 4.12 shows the emissions caused by the processes that produce the required inputs for the trigeneration system. The graphs of LCA results for the trigeneration system are included in Appendix F.

Table 4.12: The LCA Results for the Proposed Trigeneration System.

Process	**Global Warming Potential (kg CO_2-eq)**	**Acidification Potential (kg SO_2-eq)**	**Human Toxicity Potential (kg 1,4-DCB-eq)**
Ammonia Production	0.262	0.000108	0.00345
Butane Refinery	19.3	0.139	2.28
Generation of Electricity for Pump 1	67.8	0.227	3.23
Generation of Electricity for Pump 2	58.3	0.195	2.77
Generation of Electricity for Pump 3	0.275	0.000918	0.0131
Total	145.937	0.562	8.30

4.8.2 Interpretation of Life Cycle Assessment Results for the Trigeneration System

By comparing the LCA results of the cogeneration and the trigeneration systems, it can be found that the emissions due to the butane refinery process and the generation of electricity to power Pump 1 and Pump 2 are exactly the same in both systems. This is because, under similar operating parameters, the binary

vapour cycles in both systems require the same inputs. From the simulation results in Table 4.7, the powers consumed by Pump 1 and Pump 2 in the binary vapour cycle are 81.52 kW and 70.05 kW respectively. Besides that, the mass of n-butane required by the bottoming cycle of the trigeneration system is also 21 kg. These inputs are the same as the inputs of the cogeneration system. Thus, the emissions caused by the power generation and butane refinery processes follow exactly the same as the cogeneration system.

In the trigeneration system, an additional absorption cooling process takes place. The inputs required by the absorption cooling process are the electrical energy to operate Pump 3, the waste heat supplied by the n-butane cycle, and the refrigerant of the absorption chiller, which is ammonia. Based on the simulation results in Table 4.6, the mass flow rate of the ammonia-water solution is 0.20 kg/s, which means that the total mass of the ammonia-water solution in the absorption chiller is 0.20 kg. The rich ammonia-water solution composes of 52% of ammonia and 48% of water. Hence, the total amount of ammonia required by the absorption chiller is 0.104 kg.

The production of 0.104 kg of ammonia releases 0.262 kg of CO_2-eq, 0.000108 kg of SO_2-eq, and 0.00345 kg of 1,4-DCB-eq. Currently, ammonia is mainly produced through the Haber-Bosch process. This process produces ammonia (NH_3) through the reaction between nitrogen (N_2) and hydrogen (H_2). While nitrogen is the most abundant constituent in the air (about 78%) and can be easily obtained by separating it from the air, the hydrogen required by the Haber-Bosch process has to be produced through the steam methane reforming process (Frattini, et al., 2016). The steam methane reforming process involves the reaction between methane (CH_4) and hot steam and is carried out at a high temperature ranging from 850 ℃ to 950 ℃. In ammonia plants, steam methane reforming is conducted onsite to directly supply the required hydrogen to the ammonia synthesis process (Kyriakou, 2020). Hence, the emissions associated with the steam methane reforming process were also taken into account while evaluating the environmental impacts of the Haber-Bosch process. For the complete description of the steam methane reforming process, kindly refer to Section 2.9.1.

Other than steam methane reforming, the ammonia synthesis process itself is also an energy-intensive process. The reaction between nitrogen and

hydrogen requires high temperature (400 ℃ to 500 ℃) and high pressure (15 MPa to 30 MPa). The high energy requirements in both the hydrogen production and ammonia synthesis processes are usually fulfilled through the combustion of fossil fuels (Ghavam, et al., 2021). According to Capdevila-Cortada (2019), the Haber-Bosch process consumes 1% of the world's energy production and about 1.4% of the global carbon emissions are resulted from the Haber-Bosch process. This statement has also been verified by the LCA results shown in Table 4.12, as the production of 0.104 kg of ammonia for the absorption chiller releases 0.262 kg of CO_2-eq, which is almost 2.5 times higher than the mass of ammonia produced. Therefore, the production of ammonia through the Haber-Bosch process has a significant impact on global warming potential.

Similar to the binary vapour cycle, the absorption cooling cycle is also a closed cycle, in which the ammonia refrigerant is kept recirculating in the cycle (assuming no ammonia is leaked from the system). Thus, the emissions as a result of the ammonia synthesis process can be considered as one-time emissions. Furthermore, absorption chiller has the advantage of small electric power consumption. In this trigeneration system, the pump in the absorption chiller consumes only 0.33 kW of electric power. Thus, the emissions due to the generation of electricity to power the pump are negligible.

Due to the small amount of ammonia required and the small power consumption by the pump in the absorption chiller, the environmental impacts of the trigeneration system are very close to the cogeneration system. The waste heat released by the condenser of the absorption chiller was not considered by the LCA software while evaluating the global warming potential of the trigeneration system. This is because this waste heat is also emitted to the atmosphere in the form of water vapour via a cooling tower. As explained in Section 4.7.2.1, water vapour is not taken into account in the calculation of global warming potential since it only stays in the atmosphere for a relatively short duration. Thus, the operation of the solar trigeneration system is claimed to have almost similar environmental impacts as the solar cogeneration system while being able to produce an additional cooling capacity.

4.9 Further Discussion on Life Cycle Assessment

Based on the previous discussion, it can be deduced that the burning of fossil fuels is the culprit of environmental pollution. By referring to the simulation results in Table 4.7, the powers consumed by Pump 1, Pump 2, and Pump 3 for one hour of operation are 81.52 kWh, 70.05 kWh, and 0.33 kWh respectively. From the LCA results, it was found that the process of generating the electricity needed to power these three pumps releases 67.8 kg of CO_2-eq, 58.3 kg of CO_2-eq, and 0.275 kg of CO_2-eq respectively. Therefore, one can deduce that generating 1 kWh of electricity from a fossil fuel power station will release approximately 0.83 kg of CO_2-eq into the atmosphere.

In this study, the proposed cogeneration and trigeneration systems produce 3 127.5 kW of electric power from solar energy. In the case that the same amount of electric power is generated through the combustion of fossil fuels, approximately 2 595.825 kg of CO_2-eq will be released into the atmosphere when the fossil fuel power station operates for 1 hour. Similar to the other types of environmental impacts, the operation of fossil fuel power station in 1 hour releases approximately 8.69 kg of SO_2-eq and 123.849 kg of 1,4-DCB-eq into the atmosphere. In contrast, with solar power generation technology, all these emissions could be eliminated or minimized. Hence, it can be concluded that solar power generation is a much cleaner way to generate electric power since the process emits zero or negligible pollutants into the atmosphere.

4.10 Summary

In summary, the cogeneration system that generates 3 127.5 kW of electric power and 24.58 kg/h of hydrogen gas has an efficiency of 26.77%. The trigeneration system can produce similar electric power and hydrogen gas under similar operating parameters. With an additional absorption chiller, the trigeneration system can output an additional 54.97 kW of cooling capacity. Therefore, the efficiency of the trigeneration is slightly higher, which is 27.15%. The environmental impacts associated with the operation of the solar-driven multigeneration systems are mainly caused by the generation of electricity needed to power the pumps. In addition, the processes of producing the working fluids for the multigeneration systems will also emit some pollutants into the atmosphere.

CHAPTER 5

CONCLUSIONS AND RECOMMENDATIONS

5.1 Conclusions

In conclusion, all the three objectives of the project have been achieved. The proposed cogeneration system produces electric power and hydrogen gas from solar energy. The proposed trigeneration system is the cogeneration system added with an ammonia-water absorption chiller. Thus, the trigeneration system can produce electric power, hydrogen gas, and cooling capacity from solar energy. Since both the cogeneration and trigeneration systems utilize solar energy as the input source and are able to produce hydrogen gas as one of the outputs, the first objective of the project is fulfilled.

The second objective of the project was attained through the evaluation of the systems' efficiencies. On the days when the direct normal irradiation (DNI) is 0.375 kW/m^2, the solar field can supply 14 175 kW of concentrated solar energy to the cogeneration system. With the binary vapour cycle and the proton exchange membrane (PEM) electrolyzer, the cogeneration system can produce 3 127.5 kW of electric power and 24.58 kg/h of hydrogen gas. The efficiency of the cogeneration system is found to be 26.77%. On the other hand, the trigeneration system that is operating under similar conditions can generate the same amount of electric power and hydrogen gas as the cogeneration system. With the additional absorption chiller, the trigeneration system can produce an extra 54.97 kW of cooling capacity. Due to the extra limited cooling capacity delivered by the absorption chiller, the efficiency of the trigeneration system is slightly higher than the cogeneration system, which is 27.15%. It is also possible for the cogeneration system to achieve higher efficiency than the trigeneration system since the cogeneration system does not need to supply energy to the low-performance absorption chiller.

The third objective of the project was satisfied through the assessment of environmental impacts caused by the operations of the multigeneration systems. It was found that the processes of generating power and hydrogen gas from solar energy do not emit pollutants into the atmosphere. The major sources of pollution in the operation of the cogeneration and trigeneration systems are

the generation of electricity needed to power the pumps as well as the processes of producing the working fluids for the systems. In 1 hour of operation, the cogeneration system emits 145.4 kg of CO_2-eq, 0.561 kg of SO_2-eq, and 8.28 kg of 1,4-DCB-eq into the atmosphere. On the other hand, the absorption chiller in the trigeneration system only requires a small amount of ammonia refrigerant and consumes negligible power to drive the pump. Hence, the amount of pollutants emitted by the trigeneration system is quite close to the cogeneration system. It was found that the trigeneration system emits 145.937 kg of CO_2-eq, 0.562 kg of SO_2-eq, and 8.30 kg of 1,4-DCB-eq into the atmosphere when it operates for 1 hour.

5.2 Recommendations for Future Work

There are several limitations of the current project. First of all, several components in the proposed multigeneration systems, such as the heliostats and the solar power tower were excluded from the process simulations in Aspen HYSYS since these components are not available in the component list of the software. The amount of concentrated solar energy received by the binary vapour cycle was calculated based on the assumptions, which means that the accuracy of the results may be lower. To improve the accuracy and reliability of the results, it is recommended to use other simulation software to model and simulate the entire solar multigeneration systems. One of the possible software that is worth trying is TRNSYS, which is an energy simulation software that is widely used to simulate renewable energy systems. Since this program is mainly used in renewable energy simulation, the solar energy data may be available in the software and thus the solar field can be included in the simulation.

Furthermore, most of the solar power tower systems nowadays have a thermal energy storage system to store the energy obtained from the sun and use it to generate power when the sunlight is not available. In such a system, molten salt that composes of sodium nitrate ($NaNO_3$) and potassium nitrate (KNO_3) is used as the heat transfer fluid to store the solar thermal energy in a storage tank (Turchi, et al., 2018). In Aspen HYSYS, the thermal energy storage system is not able to be modelled and simulated. Thus, the thermal energy storage system was omitted from the proposed solar multigeneration systems. To make the solar-driven multigeneration systems more robust, it is recommended to include

the thermal energy storage system in the solar field. The resulting systems can be simulated through other simulation software such as TRNSYS.

In addition, as discussed in Section 2.7, another method of producing electricity and useful heat from solar energy is through photovoltaic-thermal (PVT) systems. In future work, a cogeneration or trigeneration system that operates based on PVT technology may be designed. The performance of the proposed PVT system can be evaluated through other software such as the TRNSYS program.

Last but not least, in terms of life cycle assessment (LCA), it is recommended to assess the environmental impacts of the entire multigeneration systems, including the processes of manufacturing the heliostats, constructing the solar power tower, and installing the power generation unit etc. This is because the ultimate goal of LCA is to examine the potential environmental impacts throughout the whole life cycle of a product or system.

REFERENCES

Abdullah, A.L., Misha, S., Tamaldin, N., Rosli, M.A.M. and Sachit, F.A., 2020. Photovoltaic Thermal/Solar (PVT) Collector (PVT) System Based on Fluid Absorber Design: A Review. *Journal of Advanced Research in Fluid Mechanics and Thermal Sciences*, 48(2), pp.196–208.

Adesanya, S.O. and Makinde, O.D., 2015. Irreversibility analysis in a couple stress film flow along an inclined heated plate with adiabatic free surface. *Physica A: Statistical Mechanics and its Applications*, 432, pp.222-229.

Ahmad Kamaroddin, M.F., Sabli, N., Tuan Abdullah, T.A., Siajam, S.I., Abdullah, L.C., Abdul Jalil, A. and Ahmad, A., 2021. Membrane-Based Electrolysis for Hydrogen Production: A Review. *Membranes*, [e-journal] 11(11). http://dx.doi.org/10.3390/membranes11110810.

Alanne, K. and Saari, A., 2006. Distributed energy generation and sustainable development. *Renewable and Sustainable Energy Reviews*, 10(6), pp.539-558.

Asrori, A., Soeparman, S., Wahyudi, S. and Denny, W., 2020. Investigation of steam generation performance on conical cavity receiver by different geometric concentration ratios for fresnel lens solar concentrator. *Eastern-European Journal of Enterprise Technologies*, 4/8(106), pp.6-14.

Azapagic, A., 1999. Life cycle assessment and its application to process selection, design and optimisation. *Chemical Engineering Journal*, 73(1), pp.1-21.

Bamisile, O., Huang, Q., Anane, P.O.K. and Dagbasi, M., 2019. Performance Analyses of a Renewable Energy Powered System for Trigeneration. *Sustainability*, 11(21), pp.6006-6020.

Bellos, E., 2019. Progress in the design and the applications of linear Fresnel reflectors – A critical review. *Thermal Science and Engineering Progress*, 10, pp.112-137.

Beltagy, H., Semmar, D., Lehaut, C. and Said, N., 2017. Theoretical and experimental performance analysis of a Fresnel type solar concentrator. *Renewable Energy*, 101, pp.782-793.

Brouche, M. and Lahoud, C., 2018. Review of cogeneration and trigeneration systems. *African Journal of Engineering Research*, 6(3), pp.39-54.

Capdevila-Cortada, M., 2019. Electrifying the Haber–Bosch. *Nature Catalysis*, 2, pp.1055.

Carmo, M., Fritz, D.L., Mergel, J. and Stolten, D., 2013. A comprehensive review on PEM water electrolysis. *International Journal of Hydrogen Energy*, 38(12), pp.4901-4934.

Cengel, Y.A. and Boles, M.A., 2015. *Thermodynamics: An Engineering Approach*. 8th ed. New York: McGraw-Hill Education.

Chungsangunsit, T., Gheewala, S.H. and Patumsawad, S., 2009. Emission Assessment of Rice Husk Combustion for Power Production. *International Journal of Mechanical, Aerospace, Industrial, Mechatronic and Manufacturing Engineering*, 3(5), pp.625-630.

Deng, J., Wang, R.Z. and Han, G.Y., 2011. A review of thermally activated cooling technologies for combined cooling, heating and power systems. *Progress in Energy and Combustion Science*, 37(2), pp.172-203.

Dossat, R.J. and Horan, T.J., 2002. *Principles of Refrigeration.* 5th ed. New Jersey: Prentice Hall.

Dotson, A., 2010. *Water Vapor, CO_2, and Global Warming*. [online] Available at: <https://iedro.org/articles/water-vapor-and-global-warming/> [Accessed 7 April 2022].

Dufo-López, R. and Bernal-Agustín, J.L., 2008. Multi-objective design of PV–wind–diesel–hydrogen–battery systems. *Renewable Energy*, 33(12), pp.2559-2572.

Dupeyrat, P., Ménézo, C. and Fortuin, S., 2014. Study of the thermal and electrical performances of PVT solar hot water system. *Energy and Buildings*, 68, pp.751-755.

Elsarrag, E. and Alhorr, Y., 2013. Green building practices: Optimisation of CCHP and biomass heating for maximum CO_2 reduction in a mixed-use development. *International Journal of Sustainable Built Environment*, 2(1), pp.99-108.

Engineering ToolBox, 2003. *Fuels and Chemicals - Autoignition Temperatures*. [online] Available at: https://www.engineeringtoolbox.com/fuels-ignition-temperatures-d_171.html [Accessed 12 May 2022].

Finnveden, G., Hauschild, M.Z., Ekvall, T., Guinée, J., Heijungs, R., Hellweg, S., Koehler, A., Pennington, D. and Suh, S., 2009. Recent developments in Life Cycle Assessment. *Journal of Environmental Management*, 91(1), pp.1-21.

Fletcher, J., 2021. *What is hydrogenated oil and is it safe?* [online] Available at: <https://www.medicalnewstoday.com/articles/hydrogentated-oil> [Accessed 8 April 2022].

Forabosco, F., Chitchyan, Zh. and Mantovani, R., 2017. Methane, nitrous oxide emissions and mitigation strategies for livestock in developing countries: A review. *South African Journal of Animal Science*, 47(3), pp. 268-280.

Frattini, D., Cinti, G., Bidini, G., Desideri, U., Cioffi, R. and Jannelli, E., 2016. A system approach in energy evaluation of different renewable energies sources integration in ammonia production plants. *Renewable Energy*, 99, pp.472-482.

Frima, H., 2017. New Trends in the Higher Education: Renewable Energy at the Faculty of Eletrical Engineering. *Energy Procedia*, 115, pp.18-28.

García, I.L., Álvarez, J.L. and Blanco, D., 2011. Performance model for parabolic trough solar thermal power plants with thermal storage: Comparison to operating plant data. *Solar Energy*, 85(10), pp.2443-2460.

Ghavam, S., Vahdati, M., Wilson I. A. G. and Styring, P., 2021. Sustainable Ammonia Production Processes. *Frontiers in Energy Research*, [e-journal] 9. https://doi.org/10.3389/fenrg.2021.580808.

Gong, J., Li, C. and Wasielewski, M.R., 2019. Advances in solar energy conversion. *Chemical Society Reviews*, 48, pp.1862-1864.

Gordon, M. and Weber, M., 2021. *Global energy demand to grow 47% by 2050, with oil still top source: US EIA*. [online] Available at: <https://www.spglobal.com/commodityinsights/en/market-insights/latest-news/oil/100621-global-energy-demand-to-grow-47-by-2050-with-oil-still-top-source-us-eia> [Accessed 25 January 2022].

Györke, G., Deiters, U.K., Groniewsky, A., Lassu, I. and Imre, A.R., 2018. Novel classification of pure working fluids for Organic Rankine Cycle. *Energy*, 145, pp.288-300.

Hafez, A.Z., Soliman, A., El-Metwally, K.A. and Ismail, I.M., 2017. Design analysis factors and specifications of solar dish technologies for different systems and applications. *Renewable and Sustainable Energy Reviews*, 67, pp.1019-1036.

Herath, H.M.D.P., Wijewardane, M.A., Ranasinghe, R.A.C.P. and Jayasekera, J.G.A.S., 2020. Working fluid selection of Organic Rankine Cycles. *Energy Reports*, 6(9), pp.680-686.

Hernández-Santoyo, J. and Sánchez-Cifuentes, A., 2003. Trigeneration: an alternative for energy savings. *Applied Energy*, 76(1-3), pp.219-227.

Hong, X. and Shi, F., 2020. Comparative Analysis of Small-Scale Integrated Solar ORC-Absorption Based Cogeneration Systems. *Energies*, 13(4), pp.946-960.

International Renewable Energy Agency (IRENA), 2021. *Renewable capacity highlights*. [pdf] Abu Dhabi: IRENA. Available at: <https://www.irena.org/-/media/Files/IRENA/Agency/Publication/2021/Apr/IRENA_-RE_Capacity_Highlights_2021.pdf?la=en&hash=1E133689564BC40C2392E85026F71A0D7A9C0B91> [Accessed 25 January 2022].

Kalogirou, S.A., 2004. Solar thermal collectors and applications. *Progress in Energy and Combustion Science*, 30(3), pp.231-295.

Kanoglu, M. and Dincer, I., 2009. Performance assessment of cogeneration plants. *Energy Conversion and Management*, 50(1), pp.76-81.

Khan, I., Jack, M.W. and Stephenson, J., 2018. Analysis of greenhouse gas emissions in electricity systems using time-varying carbon intensity. *Journal of Cleaner Production*, 184, pp.1091-1101.

Khan, K.A., Paul, S., Zobayer, A. and Hossain, S.S., 2013. A Study on Solar Photovoltaic Conversion. *International Journal of Scientific and Engineering Research*, 4(3), pp.1-5.

Kodama, T., 2003. High-temperature solar chemistry for converting solar heat to chemical fuels. *Progress in Energy and Combustion Science*, 29(6), pp.567-597.

Koroneos, C., Dompros, A., Roumbas, G. and Moussiopoulos, N., 2004. Life cycle assessment of hydrogen fuel production processes. *International Journal of Hydrogen Energy*, 29(14), pp.1443-1450.

Kribus, A., Zaibel, R., Carey, D., Segal, A. and Karni, J., 1998. A solar-driven combined cycle power plant. *Solar Energy*, 62(2), pp.121-129.

Kumar, S.S. and Himabindu, V., 2019. Hydrogen production by PEM water electrolysis – A review. *Materials Science for Energy Technologies*, 2(3), pp.442-454.

Kyriakou, V., Garagounis, I., Vourros, A., Vasileiou, E. and Stoukides, M., 2020. An Electrochemical Haber-Bosch Process. *Joule*, 4(1), pp.142-158.

Lakovic, M.S., Banjac, M.J., Laković, S.V. and Jovcevski, M.M., 2016. Industrial cooling tower design and operation in the moderate-continental climate conditions. *Thermal Science*, 20, pp.1203-1214.

Liang, R., Zhang, J. and Zhou, C., 2015. Dynamic Simulation of a Novel Solar Heating System Based on Hybrid Photovoltaic/Thermal Collectors (PVT). *Procedia Engineering*, 121, pp.675-683.

Liu, M., Shi, Y. and Fang, F., 2014. Combined cooling, heating and power systems: A survey. *Renewable and Sustainable Energy Reviews*, 35, pp.1-22.

Liu, W.H., Alwi, S.R.W., Hashim, H., Muis, Z.A., Klemeš, J.J., Rozali, N.E.M., Lim, J.S. and Ho, W.S., 2017. Optimal Design and Sizing of Integrated Centralized and Decentralized Energy Systems. *Energy Procedia*, 105, pp.3733-3740.

Liu, Y., Li, F., Ren, J., Ren, G., Shen, H. and Liu, G., 2019. Solar thermal power generation technology research. *E3S Web of Conferences*, [e-journal] 136(02016). http://dx.doi.org/10.1051/e3sconf/201913602016.

Mohr, S.H., Wang, J., Ellem, G., Ward, J. and Giurco, D., 2015. Projection of world fossil fuels by country. *Fuel*, 141, pp.120-135.

Msheik, M., Rodat, S. and Abanades, S., 2021. Methane Cracking for Hydrogen Production: A Review of Catalytic and Molten Media Pyrolysis. *Energies*, 14(11), pp.3107-3141.

Naeem, M., Al-Rabiah, A.A. and Mughees, W., 2014. Process Simulation of 1-Butene and N-Butane Separation By Extractive Distillation. *International Journal of Engineering Research and Technology*, 3(6), pp.747-750.

Nematchoua, M. K., 2022. Strategies for Studying Acidification and Eutrophication Potentials, a Case Study of 150 Countries. *J 2022*, 5(1), pp.150-165.

Nieva, M.A., Villaverde, M.M., Monzón, A., Garetto, T.F. and Marchi, A.J., 2014. Steam-methane reforming at low temperature on nickel-based catalysts. *Chemical Engineering Journal*, 235, pp.158-166.

Nikolaidis, P. and Poullikkas, A., 2017. A comparative overview of hydrogen production processes. *Renewable and Sustainable Energy Reviews*, 67, pp.597-611.

Norouzi, E., Amidpour, M. and Rezakazemi, M., 2019. Heat recovery steam generator: Constructal thermoeconomic optimization. *Applied Thermal Engineering*, 148, pp.747-753.

Onovwiona, H.I. and Ugursal, V.I., 2006. Residential cogeneration systems: review of the current technology. *Renewable and Sustainable Energy Reviews*, 10(5), pp.389-431.

Parida, B., Iniyan, S. and Goic, R., 2011. A review of solar photovoltaic technologies. *Renewable and Sustainable Energy Reviews*, 15(3), pp.1625-1636.

Poullikkas, A., 2009. Economic analysis of power generation from parabolic trough solar thermal plants for the Mediterranean region - A case study for the island of Cyprus. *Renewable and Sustainable Energy Reviews*, 13(9), pp.2474-2484.

Qin, J., Hu, E. and Li, X., 2020. Solar aided power generation: A review. *Energy and Built Environment*, 1(1), pp.11-26.

Rahbar, K., Mahmoud, S., Al-Dadah, R.K., Moazami, N. and Mirhadizadeh, S.A., 2017. Review of organic Rankine cycle for small-scale applications. *Energy Conversion and Management*, 134, pp.135-155.

Rahimi, N., Kang, D., Gelinas, J., Menon, A., Gordon, M.J., Metiu, H. and McFarland, E.W., 2019. Solid carbon production and recovery from high temperature methane pyrolysis in bubble columns containing molten metals and molten salts. *Carbon*, 151, pp.181-191.

Ramachandran, R. and Menon, R.K., 1998. An overview of industrial uses of hydrogen. *International Journal of Hydrogen Energy*, 23(7), pp.593-598.

Ratlamwala, T.A.H., Dincer, I. and Aydin, M., 2012. Energy and exergy analyses and optimization study of an integrated solar heliostat field system for hydrogen production. *International Journal of Hydrogen Energy*, 37(24), pp.18704-18712.

Reddy, V.S., Kaushik, S.C., Ranjan, K.R. and Tyagi, S.K., 2013. State-of-the-art of solar thermal power plants—A review. *Renewable and Sustainable Energy Reviews*, 27, pp.258-273.

Sadir, O. and Bahadir, A., 2017. Renewable energy potential and utilization in Turkey. *Journal of Engineering Research and Applied Science*, 6(1), pp.577-582.

Sánchez-Bastardo, N., Schlögl, R. and Ruland, H., 2020. Methane Pyrolysis for CO_2-Free H_2 Production: A Green Process to Overcome Renewable Energies Unsteadiness. *Chemie Ingenieur Technik*, 92(10), pp.1596-1609.

Sánchez-Bastardo, N., Schlögl, R. and Ruland, H., 2021. Methane Pyrolysis for Zero-Emission Hydrogen Production: A Potential Bridge Technology from Fossil Fuels to a Renewable and Sustainable Hydrogen Economy. *Industrial & Engineering Chemistry Research*, 60(32), pp.11855-11881.

Sharma, S. and Ghoahal, S.K., 2015. Hydrogen the future transportation fuel: From production to applications. *Renewable and Sustainable Energy Reviews*, 43, pp.1151-1158.

Sherwood, S.C., Dixit, V. and Salomez, C., 2018. The global warming potential of near-surface emitted water vapour. *Environmental Research Letters*, 13(10). http://dx.doi.org/10.1088/1748-9326/aae018

Shirazi, A., Taylor, R.A., Morrison, G.L. and White, S.D., 2018. Solar-powered absorption chillers: A comprehensive and critical review. *Energy Conversion and Management*, 171, pp.59-81.

Singer, Cs., Giuliano, S. and Buck, R., 2014. Assessment of Improved Molten Salt Solar Tower Plants. *Energy Procedia*, 49, pp.1553-1562.

Srikhirin, P., Aphornratana, S. and Chungpaibulpatana, S., 2001. A review of absorption refrigeration technologies. *Renewable and Sustainable Energy Reviews*, 5(4), pp.343-372.

Tarti ère, T. and Astolfi, M., 2017. A World Overview of the Organic Rankine Cycle Market. *Energy Procedia*, 129, pp.2-9.

The World Bank and Solargis, 2020. *Solar resource maps of Malaysia*. [online] Available at: <https://solargis.com/maps-and-gis-data/download/malaysia> [Accessed 17 March 2022].

Tian, Y. and Zhao, C.Y., 2013. A review of solar collectors and thermal energy storage in solar thermal applications. *Applied Energy*, 104, pp.538-553.

Turchi, C.S., Vidal, J. and Bauer, M., 2018. Molten salt power towers operating at 600–650 °C: Salt selection and cost benefits. *Solar Energy*, 164, pp.38-46.

Vijayakumar, P., Kumaresan, G., Kumar S.A., Faizal, U.M., Chandran, G.R.V. and Adharsh, K.S.V., 2019. *Performance evaluation of compound parabolic concentrator with evacuated tube heat pipe*. In: IOP Conference Series: Earth and Environmental Science, National Conference on Recent Advances in Fuel Cells and Solar Energy. Karaikal, India, 11-12 May 2019. Bristol: IOP Publishing Ltd.

Wagner, S.J. and Rubin, E.S., 2014. Economic implications of thermal energy storage for concentrated solar thermal power. *Renewable Energy*, 61, pp.81-95.

Wang, H., 2014. Performance Evaluation of a Small Scale Modular Solar Trigeneration System. *International Journal of Photoenergy*, [e-journal] 2014, http://dx.doi.org/10.1155/2014/964021.

Wang, R., Lam, C.M., Hsu, S.C. and Chen, J.H., 2019. Life cycle assessment and energy payback time of a standalone hybrid renewable energy commercial microgrid: A case study of Town Island in Hong Kong. *Applied Energy*, 250, pp.760-775.

Wu, D.W. and Wang, R.Z., 2006. Combined cooling, heating and power: A review. *Progress in Energy and Combustion Science*, 32(5-6), pp.459-495.

Xu, C., Wang, Z., Li, X. and Sun, F., 2011. Energy and exergy analysis of solar power tower plants. *Applied Thermal Engineering*, 31(17-18), pp.3904-3913.

Yamamoto, T., Furuhata, T., Arai, N. and Mori, K., 2001. Design and testing of the Organic Rankine Cycle. *Energy*, 26(3), pp.239-251.

Young, R.E., 2006. Petroleum refining process control and real-time optimization. *IEEE Control Systems Magazine*, 26(6), pp.73-83.

Zeng, F., Yang, C. and Yang, Z., 2011. *Typical Characteristics of Gas Turbine-Based CCHP System with Inlet Air Cooling*. 2011 Asia-Pacific Power and Energy Engineering Conference. Wuhan, China, 25-28 March 2011. New York: IEEE.

APPENDICES

Appendix A: Gantt Charts

TableA-1: Gantt Chart for Part 1 of the Final Year Project (FYP).

Tasks	W1	W2	W3	W4	W5	W6	W7	W8	W9	W10	W11	W12	W13
Understand the project scope													
Define the objectives of FYP													
Literature review: Basic concepts of cogeneration and trigeneration													
Literature review: Power generation from solar energy													
Literature review: Solar-driven cogeneration and trigeneration systems													
Literature review: Hydrogen production methods													
Proposal of solar-driven cogeneration and trigeneration systems													
Progress report writing													

Appendix A (Continued)

TableA-2: Gantt Chart for Part 2 of the Final Year Project (FYP).

Tasks	W1	W2	W3	W4	W5	W6	W7	W8	W9	W10	W11	W12	W13
Identify the weaknesses and areas of improvement based on part 1 of the FYP													
Learning to use Aspen HYSYS													
Process simulation of the cogeneration system in Aspen HYSYS													
Process simulation of the trigeneration system in Aspen HYSYS													
Learning to use GaBi software													
Life cycle assessment of the cogeneration system in GaBi													
Life cycle assessment of the trigeneration system in GaBi													
Preparing the FYP poster													
Final report writing													

Appendix B: List of Successful Simulations for the Cogeneration System

TableB-1: List of Successful Simulations for the Cogeneration System.

Steam Cycle							**n-Butane Cycle**							**Efficiency**
$P_1 = P_4$ **(kPa)**	$P_2 = P_3$ **(kPa)**	$\dot{m}_{steam}$ **(kg/s)**	$\dot{W}_{in,\ pump\ 1}$ **(kJ/h)**	$\dot{W}_{out,\ turb\ 1}$ **(kJ/h)**	T_3 **(℃)**	x_4	$P_5 = P_8$ **(kPa)**	$P_6 = P_7$ **(kPa)**	$\dot{m}_{n\text{-}butane}$ **(kg/s)**	$\dot{W}_{in,\ pump\ 2}$ **(kJ/h)**	$\dot{W}_{out,\ turb\ 2}$ **(kJ/h)**	x_8	T_8 **(℃)**	η_{cogen}
400	10000	5.0	2.235×10^5	1.210×10^7	534.5	1.0000	500	1800	22	2.237×10^5	4.188×10^6	1	104.2	25.63%
650	15000	6.5	4.427×10^5	1.092×10^7	370.5	0.8258	500	2000	21	2.464×10^5	4.575×10^6	1	120.6	23.56%
350	8000	5.5	1.950×10^5	1.095×10^7	409.4	0.9378	600	1750	24	2.197×10^5	3.760×10^6	1	105.4	23.14%
500	12000	5.5	2.970×10^5	1.153×10^7	460.6	0.9436	500	2000	22	2.581×10^5	4.544×10^6	1	106.2	24.85%
500	13000	5.0	2.935×10^5	1.251×10^7	564.7	1.0000	450	2000	21	2.522×10^5	4.677×10^6	1	103.7	26.77%
550	12000	5.0	2.698×10^5	1.214×10^7	566.4	1.0000	500	2000	22	2.581×10^5	4.483×10^6	1	102.7	25.90%
400	7500	5.5	1.818×10^5	1.052×10^7	414.3	0.9535	450	1500	22	1.790×10^5	4.068×10^6	1	108.4	22.88%
400	12000	5.5	2.971×10^5	1.189×10^7	446.7	0.9243	450	1500	22	1.790×10^5	3.968×10^6	1	101.4	24.93%

The row highlighted in green colour is the set of operating parameters that provides the highest efficiency for the cogeneration system.

Appendix C: Simulation Results and Calculation of Efficiency for the Single-Generation Power Plant

Considering a single-generation steam power plant as shown in FigureC-1. The operating parameters for this steam power plant are listed in TableC-1. Please take note that the operating parameters for this single-generation steam power plant are exactly the same as the operating parameters of the proposed cogeneration and trigeneration systems. The simulation results for the input and output energies produced by this steam power plant are tabulated in TableC-2.

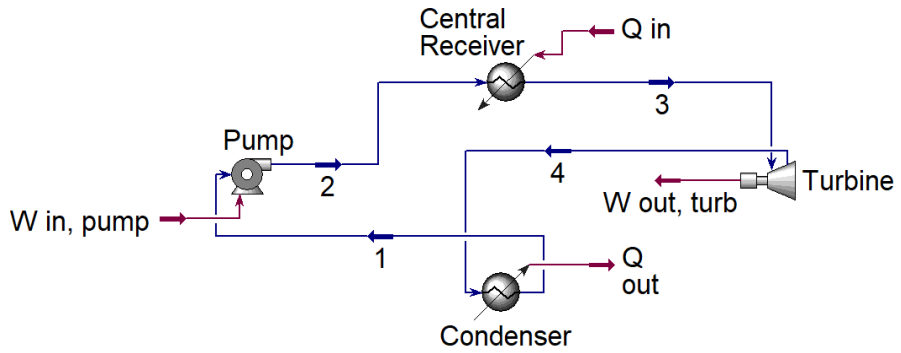

FigureC-1: The Single-Generation Steam Power Plant Modelled in Aspen HYSYS.

TableC-1: The Operating Parameters for the Single-Generation Steam Power Plant.

State Point	Pressure (kPa)	Temperature (℃)	Dryness Fraction	Phase
1	500	151.80	0	Saturated Liquid
2	13 000	153.60	0	Subcooled Liquid
3	13 000	564.70	1	Superheated Steam
4	500	165.00	1	Superheated Steam

Appendix C (Continued)

TableC-2: Rates of Flow of Energy across the Single-Generation Steam Power Plant.

Component	**Type of Energy Flow**	**Rate of Flow of Energy (kW)**	**Isentropic Efficiency**
Central Receiver	Input Heat Energy ($\dot{Q}_{in}$)	14 175.00	N/A
Pump	Input Power ($\dot{W}_{in,\,pump}$)	81.52	85%
Turbine	Output Power ($\dot{W}_{out,\,turb}$)	3 475.00	85%
Condenser	Rate of Heat Rejection ($\dot{Q}_{out}$)	10 780.56	N/A

Assuming the turbine is connected to an electric generator with an efficiency of 90%, the electric power generated by the steam power plant ($\dot{W}_{elec}$) is:

$$\dot{W}_{elec} = 0.9\dot{W}_{out,\,turb} = 0.9\ (3\ 475\ \text{kW}) = 3\ 127.5\ \text{kW}$$

Hence, the efficiency of the single-generation steam power plant (η_{SG}) is:

$$\eta_{SG} = \frac{\dot{W}_{elec} - \dot{W}_{in,\,pump}}{\dot{Q}_{in}} \times 100\%$$

$$\eta_{SG} = \frac{3\ 127.5\ \text{kW} - 81.52\ \text{kW}}{14\ 175\ \text{kW}} \times 100\% = 21.49\%$$

Appendix D: List of Successful Simulations for the Absorption Chiller in the Trigeneration System

TableD-1: List of Successful Simulations for the Absorption Chiller in the Trigeneration System.

P_{low} (kPa)	P_{high} (kPa)	T_{13} (℃)	T_{14} (℃)	T_{17} (℃)	Mixture Composition at State 13	Mixture Composition at State 17	$\dot{m}_{13}$ (kg/s)	$\dot{m}_{14}$ (kg/s)	$\dot{Q}_{gen}$ (kJ/h)	$\dot{W}_{in,3}$ (kJ/h)	$\dot{Q}_L$ (kJ/h)
200	1300	45	33.94	94.81	0.52 NH_3 + 0.48 H_2O	0.6400 H_2O + 0.3600 NH_3	0.08	0.02	1.550×10^5	476.9	7.915×10^4
300	1200	45	31.21	83.57	0.52 NH_3 + 0.48 H_2O	0.5999 H_2O + 0.4001 NH_3	0.10	0.02	1.650×10^5	494.7	8.126×10^4
300	1300	45	33.94	87.13	0.52 NH_3 + 0.48 H_2O	0.5999 H_2O + 0.4001 NH_3	0.10	0.02	1.650×10^5	549.7	8.025×10^4
300	1500	45	38.95	93.70	0.52 NH_3 + 0.48 H_2O	0.6000 H_2O + 0.4000 NH_3	0.10	0.02	1.700×10^5	659.7	7.840×10^4
300	1300	45	33.94	84.87	0.53 NH_3 + 0.47 H_2O	0.5875 H_2O + 0.4125 NH_3	0.10	0.02	1.540×10^5	551.7	8.029×10^4
300	1200	45	31.21	94.82	0.53 NH_3 + 0.47 H_2O	0.6581 H_2O + 0.3419 NH_3	0.14	0.04	3.000×10^5	695.1	1.627×10^5
300	1200	45	31.21	94.12	0.52 NH_3 + 0.48 H_2O	0.6546 H_2O + 0.3454 NH_3	0.15	0.04	3.000×10^5	742.1	1.626×10^5
300	1500	45	38.95	91.37	0.53 NH_3 + 0.47 H_2O	0.5875 H_2O + 0.4125 NH_3	0.15	0.03	2.450×10^5	993.0	1.176×10^5
200	1300	40	33.94	94.80	0.52 NH_3 + 0.48 H_2O	0.6400 H_2O + 0.3600 NH_3	0.20	0.05	4.000×10^5	1192.0	1.979×10^5

The row highlighted in green colour is the set of operating parameters that provides the highest cooling output for the absorption chiller.

Appendix E: Graphs of Life Cycle Assessment (LCA) for the Cogeneration System

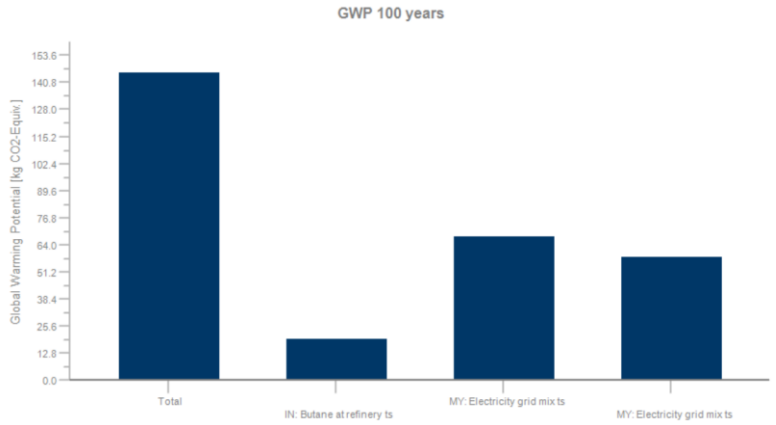

GraphE-1: Global Warming Potential of the Cogeneration System.

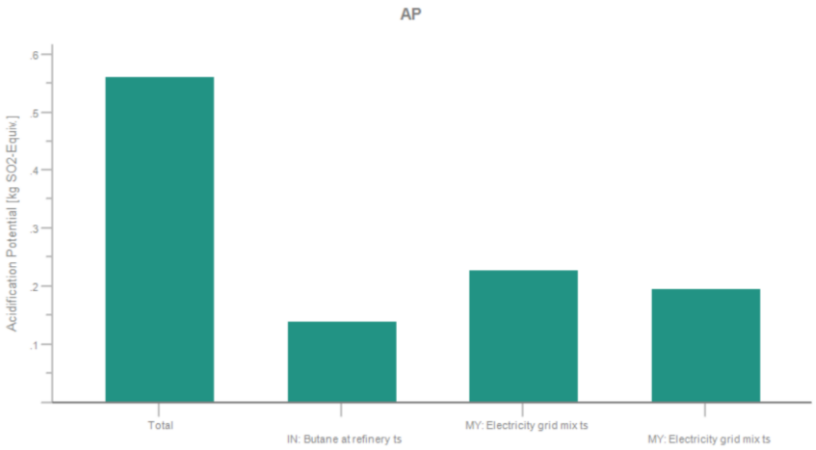

GraphE-2: Acidification Potential of the Cogeneration System.

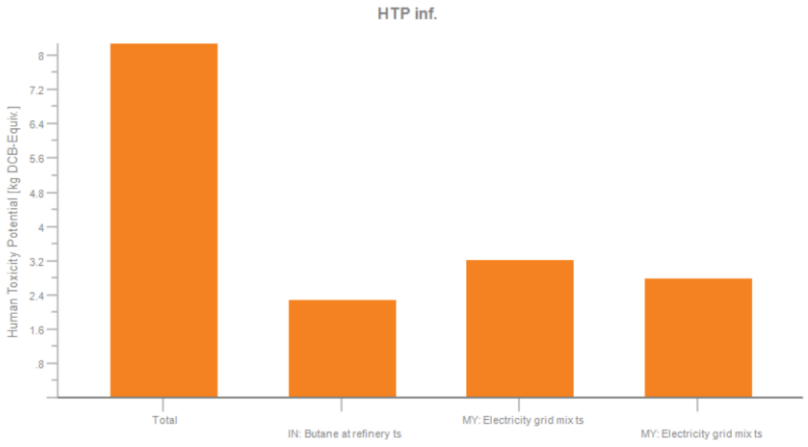

GraphE-3: Human Toxicity Potential of the Cogeneration System.

Appendix F: Graphs of Life Cycle Assessment (LCA) for the Trigeneration System

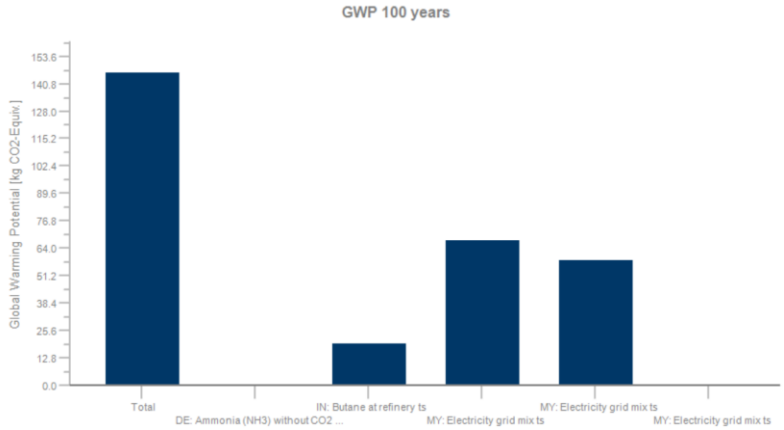

GraphF-1: Global Warming Potential of the Trigeneration System.

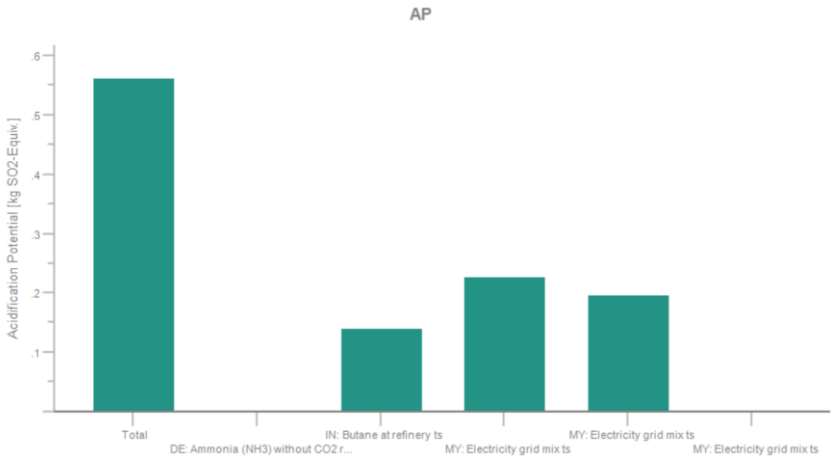

GraphF-2: Acidification Potential of the Trigeneration System.

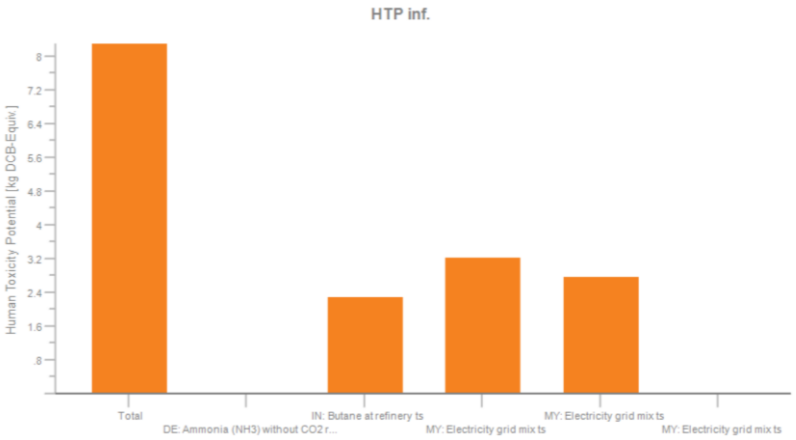

GraphF-3: Human Toxicity Potential of the Trigeneration System.